Forschungsbericht 2026-21

Analysis of Engine Noise, Acoustic Optimization of Fan Design, and Investigation of Optimal Take-Off Profiles for Certification Noise Reduction of Civil Supersonic Aircraft

Matti Gräbert

Deutsches Zentrum für Luft- und Raumfahrt
Institut für Antriebstechnik
Berlin

Deutsches Zentrum
für Luft- und Raumfahrt

Forschungsbericht 2026-21

Analysis of Engine Noise, Acoustic Optimization of Fan Design, and Investigation of Optimal Take-Off Profiles for Certification Noise Reduction of Civil Supersonic Aircraft

Matti Gräbert

Deutsches Zentrum für Luft- und Raumfahrt
Institut für Antriebstechnik
Berlin

129 Seiten
49 Bilder
16 Tabellen
198 Literaturstellen

Deutsches Zentrum
für Luft- und Raumfahrt

Herausgeber:

Deutsches Zentrum
für Luft- und Raumfahrt e. V.
Wissenschaftliche Information
Linder Höhe
D-51147 Köln

ISSN 1434-8454
ISRN DLR-FB-2026-21
Erscheinungsjahr 2026
DOI: 10.57676/axpn-6144

Akustik, Überschall, Zertifizierungslärm, Fanauslegung, Startprofile

Matti GRÄBERT
DLR, Institut für Antriebstechnik, Standort

Analyse des Treibwerkslärms, akustische Optimierung des Fandesigns und Untersuchung optimaler Startprofile zur Reduktion des Zertifizierungslärms ziviler Überschallflugzeuge
Technische Universität Berlin (Dissertation)

Mit der Entwicklung neuer ziviler Überschallflugzeuge wurde die Vorhersage ihres Zertifizierungslärms ein wichtiges Forschungsgebiet. Der Triebwerkslärm ist bei Start und Landung dominant und steht im Fokus dieser Arbeit. Es werden empirische Strahllärm- und analytische Fanlärm- und Lärmausbreitungsmodelle eingesetzt, um realistische Zertifizierungspegel vorherzusagen und Daten zum Triebwerk zu liefern. Die Einflüsse auf Start- und Landelärm durch Einschränkungen des Entwurfs von Flugzeug und Triebwerken für den Überschall sowie deren Verhalten bei niedriger Geschwindigkeit werden gezeigt. Die Triebwerksauslegung wird dabei näher beleuchtet. Ein automatischer Design-to-Noise-Prozess, primär basierend auf einem semi-analytischen Mittelschnittansatz zur Vorhersage von Aerodynamik und Akustik des Fans, wird entwickelt. Mit diesem Prozess werden je ein lärmoptimiertes einstufiges und zweistufiges Fankonzept für einen Mach 1.8-Überschallairliner entwickelt. Ihre Vor- und Nachteile bzgl. Leistungsparameter und Akustik werden untersucht. Für Überschallflugzeuge ergeben sich zudem Potentiale für die Anpassung der Startprozeduren mit dem Ziel der Reduktion von Zertifizierungspegeln. Gezielter Einsatz des Schubs sowie Anpassungen der Startgeschwindigkeiten werden im Rahmen einer Startprofilstudie untersucht. Dabei wird festgestellt, dass das oben erwähnte Airliner die in Chapter 14 festgelegten Lärmgrenzwerte mit signifikanten Abständen einhalten kann. Der Einfluss von ein- und zweistufigem Fan auf Zertifizierungspegel wird untersucht. Bei Starts, bei welchen der Fanlärm dominant ist, führt der Einsatz des zweistufigen Fans zu deutlich niedrigeren Zertifizierungspegeln. Des Weiteren wird eine Studie über den Einfluss von Unsicherheiten in der Modellierung von Flugzeugentwurf und Linerannahmen durchgeführt.

acoustics, supersonics, certification noise, fan design, take-off profiles (Published in English)
Matti GRAEBERT
German Aerospace Center (DLR), Institute of Propulsion Technology, Location

Analysis of Engine Noise, Acoustic Optimization of Fan Design, and Investigation of Optimal Take-Off Profiles for Certification Noise Reduction of Civil Supersonic Aircraft
TU Berlin (Dissertation)

As new civil supersonic aircraft are being developed, the prediction of their certification noise becomes a relevant research topic. The engine noise, which is dominant during landing and take-off, is the focus of this thesis. Empirical jet noise and analytical fan noise and noise propagation models are employed to predict realistic certification noise levels and provide engine data. The design restrictions and low-speed characteristics of aircraft and engines, and their impact on landing and take-off noise are presented. The engine design is discussed in detail. Using a semi-analytical meanline approach to predicting fan aerodynamics and fan noise, an automatic design-to-noise process for the fan is developed. With this process, a noise optimized single-stage and a two-stage fan design for a Mach 1.8 supersonic airliner are designed. Then their acoustic and performance characteristics are studied, highlighting advantages and disadvantages of each concept. For supersonic aircraft there are options to alter take-off procedures with the goal of reducing certification noise levels. Changes to the thrust application and speed management during take-off are investigated in a take-off profile variation study. It is found that the airliner mentioned above can meet Chapter 14 noise certification requirements with significant margins. The impact of using a single- or two-stage fan on those certification levels is investigated, and it is shown that on take-offs on which fan noise is dominant, significantly lower certification levels can be achieved by using the two-stage concept. Furthermore, a study is conducted on the effects of uncertainties in the airframe and liner modeling.

Analysis of Engine Noise, Acoustic Optimization of Fan Design, and Investigation of Optimal Take-Off Profiles for Certification Noise Reduction of Civil Supersonic Aircraft

vorgelegt von
Matti Gräbert, M. Sc.
ORCID: 0009-0002-1565-0527

an der Fakultät V – Verkehrs- und Maschinensysteme
der Technischen Universität Berlin
zur Erlangung des akademischen Grades

Doktor der Ingenieurwissenschaften
–Dr.-Ing.–

genehmigte Dissertation

Promotionsausschuss:

Vorsitzender:	Prof. Dr.-Ing. Andreas Bardenhagen
Gutachter:	Prof. Dr.-Ing. Dieter Peitsch
Gutachter:	Dr.-Ing. Christoph Richter

Tag der wissenschaftlichen Aussprache: 13. April 2026

Berlin 2026

Acknowledgements

This thesis was written during my 4.5-year tenure as a research associate in the Engine Acoustics department of DLR. I want to thank my colleagues for providing a pleasant working environment and constructive exchanges, which helped me learn and conduct my studies.

In particular, I would like to extend my gratitude to Robert Jaron, for his supervision of my PhD project and the numerous scientific discussions, which helped me solidify my understanding of the specifics of supersonic transport. In his role as coordinator of the SENECA project, he encouraged me to immerse myself in all facets of the research within the project and allowed me to focus on my scientific work by handling the administrative load.

Other members of the *Numerik & Prognose* group deserve special thanks as well: Antoine Moreau for sharing his expertise on the analytical models and interrelations in fan aerodynamics and acoustics of PropNoise, as well as always challenging me to work with the necessary scientific rigor. Sébastien Guerin, who always showed me compassion and took time to discuss whatever questions I had, whether they were about acoustics or the scientific process in general - Merci beaucoup à vous! Stephen Schade, whose research overlapped significantly with mine, leading to cooperation in software and modelling development. Supervising Max Marggraf as student has been a privilege and I want to thank him for the support in developing and expanding VIOLIN.

I also want to thank Fleming Kohlenberg for his open-door policy concerning all my questions about acoustic liners and the process of finishing my PhD.

Research cannot be conducted in a vacuum and I am grateful for the work of Balbir Kaur, Brig Pilger and Nico Seiffert who promptly solved all my administrative and IT issues.

A majority of the work presented in this thesis was conducted as part of the EU Horizon 2020 project SENECA (Grant Agreement No. 101006742). I would like to thank the EU for providing funding for this research and the consortium for sharing their knowledge and insights as well as allowing the publication of this work.

The high-level studies conducted for this thesis rely on extensive ground work, so I want to especially thank two parties of the SENECA consortium who made my research possible: Cristina Villena Muñoz of Cranfield University who delivered both the airliner concept design and take-off profiles, and Martin Plohr as well as his colleagues of DLR's Engine department who provided the engine cycle design and extensive engine operating data.

Jochen Kirz of DLR's Transport Aircraft Department not only headed the STORMIE project, for which I conducted the rest of my scientific work, but also provided supporting wing and inlet aerodynamics data.

I would be remiss if I did not thank those who supported me privately: friends, family, partners - in short: loved ones. You took my mind off research when I needed a break but also allowed me to focus all my energy towards this thesis when it was required. I am grateful to have you in my life.

I wish to thank Prof. Dieter Peitsch not only for reviewing my thesis, but for inspiring a passion in aircraft engine and particularly compressor design in me through his lectures at TU Berlin. Similarly, I want to thank Dr. Christoph Richter for not only being a reviewer of this thesis, but a colleague in SENECA, who helped direct the acoustics research within the project.

Writing a PhD thesis is an enormous challenge I would not have successfully conquered without many people supporting me. I am thankful for their help with this step in my life. I could not possibly acknowledge every single person here, but to those not mentioned: be aware that I recognize your contributions.

Abstract

A new generation of civil supersonic aircraft is being developed and may enter service as early as 2030. These aircraft are expected to have a bigger environmental impact than subsonic aircraft, as previous experience has shown. Besides the climate impact and en-route noise caused by the sonic boom, community noise has been a major challenge for supersonic transport. Research to quantify and minimize landing and take-off noise of a potential future supersonic fleet becomes necessary. The engine noise, which is dominant in supersonic aircraft during landing and take-off, must be predicted and reduced. To achieve both goals, empirical jet noise and analytical fan noise and noise propagation models are employed. They allow the prediction of realistic certification noise levels, which are vital to the process of setting new certification rules for supersonic aircraft. These predictions also help to reduce the certification noise levels through noise optimized design and operation by providing supporting data.

Due to their mission specifics, civil supersonic aircraft are very different from subsonic aircraft in both design and operation. The design restrictions and low-speed characteristics of aircraft and engines, which impact landing and take-off noise are presented. The engine design is discussed and it is shown that trade-offs exist between fuel efficiency in cruise and engine noise on landing and take-off.

Using a semi-analytical meanline approach to predicting fan aerodynamics and fan noise as well as analytical noise propagation models, an automatic design-to-noise process for the fan is developed and presented. Using this process, a noise optimized single-stage and a two-stage fan design for a supersonic airliner cruising at Mach 1.8 are designed. Then their acoustic and performance characteristics are studied, highlighting some advantages and disadvantages of each concept.

Supersonic aircraft can easily take off without applying maximum thrust, so there are options to alter take-off procedures with the goal of reducing certification noise levels. Changes to the thrust application and speed management during take-off are investigated in a take-off profile variation study, using the supersonic airliner mentioned above. This allows to both evaluate the effectiveness and reasonable boundaries of these procedure variations and to predict minimum certification noise levels for the airliner. It is found that the airliner can meet *Chapter 14* noise certification requirements with significant margins. The impact of using a single- or two-stage fan on those certification levels is investigated, and it is shown that on take-offs on which fan noise is dominant, significantly lower certification levels can be achieved by using the two-stage concept. Furthermore, a study is conducted on the effects of uncertainties in the airframe and liner modeling.

Zusammenfassung

Die Entwicklung einer neuen Generation ziviler Überschallflugzeuge ist in vollem Gange, eine Indienststellung wird bereits für 2030 angestrebt. Ausgehend von bestehenden Erfahrungen ist zu erwarten, dass diese Flugzeuge einen größeren Umwelteinfluss haben werden, als die heute üblichen Unterschallflugzeuge. Neben seiner Klimawirkung und dem Überschallknall im Reiseflug stellt Start- und Landelärm eine signifikante Herausforderung für den zivilen Überschallverkehr dar. Dies macht Forschung zur genauen Vorhersage und Reduktion dieses Lärms notwendig. Da der Triebwerkslärm bei Start und Landung dominant ist, steht er im Fokus dieser Forschung. Um diese Ziele zu erreichen, werden empirische Strahllärm- und analytische Fanlärm- und Lärmausbreitungsmodelle eingesetzt. Sie erlauben die Vorhersage realistischer Zertifizierungspegel, welche essentiell für die Entwicklung neuer Zulassungsregeln für zivile Überschallflugzeuge sind. Dabei werden zudem Erkenntnisse über Lärmoptimierung in Auslegung und Betrieb gewonnen.

Zivile Überschallflugzeuge unterscheiden sich, durch Eigenheiten ihrer Flugmissionen, in Auslegung und Betrieb deutlich von Unterschallflugzeugen. Die sich daraus ergebenden Einflüsse auf Start- und Landelärm werden gezeigt. Sie sind bedingt durch Einschränkungen des Entwurfs von Flugzeug und Triebwerken sowie deren Verhalten bei niedriger Geschwindigkeit. Die Triebwerksauslegung wird näher beleuchtet und gezeigt, dass ein Zielkonflikt zwischen niedrigem Treibstoffverbrauch im Reiseflug und reduziertem Lärm bei Start und Landung existiert.

Ein automatischer *Design-to-Noise*-Prozess wird entwickelt und präsentiert. Dieser basiert auf einem semi-analytischen Mittelschnittansatz zur Vorhersage von Aerodynamik und Akustik des Fans sowie analytischen Lärmausbreitungsmodellen. Mithilfe dieses Prozesses werden je ein lärmoptimiertes einstufiges und zweistufiges Fankonzept für einen Überschalllinienflugzeug mit einer Reisegeschwindigkeit von Mach 1.8 entwickelt. Ihre Leistungsparameter und Akustik werden untersucht und Vor- und Nachteile des jeweiligen Konzepts herausgestellt.

Da Überschallflugzeuge für einen sicheren Start nicht den maximal verfügbaren Schub benötigen, ergeben sich Potentiale für die Anpassung der Startprozeduren mit dem Ziel der

Reduktion von Zertifizierungspegeln. Gezielter Einsatz des Schubs sowie Anpassungen der Startgeschwindigkeiten werden im Rahmen einer Startprofilstudie am Beispiel des oben erwähnten Linienflugzeugs untersucht. In Konsequenz können sowohl die Effektivität und sinnvolle Grenzen dieser Prozeduren, als auch minimale Zertifizierungspegel für dieses Flugzeug gefunden werden. Dabei wurde festgestellt, dass dieses Überschalllinienflugzeug die in *Chapter 14* festgelegten Lärmgrenzwerte mit signifikanten Abständen einhalten kann. Der Einfluss von ein- und zweistufigem Fankonzept auf Zertifizierungspegel wird untersucht. Es kann gezeigt werden, dass bei Starts, bei welchen der Fanlärm dominant ist, der Einsatz des zweistufigen Fans zu deutlich niedrigeren Zertifizierungspegeln führt. Des Weiteren wird eine Studie über den Einfluss von Unsicherheiten in der Modellierung von Flugzeugentwurf und Linerannahmen durchgeführt.

Contents

Nomenclature

List of Abbreviations

$(V)IGV$	(Variable) Inlet Guide Vane	
AoA	Angle of Attack	
BBN	Broadband Noise	
BPF	Blade Passing Frequency	
BPR	Bypass Ratio	
CFD	Computational Fluid Dynamics	
DLR	German Aerospace Center	
$EASA$	European Union Aviation Safety Agency	
EoF	End of Field	
$EPNL$	Effective Perceived Noise Level	EPNdB
FAA	Federal Aviation Administration	
FAR	Federal Aviation Regulations	
FPR	Fan Pressure Ratio	
$ICAO$	International Civil Aviation Organization	
inc	Incidence	°
$Int.$	Interaction	
ISA	International Standard Atmosphere	
$JAXA$	Japanese Aerospace Exploration Agency	
LE	Leading Edge	
$LSWT$	Low-Speed Wind Tunnel	
LTO	Landing and Take-Off	
$MTOM$	Maximum Take-Off Mass	t

$MVDR$	Meridional Velocity Density Ratio	
$NASA$	National Aeronautics and Space Administration	
OPR	Overall Pressure Ratio	
Pax	Passengers	
PF	Potential Field	
PLR	Programmed Lapse Rate	
PNL	Perceived noise level	dB
$PNLT$	Tone-corrected perceived noise level	dB
PWL	Sound power level	dB
R	Rotor	
RSS	Rotor-Stator Spacing	
S	Stator	
SFC	Specific Fuel Consumption	
SPL	Sound pressure level	dB
SST	Supersonic Transport	
TAS	True Air Speed	ms^{-1}
TE	Trailing Edge	
TKE	Turbulent Kinetic Energy	m^2s^{-2}
TO	Take-Off	
TOB	Third-octave band	
ToC	Top of Climb	
$VNRS$	Variable noise reduction system	
VTN	Variable Throat Nozzle	

List of Greek Symbols

β	Elevation angle	$^\circ$
η	Efficiency	
λ	Wave length	m
ϕ	Roll angle	$^\circ$
ρ	Density	kgm^{-3}

List of Latin Symbols

A	Area	m^2
c	Coefficient	
D	Drag	N
D	Lieblein diffusion factor	
d	Diameter	m
f	Frequency	Hz
h	Altitude	m, ft
l	Lateral distance	m
l	Length	m
M	Mach number	
m	Azimuthal mode order	
n	Fan speed	min^{-1}
n	Noisiness	noy
n	Radial mode order	
p	Pressure	Nm^{-2}
Q	Mass Flow	kgs^{-1}
r	Distance	m
S	Cross-section	m^2
s	Solidity	
T	Thrust	N
T	Total temperature	K
t	Time	s
V	Flight speed	kts
v	Velocity	ms^{-1}
V_2	Take-off safety speed	kts

List of Subscript Notations

$\square_{\text{App}}$	Approach
$\square_{\text{cruise}}$	Cruise conditions

$\square_{\mathrm{cum}}$	Cumulative
$\square_{\mathrm{FO}}$	Flyover
$\square_{\mathrm{ise}}$	Isentropic
$\square_{\mathrm{jet}}$	Pertaining to jet
$\square_{\mathrm{Lat}}$	Lateral
$\square_{\mathrm{max}}$	Maximum
$\square_{\mathrm{opt}}$	Optimum
$\square_{\mathrm{rand}}$	Random
$\square_{\mathrm{rel}}$	Relative
$\square_{\mathrm{wet}}$	wetted

Author's notes

In this thesis, specific, uncommon terminology is used to avoid confusion. The reference noise measurements points for aircraft certification noise are called "Approach", "Lateral" and "Flyover", so the aviation term "approach" will be changed to "landing sequence" and any "flyovers" will be referred to as "flybys".

In scientific publications, the path of an aircraft (such as during landing or take-off) will often be referred to as a trajectory. However, when only two dimensions are varied, they should be called "profiles". This notation is used in this thesis.

The term "noise" is used to refer to sound in the audible domain between 20 and 20,000 Hz without any psychoacoustic evaluation.

List of Figures

List of Tables

Chapter 1

Introduction

More than 20 years have passed since the last civil supersonic flight, but passengers' desire to quickly travel long distances and cut their time on the plane in half remains. Thus, the dream of air travel faster than sound lives on. With a projected market entry as soon as 2030 [1], this dream is now closer to becoming reality than it has been since the final flight of *Concorde*. While the development of the next generation of civil supersonic aircraft is well underway, no such aircraft is in the process of being certified for service at the time of this writing - an essential step towards starting commercial operations for any new aircraft.

An important reason for this is a lack of certification rules. Unfortunately, environmental certification regulations applicable to new aircraft types only exist for subsonic aircraft and have not been written for supersonic transport (SST). These regulations impose limits on emissions and landing and take-off noise. Without applicable rules, certification is impossible and the development of new supersonic aircraft and their systems stalls: Manufacturers need reliable guidelines and rules ahead of time to design aircraft which abide by them.

When a new set of regulations is drafted for subsonic aircraft, the data which is required by the regulators is commonly extrapolated from measurements of comparable current aircraft types. Furthermore, aircraft and system manufacturers are consulted. For supersonic aircraft, this is not possible, because there are neither civil supersonic aircraft in service nor prototypes available and no established manufacturers exist. As stated by the Federal Aviation Administration (FAA), "[the] same historic lack of data to establish full supersonic noise standards continues today"[1] [2]. For this reason, data based on aircraft concepts has to be provided by companies designing those new aircraft and independent researchers who investigate the environmental impact of SST.

[1]The quote from 2018 remains accurate.

Figure 1.1: Rendering of the Boom Overture, a future supersonic airliner; Source: Boom Supersonic

As an important aspect of certification rules, the landing and take-off (LTO) noise of future civil supersonic aircraft must be accurately forecast and prediction methods evaluated and improved if necessary. Using these methods, SST LTO noise can not only be predicted reliably, but also minimized. A low-noise engine can be designed using a design-to-noise approach. By deviating from classic take-off procedures, the LTO noise can be mitigated operationally as well.

The focus of this thesis is on the design of a low-noise fan, the prediction of certification noise levels and the analysis of advanced take-off procedures. An airliner concept, cruising at Mach 1.8 will be used as a reference case. This concept was developed as part of the EU project SENECA, which will be elaborated on later in this chapter.

1.1 Context of this thesis

To understand the significance of this work, it is important to know of the history of civil supersonic aviation and its state at the time of this writing. This section's aims to provide this context, so an overview of the history and future of civil supersonic aviation and related research will be given here.

When the first generation of supersonic military aircraft had entered service in the 1950s, work on SST started in several nations, most notably in France, the UK, the USA, and the USSR. Because of concerns about the environmental impact as well as lack of profitability, only two supersonic aircraft have ever entered service in the civil sector. Those are the airliners *Concorde* made by Aérospatiale and the Bristol Aeroplane Company and *Tu-144* made by Tupolev. These are designs of the 1960s and 1970s, with the

Concorde cooperation treaty between Sud Aviation (France) and the Bristol Aeroplane Company (UK) being signed in 1962 and the initial *Tu-144* design published in January 1962 and development starting on July 26$^{\text{th}}$ 1963. They entered service in 1976 and 1975 respectively [3]. Due to the high cruise Mach number and suitable wing design, the SST airliners had a low aerodynamic efficiency (also called glide ratio) commonly expressed as the ratio of lift and drag. The details of this will be discussed in Chapter 2. Consequently, even well optimized designs such as *Concorde* and *Tu-144* had much higher thrust demand and fuel consumption than subsonic aircraft on a similar mission. *Tu-144* was removed from service in 1983 due to reliability and cost issues with few missions completed, while *Concorde* service was discontinued in 2003 due to reduced demand and increasing maintenance cost [4]. The last supersonic passenger flight to date was completed on October 24$^{\text{th}}$ 2003, so no recent experience with state of the art designs of SST exists.

Noise concerns have always been a part of SST, with the supersonic boom in cruise and engine noise on landing and take-off posing significant challenges. In 1973, even before *Concorde's* entry into service, the government of the United States of America issued a ban for civil supersonic flight over land due to environmental noise concerns [5]. Other countries adopted similar policies, leading to supersonic flight over land being banned in most of the world. These bans are largely still in place and present a major hindrance in the development of new SST, as they severely limit useful routes and thus profitable operation. In June 2025, the US government tasked the FAA with developing a noise-based certification standard to replace the ban within the ensuing 18 months [6].

Theoretical research into sonic boom reduction started in the early 1960s in the UK and US [7, 8]. Low-boom technology is supposed to reduce the overpressure and thus noise signature of the sonic boom to such a low level that supersonic flights over populated areas would be routinely possible. Focused research into low-boom aircraft designs was launched as part of the NASA HSR (High-Speed Research) in 1990 [9], but significant progress was only made with the emergence of CFD technology during the DARPA QSP (Quiet Supersonic Platform) project, particularly with the SSBD and SSBE programs (Shaped Sonic Boom Demonstration and Experiment), starting in 2000 and 2001 respectively [10, 11]. At the same time, the investigation of sonic booms was progressing in the EU as well, with project SOBER (Sonic Boom European Research Programme: Numerical and Laboratory-Scale Experimental Simulation, 2001-2004), led by Airbus [12]. After several years without any research on SST, project RUMBLE (RegUlation and norM for low sonic Boom LEvels, 2017-2020) aimed to advance the work on low-boom technology and inform EASA in discussions about potential future regulations about supersonic overland flight [13]. In Japan, JAXA investigated low-boom aircraft designs in the D-SEND (Drop test for Simplified Evaluation of Non-symmetrically Distributed sonic boom) project. The *S3* and *S4* low-boom aircraft platforms [14, 15, 16, 17] have been developed using the knowledge gained in that project. In 2025, as a product of the DARPA QSP findings and part of the ongoing CST (Commercial Supersonic Technology) effort, NASA is conducting flight tests using their *X-59* technology demonstrator to explore the real-world applications of low-boom technology as part of the QueSST mission (Quiet Supersonic Transport) [18]. By 2025, DLR have developed their own low-boom aircraft platform [19, 20].

As explained earlier, landing and take-off noise poses another challenge for SST. For *Concorde*, LTO noise standards did initially not exist, but after complaints from New York citizens and legal challenges, the FAA set noise reduction rules. According to FAR 36.301 [21], the only requirement was to minimize the noise operationally in a manner "economically reasonable, technologically practicable, and appropriate for the *Concorde* type design", since the aircraft and engine design could not be altered significantly anymore. Despite efforts from the FAA to propose general certification noise limits for SST as early as 1986 [2], this remains the only noise regulation as of Fall 2025, since neither FAR Part 36 (FAA) [22] or the ICAO (International Civil Aviation Organization) Annex 16 Vol. 1 [23] provide standards for LTO noise limits for SST.

LTO noise of SST has been researched for decades with projects such as SCR (Supersonic Cruise Research 1972-1981) and HSR (High Speed Research 1990-1999) in the US and HISAC (Environmentally friendly high speed aircraft, 2005-2009) in the EU [24] leading the way. As early as 1979, Grantham and Smith [25] assessed the LTO procedures of a supersonic aircraft with a payload of 273 passengers travelling at Mach 2.62 for community noise abatement purposes. Work on take-off procedure optimization and jet noise mitigation for modern SST concepts was started in the mid-1990s by Berton [26], and low-speed aerodynamic optimization as a means of LTO noise reduction was investigated in project EPISTLE (European project for improvement of supersonic transport low speed efficiency, 2000-2003) [27]. The goal in both cases was the minimization of thrust demand on take-off and landing.

Naturally, within the past decades, work on SST not directly related to noise has been performed as well. Project NEXST-1 of JAXA successfully experimented with low-drag SST configurations [28]. The most recent projects in Europe were:

- EUROSUP (Reduction of wave and lift-dependent drag for supersonic transport aircraft, 1996-1998) with the goal of optimizing aerodynamic efficiency en-route [29]

- SCENIC (Scenario of aircraft emissions and impact studies on chemistry and climate, 2002-2005) with the goal of improving en-route emissions predictions [30]

- SUPERTRAC (Supersonic laminar control, 2005-2008), researching the control of laminar flow in the supersonic domain [31]

- CISAP (Cruise speed Impact on Supersonic Aircraft Planform, 2002-2004), with the general goal of airframe MDO, focusing wing design optimization [32]

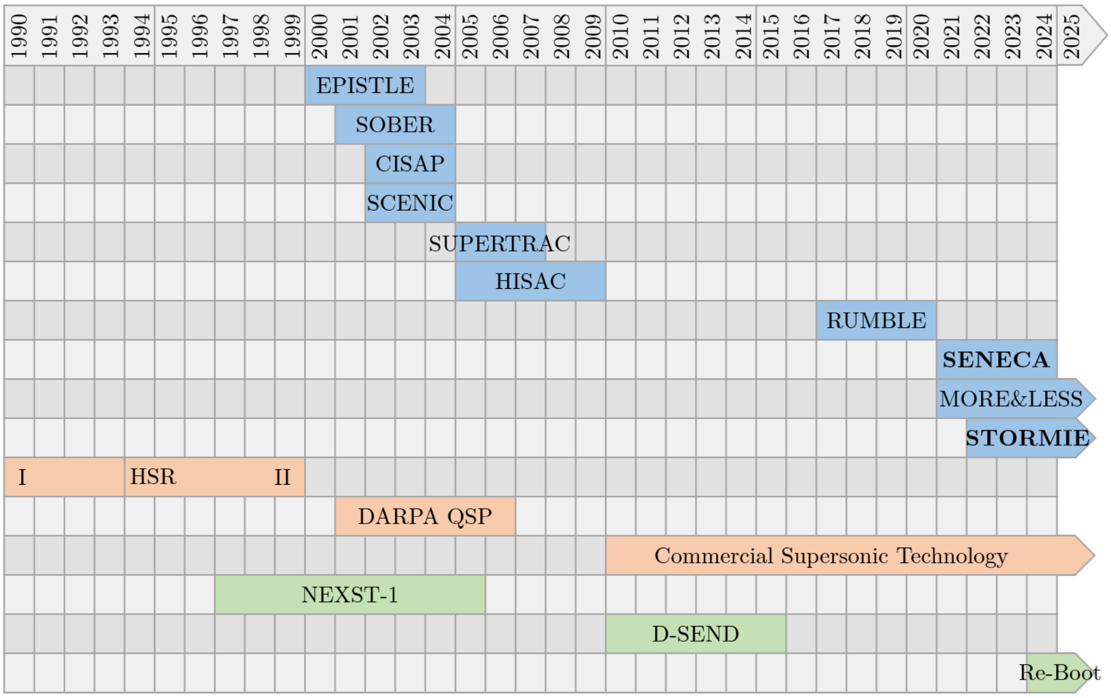

Figure 1.2: Relevant SST research projects of EU (blue), US (orange) and Japan (green)

In more recent times, there was another push to reintroduce supersonic air travel: In the 2010s and early 2020s, start-up companies were working on a new generation of SST and had made significant advancements. Most notable are Aerion and Spike Aerospace, who started work on supersonic business jets and Boom Supersonic and Exosonic who are to developing supersonic airliners. All of those companies are located in the USA.

The Aerion Corporation started designing their supersonic business jet *AS2* in 2008 and were close to a market-ready design but ceased operations in 2021 due to a lack of funding. Their 12-passenger supersonic business jet concept was supposed to travel at Mach 1.4 with a range of 4,750 NM [33]. Boom Supersonic is thought to lead development at the time of this writing, with the design having undergone multiple iterations, a planned entry into service in 2029 and supersonic test flights of a demonstrator aircraft having been completed. The *Overture* quadjet concept is supposed to carry up to 80 passengers over 4,250 NM at a cruise Mach number of 1.7 [34]. The *Symphony* engine, developed by Boom Supersonic in cooperation with Florida Turbine Technologies, is supposed to provide 155,700 N (35,000 lb-f) in thrust and have a fan diameter of 1.83 m (72") [35]. A cutaway of the engine model can be seen in Figure 1.3. No full-sized model of either aircraft or engine has been produced, but both Aerion and Boom Supersonic have reached development stages not achieved in decades.

Figure 1.3: Cutaway of the Boom Supersonic *Symphony* engine design study, source: Boom Supersonic

With the development of SST progressing, it had become imperative for ICAO to define applicable LTO noise regulation standards. Hence research of LTO noise of SST in the 2010s and early 2020s experienced a significant boost. The focus was mostly on take-off procedure optimization with the goals of researching technology to reduce the LTO noise relevant to certification and to provide the ICAO Committee on Aviation Environmental Protection (CAEP) with scientific data to base their regulations on. The state of this research will be covered in the ensuing section.

1.2 State of the art of relevant research

This thesis focuses on both the LTO and certification noise of civil supersonic aircraft and on fan noise. The status quo of research in these two fields with a focus on prediction methods will be covered here.

1.2.1 Fan noise prediction

Fan noise has been a prominent research topic for decades and consequently, many prediction, measurement and analysis methods have been developed. Fan noise prediction can be categorized in three major categories: empirical, analytical, and numerical modeling. Each of those will be covered here in brief.

- Empirical or semi-empirical methods rely on measurement data, from which physics-informed correlations are derived. They typically function with limited geometry and operation data, making them very useful at a pre-design level. They are fast and accurate inside their calibration domain, i.e. for designs similar to those used to obtain the experimental database. Outside of that domain, their accuracy diminishes, making them less suitable for exploratory studies. Additionally, the amount of measured fan noise data available to research institutions is quite limited, due to the expensive nature of those experiments, which makes the creation, improvement or tuning of such models hard. The most well-known example is the fan noise prediction model developed by Heidmann in 1979 [36], which was modified by Kontos [37], Kresja [38] and Berton [39] to expand its calibration domain. Recently, NASA has worked on another expansion to this model to suit multi-stage fans for SST. The calibration data in this case is simulated and not measured [40], and the fan design used for calibration is the GE Affinity [41]. An older fan noise prediction model for supersonic aircraft exists, called the HSRNOISE tool [42] with its calibration data based on the military XF-120 engine. Since the details of this engine are confidential, the model is hard to adapt and its practical use limited.

- Analytical or semi-analytical methods use physics-based formulae to calculate noise. The aerodynamic excitation, meaning the pressure distribution on the blade surfaces and its fluctuation is calculated first, then the noise excited by the unsteady lift. A strip theory approach is usually applied here to simplify the calculation to a quasi-2D problem at a discrete radial position of the blade. Sears [43] and Amiet [44] described such approaches with regards to the exciting unsteady pressure. To calculate the acoustic field in the entire duct, the radial strips are superposed analytically into acoustic modes using Green's function. The result is then radiated to free-field modes. In the process used most in this thesis, the aerodynamic excitation is calculated using analytical models and empirical correlations along a meanline as described by Moreau [45]. Another example of analytical fan noise modeling is the analytical broadband interaction noise prediction model developed by the University of Southampton [46]. Analytical methods are not limited by a calibration domain and are very useful for exploratory studies. They require little information about geometry and operating conditions, so they can easily be applied to fans at a pre-design level. Furthermore, they resolve the individual noise generation mechanisms and sources, allowing to assess and quantify them separately. This forms a deeper understanding of the role of fan design and operation in fan noise. While trends found with analytical methods are very reliable, their accuracy in absolute noise levels can be worse than that of numerical or empirical methods, since not all effects can be accurately modelled. These simplifications need to be addressed when discussing results of analytical fan noise studies.

- Numerical methods are commonly applied to fan noise problems. It is technically possible to resolve both the flow field, i.e. the aerodynamic excitation and the acoustic field, i.e. noise generation and propagation simultaneously using the Direct Navier-Stokes (DNS) method. However, the high computational costs make it unfeasible for industrial applications.

  This is why Navier-Stokes based hybrid approaches are taken, where the flow field is resolved using CFD methods and the acoustic field is modelled separately. Some of the most popular of these approaches, from lowest to highest fidelity (and computational cost) are:

  - Reynolds Averaged Navier-Stokes (RANS) equations based simulations combined with analytical acoustic solutions, often using acoustic analogies. For broadband noise prediction, turbulence needs to be synthesized for this approach, based on turbulence statistics provided by turbulence models such as Menter's $k - \omega$ Shear Stress Transport [47] or Kok's model [48]
  - Unsteady RANS, which is resolved in the time domain using time marching technique and used to simulate tonal noise. Turbulence needs to be modelled for this approach as well.
  - Harmonic balance (HB) or other frequency domain approaches. These methods are similar to URANS, they simulate only harmonic phenomena and consequently their scope is limited to tonal noise. Turbulence needs to be modelled for this approach.
  - Scale resolving methods such as Large Eddy Simulations (LES) [49] can resolve turbulence and are used to simulate tonal and broadband noise. Due to rapidly increasing computational cost with increasing Reynolds numbers, they are limited to subsonic flow. To reduce cost, they are sometimes used in hybrid approaches [50].

DLR's *TRACE* is an example of CFD software capable of performing Navier-Stokes based simulations for steady and unsteady flows in the time [51, 52] and frequency domain [53] as well as scale resolving simulations, e.g. LES and hybrid RANS-LES.

The Lattice-Boltzmann method (LBM) [54] is not based on the Navier-Stokes equations and can either partially or fully resolve turbulence due to simulating particle interactions and solve both flow and acoustic field at a more manageable computational cost. It can thus simulate tonal and broadband noise. Due to deteriorating accuracy with increasing Mach numbers, it is limited to high-subsonic flow. It is often used in hybrid approaches as well [55].

1.2.2 Prediction of supersonic aircraft landing and take-off noise

Several researchers and institutions currently research LTO noise of SST and several prediction processes for SST LTO noise have been developed. Most notable are NASA, DLR, JAXA, Georgia Tech, Cranfield University and Blue Ridge Research (in cooperation with Northrop Grumman) [56, 57, 58, 59, 60].

The overall goal of this research is the prediction of realistic certification noise levels to support ICAO CAEP in setting new limits for SST in 2025. Three research topics are associated with this goal:

- The improvement of noise prediction tools for SST LTO noise
- The variation of take-off (and in fringe cases, landing) procedures with the goal of minimizing certification noise levels using of so-called variable noise reduction systems (VNRS), exploring reasonable limits of these systems in the process
- The investigation of uncertainties in SST LTO noise prediction with the goal of qualifying the results of the studies in the previous categories

Early concept studies for a new generation of SST already considered LTO noise [61], but research intensified in the late 2010s across multiple projects, using a wide range of SST concept aircraft: studying NASA's *STCA* (Supersonic Technology Concept Aeroplane) design, both NASA [62, 63, 56, 64] and JAXA [65, 58] investigated the impact of VNRS on certification noise levels. This included an automatic thrust reduction called Programmed Lapse Rate (PLR), increasing the climb-out speed to exploit the aerodynamic properties of SST and the scheduled deployment of flaps to minimize certification noise levels. Similar work was conducted by DLR [66, 67, 57, 68] with the *TWO* and *THREE* aircraft as well as Georgia Tech [69, 59]. DLR also launched project STORMIE

(Supersonic Transport Open Research Models and Impact on Environment) in 2023 to create open research platforms of civil supersonic aircraft and evaluate their environmental impact. The designs of two business jets, the low-boom *FSTB-L* and the normal-boom *FSTB-N* as well as one normal-boom airliner *FSTA* [19] have been completed and published. The EU project SENECA (LTO noiSe and EmissioNs of supErsoniC Aircraft, 2021-2024 [2]) also aimed to address the need for data as a basis for new certification regulations. In SENECA, four different conceptual aircraft platforms were designed, specifically two business jets with cruise speeds of Mach 1.4 and Mach 1.6 and two airliners cruising at Mach 1.8 and Mach 2.2. For each aircraft, an engine has been developed and optimized to reduce LTO noise and emissions. This thesis focuses on the noise assessment of the Mach 1.8 Airliner, with a particular emphasis on fan noise. The EU project MORE&LESS (MDO and REgulations for Low-boom and Environmentally Sustainable Supersonic aviation) was started in conjunction with SENECA. The environmental impact of three aircraft concepts with a Mach range of 2.0 to 5.0 is evaluated with regards to LTO noise, sonic boom, emissions, and sustainable fuels. Details of SENECA and MORE&LESS were described by Jaron and Viola [70].

Table 1.1 lists the SST concepts currently investigated most intensively, with *Concorde* included for reference.

Aircraft	**Source**	$\mathbf{M_{cruise}}$	**Range [NM]**	**Pax**	**MTOM [t]**
FSTB-L	DLR [19]	1.4	4000	8	47.4
Two	DLR [71, 67]	1.4	4000	8	55.4
Three	DLR [71, 72]	1.6	4000	8	51.0
STCA	NASA [63]	1.4	4240	8	54.9
E-5	CU[2] [73]	1.4	4000	6	41.6
E-19	CU [74]	1.6	4000	8	45.0
Business Jet	GT[3] [69]	1.4	4250	8	52.8
S3	JAXA [14, 15]	1.6	3500	50	70.0
S4	JAXA [16, 17]	1.6	3500	50	68.0
Airliner	GT [59]	1.7	4250	65	199.2
Airliner	CU [75]	1.8	4000	100	144.3
Concorde	[3]	2.0	3600	100	186.9
Airliner	CU [76]	2.2	4000	100	156.0
FSTA	DLR [19]	1.7	4250	80	185.5

Table 1.1: Overview over SST concepts currently investigated with SENECA Mach 1.8 airliner in bold; *Concorde* included for reference

[2]https://seneca-project.eu/
[2]Cranfield University
[3]Georgia Institute of Technology

To qualify the results of LTO noise prediction, uncertainty studies have begun to gain relevance in past years, with studies being conducted by DLR, JAXA and NASA [58, 77, 72, 78, 79, 80].

A major difference between the work presented in this thesis and other studies on certification noise levels of SST is the treatment of fan noise. Other studies use empirical fan noise models. NASA's ANOPP2 (Aircraft NOise Prediction Program 2) framework [81] is the most popular choice which employs the Heidmann models for turbofan noise. However, these models have drawbacks when applied to SST fan noise problems which are often outside their calibration domain. For example, multi-stage fans or inlet guide vanes (IGVs) are not within the scope of most empirical models. The HSRNOISE fan noise model [42] described in the preceding section has shown decent agreement with the tonal noise emitted by a two-stage fan, only under-predicting the sound power levels by 2 dB. Precision of broadband noise prediction with this model could not be determined reliably by Stephens [82]. The need for a physics-based approach to predicting supersonic aircraft fan noise was pointed out as a response [83], but use of such fan noise models has only recently started at NASA [40].

1.3 Goals and structure of the thesis

The goal of this thesis is to develop an LTO noise prediction method for SST based primarily on analytical models, which is an improvement over current methods in both scope and quality. It will allow a more accurate assessment of fan noise trends on landing and take-off and provide opportunities for a noise optimized fan design process. The application of the improved methods in the SENECA project yielded aeroacoustically optimized fan designs and allowed for the evaluation of optimal take-off trajectories. The lessons learned during the work on project SENECA and their impact on the later work in project STORMIE will be presented.

Since civil supersonic aircraft are conceptually different from ordinary subsonic aircraft, Chapter 2 of this thesis will explain relevant design features in airframe and engines of SST. The impact on LTO and certification noise of those design features and specific components will be discussed briefly.

Specifics of engine noise of supersonic aircraft are covered in the ensuing Chapter. The noise originating from individual components of the engine is investigated, with a deeper look into the most relevant noise sources: fan and jet. The noise generation mechanisms, their modeling and noise mitigation technologies of these two sources will be addressed. Focus is put on the analytical fan noise prediction approach used in this work, with its advantages and disadvantages.

In Chapter 4, aircraft certification noise will be treated in detail. The theory and history behind it, as well as current developments pertaining to SST and discussions about noise certification are covered. A particular focus is put on VNRS, which are highly relevant to the LTO noise of SST. Then the measurement and calculation procedures to obtain certification noise levels are conveyed. The physics-based modeling approach taken in this thesis is explained, highlighting its advantages.

Fan design for civil supersonic aircraft engines is covered in Chapter 5. First, the newly developed noise-optimized design process for such fans is explained. The aerodynamic and acoustic specifics of the resulting single- and multi-stage fan designs are discussed.

In Chapter 6, the methods of minimizing certification noise levels for SST are explored. The potential of VNRS is evaluated in a take-off profile variation study. The impact of single- and two-stage fan concepts on certification noise along two representative take-off profiles is presented. Furthermore, uncertainties in the aircraft pre-design and acoustic liner assumptions are discussed and their impact on certification levels investigated.

Finally, the conclusions from the work presented in this thesis are drawn in Chapter 7. This includes an evaluation of the methods used and developed, the impact of the results of the studies presented in this thesis and an outlook on possible future work on the subject.

Chapter 2

Differences Between Supersonic and Subsonic Transport

Even for civil applications, there are significant design differences between subsonic and supersonic aircraft. As is the case for all aircraft, there are different, often conflicting design goals for SST. They are designed for maximum economic gain while maintaining maneuverability and safety at low speeds, without exceeding certification noise limits as well as abiding other regulations adhering to safety and the environmental impact. This chapter will cover the most relevant boundaries and design goals and their impact on the design of supersonic aircraft and their engines. The emphasis lies on characteristics which impact LTO noise.

2.1 Airframe and wing design

Supersonic aircraft have specific design characteristics for their airframes, such as wing shape, size and profiles, the airframe shape and landing gear dimensions. These will be discussed here. As for every aircraft, drag minimization is a major design goal. This is particularly relevant to SST designs, since they incur high drag due to their high cruise speeds. Yoshida [84] gives a drag breakdown for *Concorde* and potential future SST (cruising at Mach 2.0) with the same mission parameters, indicating the significant potential in drag reduction for an optimized design. In Figure 2.1, the individual components of the drag force F_D are listed. While it is impossible to reduce the wave and induced drag caused by lift significantly, friction and volume-induced wave drag minimization are clear design goals.

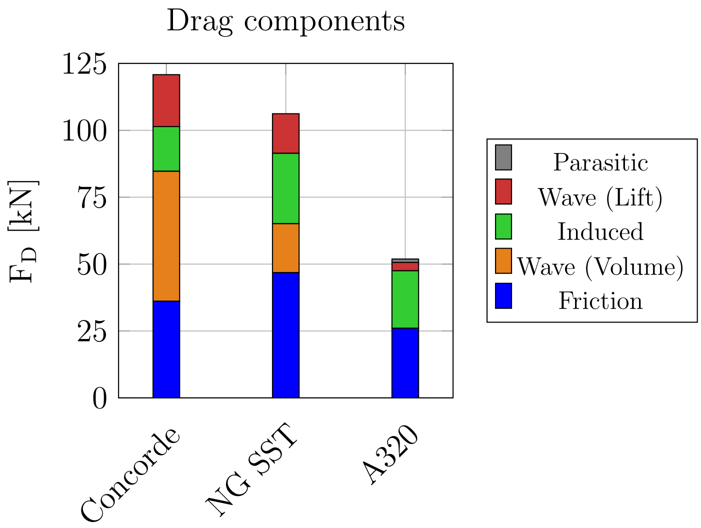

Figure 2.1: Breakdown of cruise drag estimates for *Concorde*, a Next Generation SST (M_{cruise}=2.0) and an A320 (M_{cruise}=0.78)[2]

Friction drag is defined as:

$$D_{\text{fric}} = \frac{1}{2} c_{\text{fric}} \rho v^2 A_{\text{wet}} \tag{2.1}$$

and thus, scales with the square of the aircraft's speed. While the friction coefficient c_{fric} depends on material properties, which are usually not known at the concept design level, and the ambient density ρ cannot be changed, the minimization of the wetted area A_{wet} is a general design goal. This is a true for all aircraft but even more important to SST due to the large v^2. This has an impact on the design of all aircraft systems.

Wave drag will be discussed in reference to area ruling.

2.1.1 Wing design

In supersonic flight, lift is generated by accelerating the air over the wing through expansion shocks and decelerating the air under the wing through compression shocks. Camber does not generate additional lift but significant extra drag in supersonic regimes, so supersonic aircraft wing profiles are thin and symmetrical as opposed to curved subsonic aircraft wing profiles. Slender wings, which are often used for supersonic aircraft, have been shown to produce similar lift coefficients c_L at identical angles of attack (AoA) over a wide range of Mach numbers [88, 89]. Since total lift L is defined as $L = \frac{1}{2} c_L \rho v^2 A_{\text{wing}}$ and scales with v^2, supersonic aircraft can generate high lift at small angles of attack at

[2]Data sourced from Yoshida, Blackall, Hill and Airbus [84, 85, 86, 87]

supersonic speeds. At these high speeds, the wings also incur high drag, through both viscous friction and wave drag. This means that a small wing area provides sufficient lift and is preferable for supersonic flight, so the minimum wing size of SST in dependent on safe low-speed LTO operations.

The delta wing shape has proven to be a popular choice in both civil and military aircraft [90]. It provides a good compromise between high- and low-speed aerodynamic properties. The swept, slender planform helps keep the flow moving normal to the leading edge at subsonic speeds for drag reduction in cruise. At low speeds, the lift is generated by suction from eddies forming on the top surface due to the flow detaching at the sharp leading edge (see Figure 2.2). This process is stable in a wide range of AoAs and allows for a high peak lift. While conventional wings usually peak in lift at AoAs of 10° and stall at 12-13° with a sudden drop in lift, the lift coefficient of delta wings scales linearly with AoA until 30° or even 40° [91].

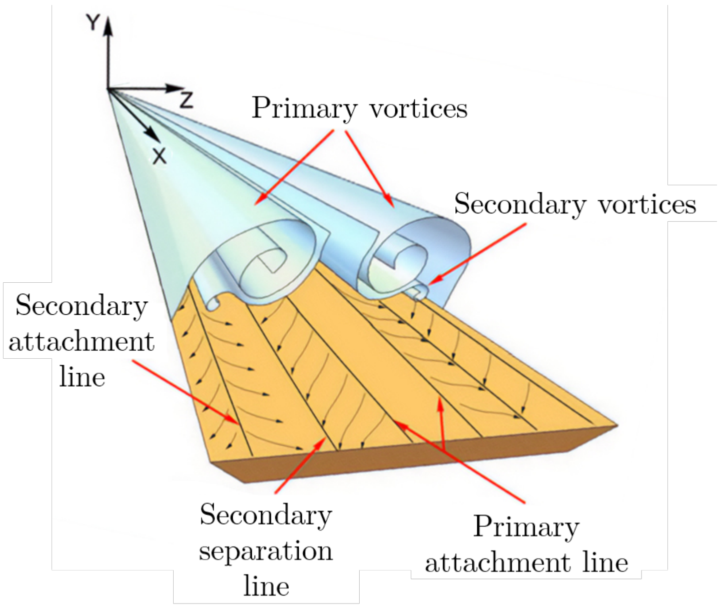

Figure 2.2: Flow around a delta wing at low speed as published by Sidorenko et al. [92]

Due to the thin, symmetrical profiles, the aerodynamic efficiency (or glide ratio, defined as the ratio of lift and drag coefficients c_L/c_D) at low speeds is poor, so lift is produced at a high drag penalty. Because of the minimal wing size to minimize cruise drag, high AoAs are necessary in low-speed operation to generate the required lift. This further increases the drag penalty. As an example, *Concorde* only had a glide ratio of 4 on take-off [3] and high-fidelity simulations predict a glide ratio of 6 for the *FSTB-L* on take-off [93]. Consequently, the delta wing is a very energy sensitive wing design, which puts bigger emphasis on a specific phenomenon that all aircraft share: below a critical speed, called the minimum drag speed, traveling faster incurs a lower drag penalty. This operating range is called the region of reverse command. For supersonic delta wings, the minimum drag speed is quite high, for example 296 kts for the NASA *STCA* [94]. In other words, during LTO operations flying faster requires less thrust than flying at lower speeds. *Concorde* made use of this by keeping its air speed high until very late in the landing sequence to reduce the thrust demand and consequently the landing noise [3].

2.1.2 Area ruling

Besides high friction drag due to high speeds, bodies traveling at supersonic speeds also incur wave drag D_{wave} which is a result of the compression shocks. There is an analytic formula for wave drag, derived from Kármán-Moore's linearized supersonic flow theory [95]:

$$D_{\text{wave}} = \frac{\rho v^2}{2\pi} \int_0^l \int_0^l S''(x_1) S''(x_2) ln|x_1 - x_2| dx_1 dx_2 \qquad (2.2)$$

S'' denotes the second derivative of the cross section of the body $S(x)$, l is the length of the body and $x_{1,2}$ are longitudinal coordinates (see Figure 2.3).

Its solution for minimum drag is the Haack-Sears body [96], a representation of which can be seen in Figure 2.3. It commonly serves as a basis for supersonic aircraft designs. As can be seen in Equation 2.2, in a supersonic regime, the drag scales with the square of $S(x)$. In transonic regimes it scales with the second derivative of the cross section. A resulting design rule for supersonic aircraft is that the cross section needs to be minimized and smoothly distributed along the longitudinal axis for minimum wave drag. Where components of the aircraft such as engines and wings are placed, the fuselage geometry needs to be constricted. These constrictions reduce the aircraft's ability to carry its payload and thus need to be minimized. This puts constraints on the engine and wing design: the cross section of wings and engines must be minimized and their positioning is limited as well.

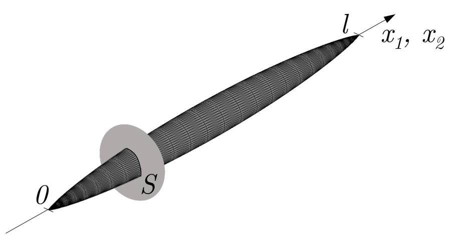

Figure 2.3: Example of a Haack-Sears body with relevant variables

2.1.3 Landing gear

Due to the high angle of attack required to generate sufficient lift on take-off and landing, the landing gears of supersonic aircraft need to be particularly tall to avoid tail strikes, as stated by Takahashi [97]. Since the turbulence caused by the landing gear is a major contributor to airframe noise (as was confirmed through the measurements made by Fink [98]), the larger landing gear has the potential to contribute significantly to the LTO noise of SST. For the HSCT airframe, this was confirmed through wind tunnel tests by Herkes et al. [99]. Since the aircraft discussed in this thesis are not developed further than the concept stage, this contribution cannot be quantified beyond rough estimations. It will not be investigated in detail but its potential impact should not be neglected.

2.2 Engine design

As was discussed above, aircraft and mission design sets restraints on the engine design space. The general cycle and geometric design as well as component design are affected by these restraints. Aircraft engine technology is still evolving significantly, but in order to provide regulators with realistic results, only technologies with a forecast entry into service as late as 2030 are considered in the engine design.

2.2.1 General design

The engine delivers the thrust for the aircraft, so to understand the impact of design constraints, it is helpful to look at the equation for installed thrust as proposed by Adamidis et al. [100]:

$$T_{\text{inst}} = T_{\text{uninst}} - D_{\text{spill}} - D_{\text{bleed}} - D_{\text{bypass}} - D_{\text{afterbody}} \tag{2.3}$$

with uninstalled thrust defined as:

$$T_{\text{uninst}} = (Q_{\text{air}} + Q_{\text{fuel}}) \cdot v_{\text{jet}} - Q_{\text{air}} \cdot v_{\infty} + (p_{\text{exhaust}} - p_{\infty}) \cdot A_{\text{exhaust}} \tag{2.4}$$

Q denotes the respective mass flow, p the static pressure and A_{exhaust} the exhaust area.

While spillage drag D_{spill}, bleed drag D_{bleed} and bypass drag D_{bypass} are throttle-dependent terms which are more relevant to detailed design, afterbody drag $D_{\text{afterbody}}$ scales with engine size.

Boeing's PIPSI (Performance of Installes Propulsion Systems - Interactive) tool [101] models afterbody drag as $D_{\text{afterbody}} = c_{D_{\text{afterbody}}} \cdot p_\infty \cdot S_{\text{max}}$, i.e. proportional to the engine maximum cross-section. $c_{\text{D}_{\text{afterbody}}}$ is dimensionless and depends on detailed geometric data.

Friction and wave drag are not included in this equation, as they are deemed airframe drag terms. At supersonic speeds, they scale with the engine's wetted surface A_{wet} and cross-section S (see Eq. 2.2) respectively. Thus, the engines have to be as small as possible. Both diameter and length should be minimized, but diameter reduction is more critical due to its impact on wave and afterbody drag.

Cycle design

The overall pressure ratio (OPR) of aircraft engines is limited by the maximum compressor outlet temperature. This limit exists since the temperature at the turbine inlet is limited by cooling and material performance and the gas temperature rise in the combustion chamber is required to deliver power to the engine. Due to the external compression in the inlet in supersonic flight, the temperature at the fan inlet plane of supersonic aircraft is already much higher than for subsonic aircraft engines, so compression is more limited. A low OPR reduces the thermodynamic efficiency of the Brayton Cycle run in the engine, but this will not be expanded on in this thesis.

The constrained engine diameter exacerbates a problem of general engine design: bypass ratio (BPR) is limited by nacelle drag and the minimum core size. A high bypass ratio is generally desirable to increase the mass flow through the engine, which benefits both engine noise and efficiency. Propulsive efficiency η_{prop} is defined by Bräunling [102] as:

$$\eta_{\text{prop}} = \frac{2}{1 + \frac{v_{\text{jet}}}{v_\infty}} \tag{2.5}$$

At a low BPR, the air mass flow Q_0 through the engine is severely limited. To provide sufficient thrust with a small mass flow, jet velocity v_{jet} must be much higher than flight speed v_∞ (see Equation 2.4). This leads to a low propulsion efficiency as can be seen in Equation 2.5. The high velocity gradients between ambient air and jet exhaust $(v_{\text{jet}} - v_\infty)$ also lead to large vortex structures which cause strong jet noise.

The BPR cannot be increased by reducing the engine core size without reducing the power output or compromising reliability, so a trade-off exists between high BPR and low drag and thus fuel consumption as shown by Plohr et al. [103] and Papamoschou et al. [104]. Calder and Gupta determined that the BPR for ideal cruise fuel consumption at Mach 2.0 lies between 0 and 0.3 [105], although this relies on 1970s technology assumptions and cores with a lower power density compared to current engine technology.

The exhaust must be kept subsonic in LTO operations to avoid jet noise levels far above certification limits. This will be expanded on in Section 3.3. Therefore, a trade-off exists between LTO jet noise and fuel efficiency, commonly expressed as specific fuel consumption (SFC), as demonstrated by Calder [105] as well as Plohr [103]. For the SENECA M1.8 airliner engine, Plohr investigated the SFC cost of keeping the jet subsonic on take-off in a preliminary, exploratory study, the results of which are shown in Figure 2.4. It is clear that the engine was designed with a focus on low LTO noise at the cost of cruise SFC.

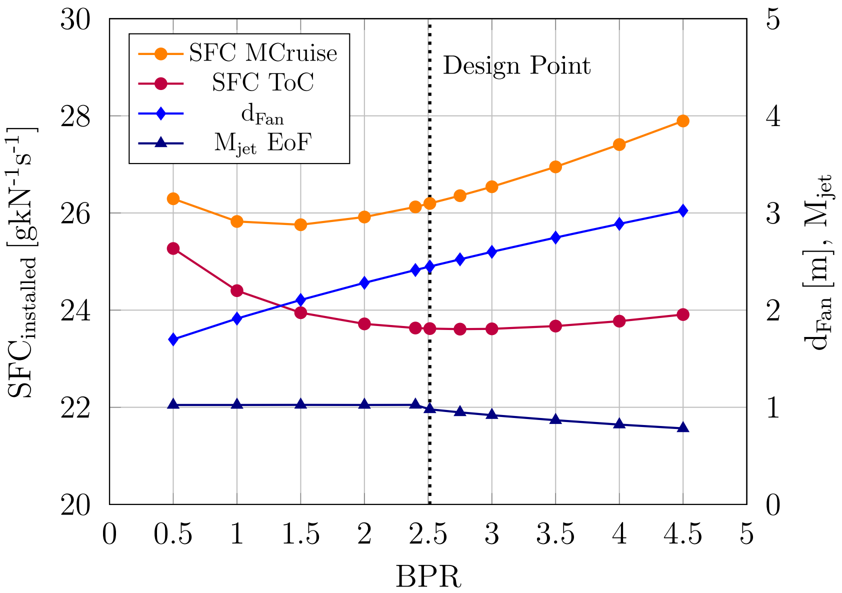

Figure 2.4: SFC at Top of Climb (ToC) and Mid Cruise (MCruise), fan diameter (D_{Fan}) and End of Field exhaust jet Mach number (M_{jet} EoF) as function of the design point BPR for the installed engine, as shown by Plohr [103]

Subsonic aircraft have the highest thrust requirement at take-off and their engines need to be sized and designed accordingly. Supersonic aircraft on the other hand have a high thrust demand in supersonic climb and cruise, with Top of Climb (ToC) being the most critical point with regards to turbine entry temperature due to the high altitude and thrust requirement. It also marks the beginning of the cruise, so it is the most common design point for SST engines, being also representative of the cruise operating conditions. The high thrust must be maintained for the entire cruise instead of short periods as is usual for subsonic aircraft. This puts high stress on the engine core which already led to issues on the *Concorde's* Olympus 593 engines [106]. The high thrust demand at ToC and in cruise means that there is a thrust surplus on take-off, meaning the engines can provide a much higher thrust than is necessary for a safe take-off. The thrust surplus allows an adjustment of take-off procedures to minimize engine noise. These adjustments, implemented as part of variable noise reduction systems (VNRS), are discussed in Section 6.1.

The high cruise speed entails a high thrust demand which can only be satisfied with very high jet velocity v_{jet} since the speed of the aircraft v_0 is already very high. To achieve supercruise, which is supersonic flight without reheat (i.e. the use of an afterburner), a nozzle pressure ratio $NPR > 2$ is required (≈ 1.9 to relax the jet to Mach 1.0). To provide this NPR and sufficient thrust in cruise, supersonic aircraft engines require a much higher fan pressure ratio (FPR) than those of subsonic aircraft.

To illustrate the specifics of the cycle design of civil supersonic engines, the SENECA M1.8 airliner engine is compared to two engines with similar thrust in Table 2.1: a 1980s civil subsonic design (V2500) and a military design capable of supercruise (F119). Even the old V2500 design has a much higher BPR and OPR than the supersonic aircraft engines. The BPR of the SENECA engine is higher than that of the F119 due to take-off noise considerations, but this results in a much higher cruise SFC due to the additional drag at supersonic speeds. As mentioned above, the lower BPR necessitates a higher FPR to provide sufficient thrust.

Engine	**Thrust**	**BPR**	**OPR**	**FPR**	$\mathbf{SFC_{cruise}}$	$\mathbf{M_{cruise}}$
F119[3] [107]	116 kN	0.30	26	≈4	17.28 $\text{gkN}^{-1}\text{s}^{-1}$	1.5
SENECA M1.8	133.4 kN	3.19	24.3	2.09	27.6 $\text{gkN}^{-1}\text{s}^{-1}$	1.8
V2530 [108, 109]	133.0 kN	4.60	32.8	1.62	16.3 $\text{gkN}^{-1}\text{s}^{-1}$	0.81

Table 2.1: Comparison between military, SST, and representative civil engine

The BPR and FPR of supersonic aircraft engines designed in multiple projects can be seen in Figure 2.5. There is a clear distinction between designs with a low specific thrust and a higher BPR (ASCENT designs [69, 59] and SENECA M1.8 airliner engine) that are optimized for low LTO noise and designs with a high specific thrust that have lower BPRs at higher M_{cruise}, optimized for cruise efficiency (STORMIE and other SENECA designs).

[3] Since military data is confidential, this data relies on expert estimates

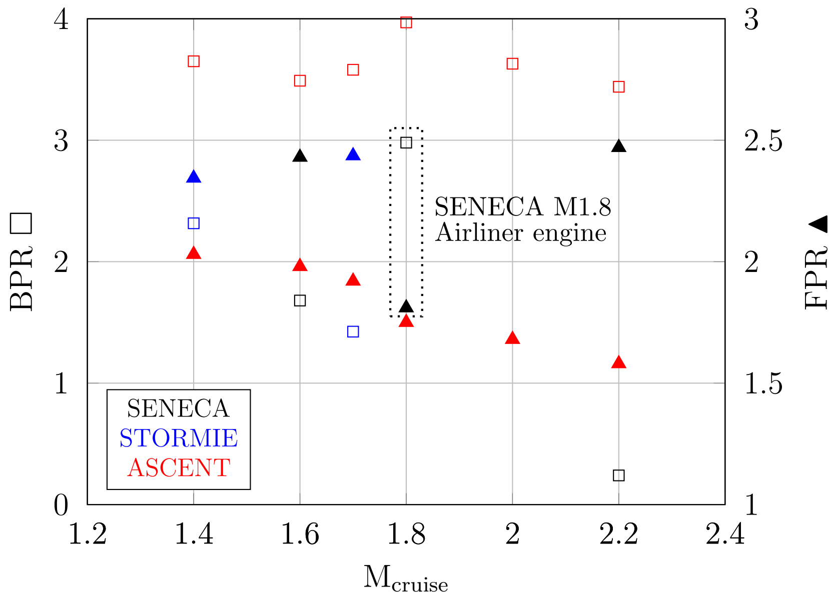

Figure 2.5: Bypass and fan pressure ratios of supersonic engine designs developed in the SENECA, STORMIE and ASCENT projects at the final mission Top of Climb operating point

Even for engine cycles with a low specific thrust, the BPR is much lower than for subsonic aircraft engines. Their FPRs are decreasing with higher M_{cruise} due to the stronger external inlet compression (see ensuing section).

For engines with a high specific thrust, the FPRs remain in a similar range with decreasing BPRs with increasing M_{cruise}. This keeps drag and thus SFC low, but poses challenges for LTO noise due to low BPRs generally leading to strong jet noise and high FPRs leading to strong fan noise.

The SENECA M1.8 airliner engine design is a consequence of a mismatch of aircraft, mission and engine design and impacts the engine noise which will be discussed in later chapters.

Component design

The restrictions and demands on a supersonic aircraft engine do not only affect its cycle, but also its component design. The core can remain essentially identical, but other components need to be designed very differently than those of subsonic aircraft engines.

Fan

To reach FPRs of 2.0 or more, high pressure fan designs differ from regular subsonic aircraft engine fans. If a single-stage fan is used, the rotor needs to be highly loaded and run at very high transonic speeds (example: [110]). Consequently, a single-stage rotor must be a high-solidity wide-chord design to control the loading and provide acceptable flow stability.

A two-stage fan design offers an alternative as the pressure increase can be distributed over its two stages, reducing the required fan speed and aerodynamic loading. The lower aerodynamic load allows more slender, low-solidity blade designs. Disadvantages of a two-stage fan design are its increased weight and complexity as well as larger dimensions when compared to a single-stage design. Since both fan speed and stage loading are significant for fan noise generation, this design choice has an impact on LTO noise and thus certification noise levels. This is elaborated on in Section 3.2.

The contour of the flow channel must be adopted to the high FPRs. In high power operation, the air gets compressed significantly, reducing the volume flow downstream. To stabilize the flow, a strongly converging channel geometry with a high meridional velocity density ratio (MVDR) is required. Without it, the DeHaller stability criterion would be violated. The DeHaller number as formulated by DeHaller [111] is defined as the ratio of absolute rotor outlet and inlet speeds and should be kept above 0.69. In low power settings, when air is not compressed in the same capacity, the contracting channel geometry acts as a nozzle, effectively throttling the flow. This leads to low mass flow through the first stage(s) and high loading and incidences on the front rotor and high negative incidences and flow detachment on the rear stator. Especially the high loading and incidence of the front rotor have a relevant impact on the fan noise which will be discussed in detail in Chapter 5. To combat the negative incidence in the rear stator, the flow channel can diverge between the (rear) rotor and stator.

Inlets

Inlets of SST work differently than those of subsonic aircraft. Since the inflow is supersonic, it needs to be slowed to a suitable Mach number with a shock system instead of a diffuser geometry. This dictates a long inlet with a variable spike or ramp geometry to control the shock system. The higher the flight Mach number, the higher the pressure increase inside the inlet. Therefore, the FPR generally decreases with increasing flight speed, as can be seen in Figure 2.5. Since the inlet frontal area is not variable, the inlet cannot deliver the perfect mass flow to the engine in all operating conditions. Any excess mass flow is expelled through spillage or bypass systems. Since spillage drag D_{spill} is significant at supersonic speed, the inlet needs to match the fan mass flow in cruise configuration to minimize drag penalties.

An effect of this strict sizing requirement which has been observed repeatedly is that the inlet cannot allow a sufficient airflow to the fan on take-off. To solve this problem, auxiliary openings and blow-in doors need to be included in the design. The inlet of *Concorde* had an auxiliary inlet for this purpose [85]. Modern SST inlet designs may also require an "opening" geometry [93, 112]. Auxiliary inlets introduce inflow distortion [113] which causes additional fan noise and have a significant impact on the radiation of fan noise into the free-field, as demonstrated by Stephens et al. [112]. There is another impact on fan noise: The application of liners in the inlet is one of the most effective means of fan noise mitigation and primarily depends on the area to which they can be applied and available nacelle depth (this will be discussed in detail in Section 3.2.4). Their effect is significantly reduced if fan noise can exit the engine through auxiliary openings before passing the entire liner segment.

Nozzle

SST engines can only produce an optimally expanded jet at varying supersonic speeds with a variable convergent-divergent nozzle: With a sufficient nozzle pressure ratio (NPR) and mass flow, the flow is choked and the nozzle exit area determines the exhaust (or jet) Mach number, pressure, and temperature. An optimally expanded jet is essential for a high propulsion efficiency in supersonic flight. Consequently, supersonic aircraft need a variable divergent section to their nozzle. For LTO operation, when the jet is supposed to be subsonic, the flow must remain unchoked to avoid high losses. The divergent section should thus be closed to have the same diameter as the throat.

2.2.2 Variable features

SST engines must cover a particularly large envelope: constant high thrust in cruise and very low thrust in idle. Covering this entire envelope can cause surging at low power settings and choking at high power settings. Variable features are used to mitigate these risks and keep the airflow through the fan and compressor section of the engine stable throughout its operating envelope. The most common variable features, which can be applied individually or in combination, are:

- Variable inlet guide vanes (VIGVs): a variable stator row is added in front of the fan, preconditioning the fan inflow by adding swirl in the desired direction. At low thrust settings with low mass flow, the vanes are closed to reduce the fan incidence and avoid surging. During transient operation, the surge margin can be maintained by a proactive use of VIGVs to regulate the mass flow. In high thrust operation, the vanes are fully open. Closing the VIGVs shifts the throttle line of a fan to lower FPRs and decreases the isentropic efficiency but increases the surge margin at the same time, as shown by Mallett et al. [114]. As an additional blade row, any sort of IGV causes increased fan noise, as stated by Stephens [82].

- Variable Throat Nozzle (VTN): A variable throat nozzle opens and closes the throat (narrowest part) of the nozzle, which regulates the mass flow and fan pressure ratio. Opening it reduces the FPR and increases mass flow. It can move the engine along a fan throttle line without changing the resulting thrust, allowing a fan operation on an ideal working line [115]. An additional advantage is that the jet velocity can be lowered in LTO operations by opening the nozzle; without a VTN, reaching a similarly low jet velocity would require a much bigger engine which results in a massively reduced cruise fuel efficiency as shown in the preceding sections.

Due to its capabilities in reducing jet noise, the VTN is favored for civil SST applications and was chosen for the design of the engine for the SENECA M1.8 airliner. Opening the nozzle affects the fan aerodynamics and has an impact on fan noise, as will be shown in later chapters. When fully opened, it increases the mass flow and with it the fan's surge margin, which is most critical at low thrust. This was demonstrated for subsonic aircraft engines by Guynn et al. [116], but is also applicable to supersonic aircraft engines. When closed, it decreases mass flow and avoids choking, which is most critical at high thrust. This can be seen in Figure 2.6 and means that a nozzle schedule depending on the operating point is necessary.

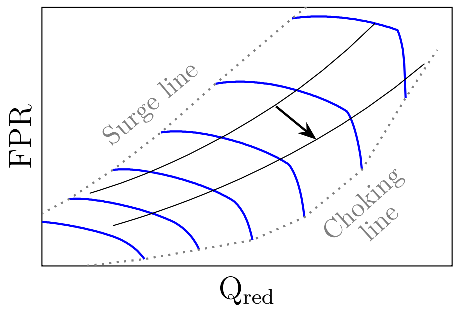

Figure 2.6: Generic SST fan map showing the shift of working lines when the nozzle throat is opened

Due to their movable parts, variable features are particularly likely to cause parasitic noise. Their wetted surfaces often do not form perfectly smooth topologies, so additional turbulence and thus noise is created. They also add complexity and weight to the engine, which is why they are only included in aircraft engine designs if necessary.

2.3 SENECA airliner design

The supersonic airliner concept most prominently investigated in this thesis is the Mach 1.8 airliner designed as part of project SENECA by Cranfield University [75]. The design is based on NASA's N+2 study [117] and was adapted using the in-house design tools at Cranfield University.

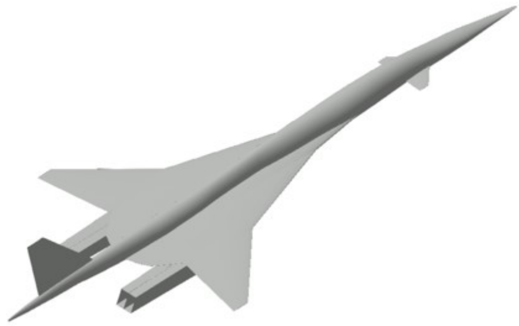

Figure 2.7: SENECA Mach 1.8 Airliner

It was originally designed to be a twin-jet design, but the resulting engine core dimensions were much larger than any existing cores, so a quad-jet design was chosen instead with more reasonable engine dimensions. The engine cycle was designed by DLR [103], but no components were designed in detail initially.

This airliner will be referred to as the SENECA M1.8 airliner throughout the rest of the thesis.

M_{cruise}	1.8	**Number of engines**	4
Pax	100	**Engine Architecture**	Two-stage fan, VTN
Range [NM]	4000	**T_{net} per engine [kN]**	133
MTOM [t]	144.3	**SFC [$gkN^{-1}s^{-1}$]**	17.1
Wing area [m^2]	427.3	**BPR**	3.19
Wing loading [kgm^{-2}]	337.65	**OPR**	21.9
Overall length [m]	71.6	**FPR**	1.94
Span [m]	35.0	**d_{Fan} [m]**	1.64

Table 2.2: Aircraft specifications and engine specifications at sea level, EoF, ISA+15 K at Mach 0.25

Chapter 3

Engine Noise of Supersonic Aircraft

For the LTO noise of subsonic aircraft, noise caused by the wing, flaps and especially the landing gear is becoming increasingly relevant, because their engines are becoming progressively less noisy due to rising bypass ratios, low-noise fan designs, and the effective use of liners. For civil supersonic aircraft on the other hand, it is expected that the propulsion system is the dominant noise source during take-off and landing, despite their tall landing gear. Studies on a supersonic business jet conducted by Nöding et al. [67] support this, as engine noise is found to be dominant over airframe noise by 15 dB. Even with a noise optimized engine, this assumption will most likely remain valid.

Consequently, a rigorous investigation of the engine noise of supersonic aircraft is needed. The goal of this chapter is to evaluate the most relevant aspects of SST engine noise. The associated noise generation mechanisms are explained as well as the approaches applied to model them in this thesis. Finally, fan and jet noise mitigation technologies are discussed.

Engine noise can be categorized into two categories: broadband noise, which is distributed over a large range of frequencies and tonal noise at discrete frequencies. Broadband noise (BBN) and tonal noise will be treated separately because they are caused by different noise generation mechanisms.

3.1 Component noise sources

Several components of turbomachinery cause noise in operation. The most obvious are the outward facing components, with the fan and turbine facing the engine inlet and exit plane and the jet, which is a noise source located entirely outside the engine. Fan, turbine and compressor cause noise typical for ducted rotor-stator stages: excitation of bladed rows by unsteady flow phenomena and in the case of transonic fans and compressors, buzzsaw noise as a result of the propagation of blade-attached shocks. In the context of fan noise, the noise generation mechanisms will be discussed in detail in the ensuing section.

The hot exhaust jet of an aircraft engine causes broadband noise along the jet plume, making it a distributed source. It will be covered in more detail later in this chapter.

The combustion chamber causes a low-frequency broadband noise with small tonal components, commonly described as combustion chamber rumble [118]. It will not be expanded on in this thesis. It is not expected to contribute significantly to the noise of supersonic aircraft engines since the low BPR makes jet noise the dominant low-frequency broadband noise source of the engine.

Other engine components which cause noise, but will not be elaborated on here, are mixer and nozzle. Proper designs should not cause excessive, parasitic noise and their noise generation is modelled either as part of the jet noise, or requires numerical prediction methods which are outside the scope of this thesis.

Fan and jet noise are usually considered as the most relevant sources. It is assumed that turbine and compressor noise are considered in their design and that they will not be dominant over fan and jet noise. Furthermore, both these noise sources experience significant shielding and scattering by propagating through a transonic fan or mixer and bypass jet respectively. The assumption that they would not be dominant noise sources in a real engine is thus plausible.

As mentioned in the previous chapter, variable geometry components like nozzle and intake can cause parasitic noise since their geometries are not smooth in all positions, creating small gaps and crevices instead. For investigations in this thesis, it is assumed that there is no parasitic noise in a relevant capacity, so it can be neglected.

3.2 Fan noise

While jet noise is strongly dependent to engine cycle design and hard to reduce on a component level, as will be discussed later in this chapter, fan design offers a larger choice of parameters. Some have a significant impact on fan noise, so optimization on a component level is much more viable. It will thus be the focus of this thesis. This section will cover the physical background of fan noise, which is relevant to its reduction, as well as the tools most suited to model it. Since the aircraft and engine investigated in this thesis are only developed on a concept level, there are no detailed 3D-designs available for any engine components. Consequently, the fan noise prediction must be realized on a pre-design level with little geometric and operational data available. Meier zu Ummeln [119] outlined the associated challenges, as the lack of fully developed geometries constraints on the methods which can be applied to fan noise predictions.

3.2.1 Noise generation mechanisms

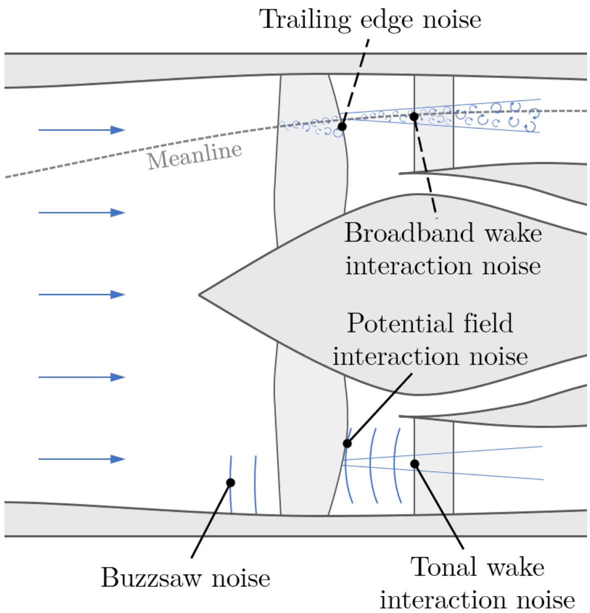

Figure 3.1: Main fan flow phenomena and noise source mechanisms

Fan noise can be separated into two categories: self noise and interaction noise. Self noise is caused by the blades or blade rows themselves, while interaction noise is caused by the interaction of a blade row with unsteady flow phenomena, commonly caused by another blade row. These categories will be explored separately, since their respective noise generation mechanisms are different in nature.

A sketch illustrating the fan noise sources covered in this section can be seen in Figure 3.1.

Self noise

- **Trailing edge noise** is a form of broadband self-noise, in which the turbulent pressure fluctuations in the boundary layer along a blade surface are scattered on the blade's sharp trailing edge [120]. It is driven by the strength of the turbulent pressure fluctuations and the flow velocity.

- **Buzzsaw noise:** For any transonic rotor, an outer section of any blade is supersonic, which causes a shock which is attached to the rotating blade. These shocks propagate both toward the neighboring blade within the row and upstream toward the inlet, where they form a saw-tooth shaped pressure signal [121, 122]. This signal is perceived as tonal buzzsaw noise when exiting the inlet. When ideal, identical blades and blade angles are assumed, only tones in the blade passing frequencies (BPFs) are emitted, but in real-life applications, buzzsaw noise is perceived as multiple pure tones [123]. This happens due to small variations in blade angles caused by manufacturing tolerances, so the shocks propagate at different angles and merge. For all fan noise studies in this thesis, non-ideal blades are assumed with random deviations of the blade angles of $\pm 0.4°$.

Interaction noise

Rotor-stator interaction noise is the most prominent group of noise sources in fan noise and has been studied extensively. It is caused by the interaction of unsteady flow phenomena caused by one blade row with another blade row [124]. The generated unsteady lift on the blade surface is a noise source which can be categorized as a dipole source [43]. The unsteady disturbances considered in this thesis are the potential field and wakes of blades.

- **Potential field interaction noise** is caused by the potential pressure field of blades in a flow propagating up- and downstream and interacting with the respective upstream trailing edges or downstream leading edges. Potential field interaction noise is tonal and is excited in the azimuthal mode order m according to Tyler and Sofrin [125], with $m = nB - kV$ (B being the number of rotor blades, V the number of stator vanes and n, k being indices).

- **Wake interaction noise:** The flow around bodies such as blades forms boundary layers on their surfaces which result in a wake. The interaction of these wakes with downstream leading edges causes both broadband and tonal noise. The tonal noise is caused by the resulting periodic unsteady lift, similar to potential field interaction noise and is excited in Tyler-Sofrin modes as well. Broadband wake interaction noise is caused by the interaction of the leading edges with wake turbulence which leads to unsteady lift of a stochastic nature [126]. Wakes can be characterized by the wake's area A_{wake} and turbulent kinetic energy TKE.

The dimensionless wake area A_{wake} is defined as the wake velocity deficit Δw integrated over the blade spacing s, normalized with the mean streamwise flow velocity $\overline{w}$ and the blade spacing (see Figure 3.2):

$$A_{\text{wake}} \equiv \int_0^s \frac{\Delta w(y)}{\overline{w}} \frac{dy}{s} \tag{3.1}$$

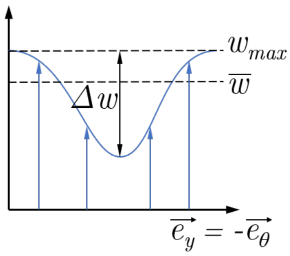

Figure 3.2: Sketch of a wake, the mean flow $\overline{w}$ and deficit velocity Δw

Turbulent kinetic energy TKE is defined as:

$$TKE \equiv \frac{1}{2}\left(\overline{(u')^2} + \overline{(v')^2} + \overline{(w')^2}\right) \tag{3.2}$$

With u', v' and w' being the turbulent velocity components of the flow in the wakes. TKE is determined empirically in the fan noise prediction tool *PropNoise*, which will now be described in detail.

3.2.2 Modeling

There are many approaches to fan noise modeling, as has been explained in Chapter 1. The simplified, comprehensive, analytical approach taken in calculating the fan noise in this thesis, as described by Moreau [45], will be explained in more detail. It is implemented as part of the DLR in-house tool *PropNoise* and allows for the aerodynamic, thermodynamic and aeroacoustic simulation of a fan. The noise generation models are in principle based on Lighthill's acoustic analogy [127] and can be considered an evolution of the work of Ffowcs Williams and Hawkings [128] as well as Goldstein [129]. *PropNoise* has previously been compared to Kontos' empirical fan noise model and found to reproduce trends very well [130]. Since the aerodynamics and thermodynamics of the fan are calculated for any given operating point, the tool can predict the aerodynamic and consequently the acoustic characteristics of a fan off its working line quite well.

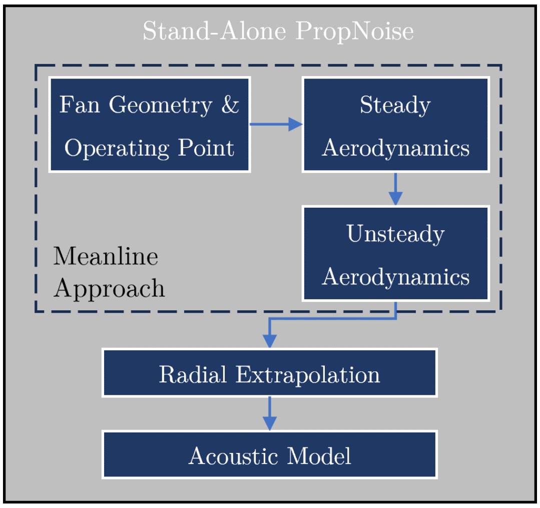

Figure 3.3: Schematic showing the process fan noise calculation in the *PropNoise* stand-alone mode

Since only rudimentary geometry data is available in the concept design stage of the fan, a meanline approach is taken. This allows the aeroacoustic evaluation of a fan design based on very limited geometry and operational data using the *PropNoise* stand-alone mode. Its general process is shown in Figure 3.3: First, analytical models, supported by empirical correlations are used to calculate the steady aerodynamics of each row. Then, the unsteady flow phenomena which are relevant to noise generation are modelled: the potential field and wakes of the blade rows, before the results get extrapolated to the entire channel height. Aerodynamic, thermodynamic and performance parameters are also calculated and provided.

For the noise prediction, strip theory is applied (as described in Chapter 1) to simplify the 3D problem into a quasi-2D problem with the strips being superposed later. From the unsteady flow phenomena, the excitation, i.e. the fluctuation of the pressure distribution on the blade surfaces is calculated. All resulting noise sources are calculated separately. The following tonal sources relevant for turbofans can be modelled by *PropNoise*:

- Tonal wake interaction noise
- Potential field interaction noise
- Buzzsaw noise

as well as the following broadband sources:

- Broadband wake interaction noise
- Trailing edge self-noise

The propagation of these noise sources in modes inside the duct and into the free-field is performed purely analytically.

For the prediction of buzzsaw noise, an analytical model describing the pressure signature of the shock system upstream of a transonic rotor has been developed by Moreau [131]. It models both shock generation and propagation. The generation and propagation of the shocks are modelled in the spatial domain rather than the frequency domain since the shocks are treated as a phenomenon of gas dynamics rather than a purely acoustic one. The model predicts the pressure jump and azimuthal position of each rotor induced shock at a given axial position.

Some significant assumptions are made in this model:

- Strip theory is applied, so strips are calculated independently as a 2D problem and shocks propagate along the unwrapped stream surface, they cannot propagate away from the engine axis
- The background flow is assumed to be circumferentially uniform, so scattering due to interaction with inflow distortion is not considered
- The inflow is purely axial

Some simplifications are made for the prediction of all noise sources:

- The blades are modelled as thin plates with dipoles distributed on their surfaces
- The inlet is assumed to be a circular duct
- A simplified engine geometry without core or bifurcation is assumed
- Transmission effects of noise passing through blade rows are ignored. The scattering of acoustic energies into other modes, and transonic rotor shielding would be the most relevant effects.
- The inflow is assumed to be perfectly uniform in axial direction
- The variable intake is closed in LTO operation, all upstream acoustic radiation happens through the inlet plane

3.2.3 Additional sources for multi-stage designs

For a multi-stage fan design, which is common for high FPR fans, there are more rows and thus more noise sources to be expected. For clarity, this will be discussed for a two-stage fan design since it is the simplest multi-stage design. There is wake and potential field interaction between all neighboring rows, buzzsaw noise is emitted by both rotors if they are running in a transonic regime and all rows produce trailing edge noise.

However, some noise sources can be neglected: the buzzsaw noise of the second stage rotor (R2) is only radiated forward, passing through two rows. While the stator row transmission effects are likely limited to scattering and reflection, the front rotor row (R1) shields the second stage buzzsaw noise: R1 is also transonic but has a higher blade tip Mach number, since both rotors are running at the same speed and have approximately the same radius, but the inflow temperature of R2 is higher, leading to a higher speed of sound. This means that a larger span of the R1 blades than R2 blades are covered by shocks. Thus, no acoustic energy can be transmitted through the outer part of the duct where the R2 shocks are located. Consequently, R2 buzzsaw noise can be considered inherently shielded.

For multi-stage compressors, only interaction noise between neighboring rows is relevant. While there could theoretically be interaction noise between non-neighboring rows, it can be neglected for the following reasons:

- Both potential field and wakes are disrupted when propagating through a blade row, getting "chopped up" and scattered, which leads to a weaker excitation
- Because the rotors are on the same shaft, there is no periodic interaction between neighboring rotors, so tonal interaction can only occur between neighboring rows or after transmission through two additional rows.
- The unsteady flow phenomena dissipate with propagation, as was demonstrated by Jaron [132] with potential fields showing a much faster decay than wakes, so the excitation will always be much stronger on a neighboring row than on non-neighboring rows. Consequently, the interaction noise between neighboring rows will be assumed to be dominant over that between non-neighboring rows.

Since the potential field decays much faster with axial distance than wakes, it is easy to choose the axial distances between rows in such a way that potential interaction noise is never dominant over wake interaction noise. This is a design goal for all civil fan designs and should only be broken when external factors severely limit the design space. For all fan designs investigated in this thesis, potential field interaction noise can be neglected.

This makes the relevant noise sources:

Noise source	**Exciting and excited components**
Tonal Wake Interaction	R1 → S1, S1 → R2, R2 → S2
Broadband Wake Interaction	R1 → S1, S1 → R2, R2 → S2
Buzzsaw Noise	R1
Trailing Edge Noise	R1, S1, R2, S2

Table 3.1: Relevant fan noise sources for a two-stage fan considered in this thesis, R denotes a rotor and S a stator

3.2.4 Fan noise reduction methods

Several methods exist to mitigate fan noise. It can either be reduced at source through both low-noise design and operation or during propagation through the duct by exploiting attenuation effects.

Consequently, they are relevant to design a low-noise fan and to accurately predict the LTO engine noise. The most relevant aspects to fan noise reduction for a concept stage will be covered in this section.

Cut-off design

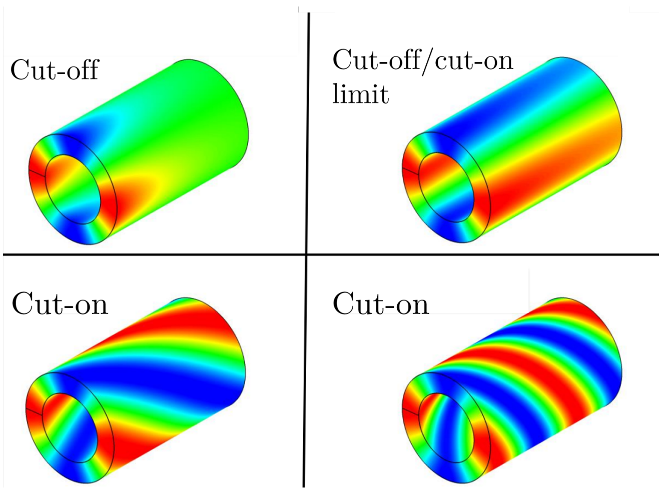

Figure 3.4: Example of propagation of acoustic mode in circular duct without mean flow to illustrate cut-off effect. Adapted from Guerin [133].

Certain azimuthal mode orders cannot propagate throughout the duct and will decay exponentially - these are called cut-off modes. An example of how a mode propagates in a circular duct depending on whether it is cut-off or cut-on can be seen in Figure 3.4. Since interaction modes are excited as Tyler-Sofrin modes with a mode order of $m = nB - kV$, it is in some cases possible to move the majority of the energy of a tonal interaction source into cut-off. This can be achieved with an advantageous selection of blade numbers, typically with much higher stator than rotor blade counts. The cut-off factor α_{mn} which is used as the cut-off criterion in *PropNoise* is defined as:

$$\alpha_{mn} = \sqrt{1 - (1 - M_x^2)\left(\frac{\sigma_{mn}}{kR}\right)^2} \tag{3.3}$$

Where R is the duct radius, k the wave number, M_x the axial Mach number and σ_{mn} the non-dimensional transverse wave number. When the imaginary part of α_{mn} does not equal 0, the mode is cut-off. This means the cut-off criterion can be simplified to:

$$\frac{\sigma_{mn}}{kR} > (1 - M_x^2) \tag{3.4}$$

Azimuthal modes m go cut-on for n=0 first, making it the critical radial mode. For this radial mode, the approximation $\sigma_{m,0} \approx |m| + 0.8|m|^{1/3}$ can be used to evaluate whether a mode will be cut-on.

A more simplified empirical rule to achieve a cut-off design is provided by Bräunling [102]: $V/B \geq 1.1 \cdot (1 + v/a) \cdot h$ with v being the tangential rotor speed, a being the speed of sound and h being the flow channel height.

Blade loading and incidence control

The loading of blades has a direct impact on the wakes they cause. Higher loading leads to a higher negative pressure gradient on the suction side and thus a thickening of the boundary layer. Downstream of the blades, the boundary layers of both suction and pressure side then form wakes with a larger wake area and higher turbulence, as demonstrated by Ravindranath and Lakshminarayana [134]. This increases broadband wake interaction noise significantly. The higher loading increases the swirl in the flow, leading to more curved wakes along the channel height. Consequently, a phase shift in tonal interaction noise along the blade span emerges which cause radial inferences. This results in reduced tonal wake interaction noise. These phenomena have been comprehensively demonstrated by Ginder [135], Moreau [136] and Jaron [132] among others. Depending on the dominant noise source, it can be acoustically beneficial to increase or decrease blade loading in both design and operation. However, flow stability is imperative, so the ability to increase blade loading is limited.

Incidence is generally linked to blade loading. Large incidences also lead to a thicker boundary layer on the suction side which again causes larger, more turbulent wakes. In extreme cases, the flow can detach, amplifying this effect. This increases broadband interaction noise as well as trailing edge noise. Operating the fan at minimum incidence angles reduces the its broadband noise emissions.

Relative Mach number

Supersonic fan tip speeds cause buzzsaw noise which is usually the dominant forward-radiating engine noise source. Keeping the entire fan subsonic effectively eliminates this dominant, tonal noise source. Supersonic tip Mach numbers $M_{\text{tip,rel}}$ have two conflicting effects on buzzsaw noise: with increasing $M_{\text{tip,rel}}$ a larger section of the rotor blade span has a shock attached, but the reduced shock strength and shallower propagation angle reduce the shock strength at the engine inlet plane. Aerodynamically shocks can be necessary as they help generate the rotor row's pressure increase, allowing for a higher FPR without increasing blade loading, so higher fan speeds stabilize the flow. The corresponding acoustic trade-off was investigated by Moreau [136]: lower rotor speeds reduce buzzsaw noise but the increased loading leads to an increase in broadband self- and interaction noise and a reduction in tonal interaction noise. With this information in mind, it is a clear design goal to produce a fan with a low tip Mach number while maintaining stability and manageable loading for aeroacoustic optimization. In operation, low power settings can keep the fan subsonic and eliminate buzzsaw noise.

Other tonal and broadband noise sources scale with the inflow Mach number into the excited component to the fifth to sixth power[1], as found by Morfey [137] and Glegg [138]. A reduction in the relative Mach number consequently reduces fan noise. This can only be achieved by limiting mass flow and fan speed, i.e. the power setting, leading to the obvious conclusion that lower power settings reduce fan noise.

Acoustic liner

Acoustic liners play a significant role in attenuating fan noise. Single degree of freedom liners are designed to dampen discrete frequencies, which is conventionally achieved in two ways: When an open cavity is used as a resonator ($\lambda/4$ liner), the sound waves are reflected at the back of the cavity, creating destructive interference with the original sound wave at the resonance frequencies [139]. This design is not commonly used to attenuate fan noise because of the increased drag and potential of cavity noise associated with an open cavity.

[1] Depending on whether the source is compact

A Helmholtz resonance design liner is a cavity with three dimensions significantly smaller than the relevant sound wave length λ, covered with a hole sheet. When it is excited at its eigenfrequency acoustic energy dissipates through friction at the thermoviscous boundary layer at the hole walls when the sound waves move through the holes [140]. Conventional single-degree-of-freedom (SDOF) liners only attenuate sound significantly in the vicinity of their design resonance frequency. This makes liners particularly effective in dampening tonal noise and much less effective in dampening broadband noise. Multi degree of freedom liners use the principles of the Helmholtz resonance and combine different resonators [141]. They have a broader effective bandwidth but are more complex and require more space and been in use since at least 1992 [142].

For current subsonic aircraft engines liners have been proven effective in reducing fan noise. Their impact can be expected to be much more significant for supersonic aircraft engines: the geometry with a long inlet and bypass allows for a large surface to which liners can be applied, especially in relation to the small diameter. The small diameter also dictates higher rotational speeds, causing higher frequency tones which can be attenuated more easily even with shallow liners, since the eigenfrequencies of acoustic liners with shallow cavities are higher.

However, designing a liner is outside the scope of this thesis. This is why a simplified approach is chosen which assumes a perfectly tuned liner with the following properties:

- A flat rate noise attenuation over all frequencies depending on whether they are tonal or broadband sources.
- The liner attenuation scales linearly with liner length
- Since discrete frequencies can be dampened with liners much more efficiently, the liners are assumed to be capable of attenuating broadband sources by -10 dB per l/d (where l is the liner length and d is the duct diameter) and tonal sources by -20 dB per l/d
- The liner is designed for take-off and will work with 100% effectiveness in any take-off setting; for the lower fan speeds on approach, the effectiveness is 70% (i.e. -14 dB or -7 dB per l/d)

The attenuation across all frequencies as opposed to attenuation in a small frequency range entails the assumption that when dominant tones are dampened, no previously non-dominant tone emerges as dominant. The estimated attenuation is loosely based on papers by Rice [143, 144, 145, 146] who studied the large-scale impact of liners. To verify that the assumed attenuation is in a realistic range, it is compared to theoretical optimum attenuation, a proven liner model and in-flight measurements:

For a duct with infinite depth liners, no background flow and no reflection, Cremer [147] found the theoretical maximum attenuation of single mode plane waves to be -19 dB per l/h for low frequencies and -3.5 dB $\cdot\lambda$/h (with λ being the wave length) per l/h. While Unruh [148] studied the impact of finite liner tuning lengths on plane waves of a singular mode in ducts, he found a peak attenuation of ≈22 dB per l/h at $f \cdot h/c = 0.4$ (f being the frequency and c the speed of sound). While the exact $f \cdot h/c$ depends on fan design and operation, 0.4 can be considered in a realistic range based on preliminary studies. Since plane waves are normal to the lined surface, they are attenuated less than actual engine noise, whose modes will graze the surface at an angle below 90°. Hence, this can be seen as a very conservative attenuation estimation of fan noise when liners of ideal tuning lengths are assumed. Since a real engine does not have ideal liners, it is reasonable to assume that the assumed attenuation (-20/-10 dB per l/d) is optimistic but realistic when compared to theoretical maxima.

A preliminary single point study using *PropNoise* on the SENECA M1.8 airliner fan noise with an extended Helmholtz resonator model [149] indicates that the attenuation assumed here is a rough match with peak attenuation of Helmholtz resonators. As opposed to the results of Cremer and Unruh, this includes real acoustic modes and background flow. When operating point and thus dominant BPFs matched the liner design, peak tone SPLs were attenuated by 30.6 dB through the inlet (20.4 dB per l/d) and by 57 dB (9.5 dB per l/d) through the bypass. Peak broadband noise SPLs were attenuated by 12.8 dB (8.53 dB per l/d) through the inlet and 15.8 dB (2.63 dB per l/d) through the bypass. This indicates that the assumed attenuation of upstream radiating noise is generally realistic while the assumed attenuation of downstream radiated noise might be too optimistic.

Wong et al. [150] tested an advanced liner design using the LEAP-1B engine on a Boeing *737-MAX7* with an approximated l/d ≈ 0.25. The tonal sound power (PWL) of the forward arc was attenuated by a maximum of 12 dB during take-off and 4 dB during approach. Broadband sound power attenuation was at 2-4 dB depending on frequency and radiation angle with better attenuation for approach than take-off. While the LEAP-1B is very different from a supersonic aircraft engine, the liners function in the same manner and their performance can be considered representative.

These comparisons show that the assumed attenuation is optimistic but ultimately in a realistic range.

The impact of these assumptions will be explored in Chapter 6.

3.3 Jet Noise

According to Lighthill [127], installed jet noise power level scales approximately with the eighth power of jet velocity. Due to the small bypass ratio and associated high velocity, the jet is a strong noise source in high power settings like at take-off. Since it is generated almost entirely outside the engine, it is essentially impossible to attenuate which makes it the dominant noise source in low BPR engines over fan noise [151]. This means reducing jet noise at source is essential for SST engine noise reduction.

3.3.1 Noise generation mechanisms

Jet noise is created through two major mechanisms: mixing noise and shock noise. Mixing noise in created when the fast and hot flow encounters slower flow and turbulent structures develop along the resulting shear layer. Smaller structures causing high frequency noise are located closer to the nozzle while larger structures, causing low frequency noise are observed further downstream. Mixing noise is caused between the jet and the ambient air but also between core jet and bypass jet for any engine with a bypass flow. Shock noise is only created when the jet is supersonic. If the pressure in the jet is higher than ambient pressure, the resulting expansion waves will be reflected on the shear layer and form shock cells where they converge. The turbulent mixing structures in the shear layer interact with the shock cells downstream and cause shock noise. Both kinds of jet noise are generally broadband noise sources, but shock noise can cause narrow-band screech.

3.3.2 Jet noise modeling

Jet noise prediction is its own field in aeroacoustics research. There are multiple methods to predict jet noise, and low fidelity semi-empirical models and high-fidelity numerical methods are the most popular. Due to the stochastic nature of the turbulent structures responsible for mixing noise, purely analytical models are not particularly accurate for this application.

The model chosen to calculate the jet noise in the context of this thesis is the Stone model of 1983 [152]. This semi-empirical model assumes two coaxial jets: the core and bypass jet. Since the engines studied in this thesis have an internal mixer and a plug exhaust, but no detailed geometry is designed, the assumption is made that mixing is 100% complete at the nozzle exit plane. This means a perfectly mixed single stream is assumed for jet noise prediction and no noise results from the internal mixing process. By omitting the bypass flow, the model can easily be adapted to work on a single jet. It is based on physics-informed equations which were fitted to empirical experimental data. Jet mixing noise is predicted based on experimental data and empirical correlation of Olsen and Friedman [153] of the interaction of outer stream and inner jet. The effect of a primary nozzle plug is included in the prediction, but was not validated by Stone until 1999 [154]. Stone also developed a jet noise model for supersonic business jets [155]. The engine design considered in this thesis is not geometrically detailed enough to benefit from the advancements in the model. It was also deemed closer in design to the reference engines of the 1983 model.

The modeling of shock noise for a supersonic jet is based on an extension of the method of Harper-Bourne and Fisher [156]. The predictions cover 180° angular range and assume an axisymmetric distribution of jet both mixing and shock noise, effectively providing a full sphere. Validation with static data showed good agreement in sound pressure level and there are no inherent limitations to the model.

To increase the reliability of jet noise prediction, the SENECA project consortium has conducted a successful jet noise prediction benchmark test using different versions of Stone's semi-empirical jet noise prediction model [157]. That activity is complemented by small-scale jet noise tests conducted at the NLR [158], as well as numerical simulations on a realistic nozzle configuration [159]. When compared to the results of these studies for the single, fully mixed stream which is assumed in the SENECA M1.8 airliner applications, the Stone models developed in 2009 (experimental and numerical) and 1983 (numerical) showed good agreement and can thus be considered reliable.

3.3.3 Jet noise reduction technology

Since jet noise can be separated into shock and mixing noise, it is reasonable to consider both individually.

Shock noise can be fully eliminated by avoiding supersonic jet velocities. At subsonic speeds, no shock cells form and no jet shock noise is excited. Due to the high intensity of shock noise, this must be a design goal for any aircraft that needs to comply with noise restrictions. For the SENECA M1.8 airliner, this design restriction was respected, as explained in Chapter 2 (see Figure 2.4). This means shock noise will not be present in the considered design and will not be elaborated on.

Mixing noise is driven by jet temperature as well as the velocity gradient in the shear layers between the jet and the ambient air or secondary jet, in the case of coaxial jets. This was proven in many studies, for example by Cocking [160] and Powell [161] respectively. Since no workable concept for cooling the exhaust jet exists yet, it is depended on the engine power setting: lower power reduces the jet velocity and temperature, both of which are favorable for low jet mixing noise.

There are various means of reducing the velocity gradient in the shear layers. Reducing the jet velocity is highly effective, which can be achieved in two ways:

- Operationally, by applying as little thrust as possible. How to reduce thrust requirements in SST operation is expanded on in Section 6.1.
- In design, by maximizing the mass flow during take-off and achieving the required thrust at lower jet velocities. This can be achieved by maximizing BPR, potentially using a variable cycle design, or by using a variable nozzle as described in Section 2.2.2.

Mixing noise can also be reduced by manipulating the mixing process. Internal mixers or nozzles with lobes or tabs, such as chevrons, generate axial vorticity and enhance mixing. This breaks down large turbulent structures into smaller ones which speeds up the jet core decay, but also transfers energy from lower to higher frequencies. This can negatively impact the perception of the noise, which makes the design of aeroacoustically optimized mixers and mixer nozzles very delicate, as demonstrated by Mengle et al. [162]. A successful design has been shown to achieve a significant reduction in effective perceived noise by Saiyed et al. [163].

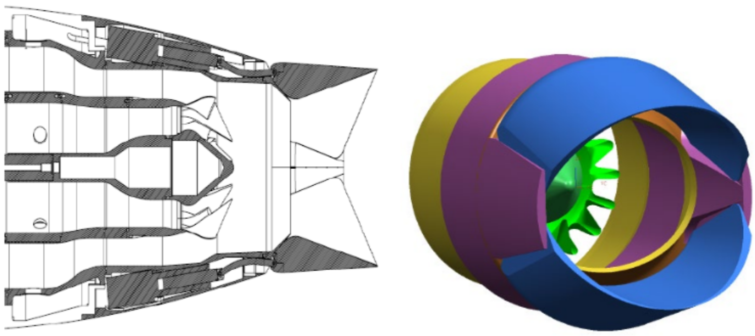

Figure 3.5: Example of Mixer-Ejector Nozzle Design as published by Sokhey et al. [61]

Mixer-ejectors are another measure which can reduce jet noise. The concept of ejectors has existed for a long time with most applications being in hydraulic pumps. Ejectors are shrouds around an open jet with a significant clearance (see Figure 3.5), allowing outside fluid from either a secondary jet or an ambient fluid, in this case air, to be pulled into the jet. The turbulent mixing along the outer shear layer of the primary jet causes a suction force on the outside air. Ambient air being pulled in increases the jet mass flow and reduces jet velocity compared to the primary jet. Combining the ejector with a mixer to enhance the mixing of outer and inner flow makes it a mixer-ejector nozzle. The resulting mixing and reduction of jet velocity promises a stark decrease in jet noise, but the implementation without causing parasitic noise is not easy, as shown by Morgenstern et al. [61]. Zaman et al. [164] demonstrated that achieving even mixing is difficult; pockets of high velocity jet remain in many cases which negate the benefits of the mixed flow. Furthermore, ejectors can produce parasitic tonal noise through flow resonance, which should be avoided within the entire operating range. They also add complexity and cause a significant increase in friction drag and weight. The concept of mixer-ejectors is still at a low technology readiness level and has not been conclusively proven viable for SST applications. Since a possible entry into service around 2030 is not realistic, it will not be considered further in this thesis.

Eccentric jet positioning in co-axial jets is explored as another option to reduce jet noise by eliminating strong Mach wave radiation, as demonstrated by Papamoschou [104]. This requires a more detailed nozzle design than is available in this work, so it will not be investigated any further.

Chapter 4

From Engine Noise to Aircraft Certification Noise

Like many other vehicles, aircraft need to be certified to be permitted to operate in civil applications. Due to the international nature of air travel, these certification rules are dictated by ICAO as the international regulatory agency. Noise certification is a major step in certification and will be discussed in detail here.

As explained in the Introduction (Chapter 1), there are no noise certification regulations in place for SST as of 2025. However, starting in the 2010s, there have been discussions about establishing rules equivalent to those of subsonic aircraft. It is suggested by the International Council for Clean Transportation that the current noise limits for subsonic aircraft will be codified as limits for SST [165]. For this reason, the existing subsonic aircraft regulations will be discussed in the ensuing sections.

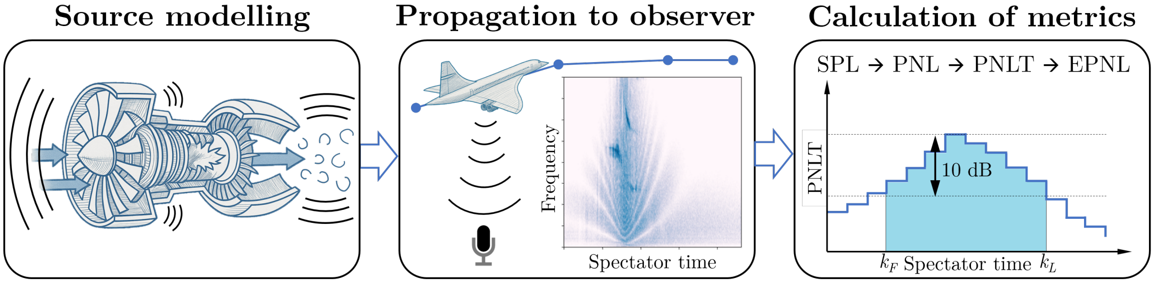

Figure 4.1: Schematic showing the process of certification noise level prediction

Since optimizing the engine components of SST aircraft for minimal certification noise levels is a goal of this thesis, their specific impact must be evaluated. To provide this information a reliable process of predicting certification noise levels from the engine source noise, which was covered in the previous chapter, must exist. The general process is depicted in Figure 4.1. Both the modeling of noise propagation to the observer and the calculation of certification metrics will be explained in this chapter.

4.1 Noise certification regulations

The rules regulating noise certification of new subsonic aircraft are listed in ICAO Annex 16 - Volume I [23]. Both the procedures used to determine an aircraft's certification noise levels and their limits are described there.

The metric used to determine certification noise levels are Effective Perceived Noise Levels (EPNL). It is supposed to represent the subjective perception of noise instead of purely physical attributes such as sound power or pressure levels. To demonstrate the impact of acoustic phenomena on EPNL, a cursory explanation of its calculation will be given here.

4.1.1 Calculation of EPNL

Following the procedure detailed in ICAO Annex 16 - Volume I [23], a microphone is used to record the sound pressure levels (SPL) during the flyby of the certifiable aircraft. Measurements are to be taken every 0.5 s and the frequency spectrum is to be simplified to third-octave bands (TOBs).

A frequency weighing for each time step j is performed because the human perception of noise is strongly linked to loudness [166, 167], which is frequency-dependent. For this purpose, first a perceived noisiness n is determined for each TOB. This step uses the Noy scale, developed by Kryter [168] which is based on loudness equivalence. A mathematical formulation of the Noy lookup-tables exists [169], but it will not be elaborated on here for the sake of brevity. As the next step, the total perceived noisiness N of for each j is calculated:

$$N = 0.85 \cdot n_{\text{max}} + 0.15 \cdot n_{\text{sum}} \tag{4.1}$$

Here, n_{max} is the maximum noisiness across all TOBs and n_{sum} the sum of all noisinesses n of the TOBs. N is thus no longer frequency dependent. It is then converted to a Perceived Noise Level (PNL):

$$PNL = 40 + 10 \cdot log_2 N \tag{4.2}$$

Kryter [168] explains that PNL represents the subjective impression of a complex sound as opposed to pure loudness-equivalence, which can only be applied to pure tones or bands of sounds. It was developed specifically to evaluate aircraft noise and has been used for this purpose since 1959.

Humans tend to react to tonal noise more negatively than to broadband noise [170, 171], so a tone correction is performed as well: tonal properties in the recorded spectrum are penalized to obtain PNLT (tone-corrected PNL). The tone correction is based on the "slopes" of SPLs between neighboring TOBs. If they eclipse a critical value, a penalty is determined and applied. The precise procedure will not be described for the sake of brevity.

Finally, the duration of the noise recorded during the flyby is taken into consideration, since duration also impacts the human perception of noise [172]. From the maximum PNLT (PNLTM) value in the time series, the so-called 10 dB-down time T can be determined between j_F and j_L. j_F is the first point in the time series for which $PNLT(j_F) > PNLTM - 10\,dB$ is true. j_L is either the last point after j_F, for which $PNLT(j_L) > PNLTM - 10\,dB$ is true, or the ensuing point (i.e. the first point for which $PNLT(j_L) < PNLTM - 10\,dB$ is true), depending on which is closer to $PNLTM - 10\,dB$. From that, EPNL are calculated as:

$$EPNL = 10log_{10}\left[\frac{1}{T}\sum_{j_F}^{j_L} 10^{\frac{PNLT(j)}{10}}\right] \tag{4.3}$$

As a consequence, a short, sharp peak yields a shorter effective duration and thus lower EPNLs.

To summarize, the following parameters have a significant impact on EPNLs:

- SPL received at the microphone position
- Frequency distribution of the acoustic spectrum
- Presence of tones in the acoustic spectrum
- Effective duration of the noise

4.1.2 Measurement setup

During the take-off or landing, SPL are recorded in three distinct reference noise measurements points, one on landing and two on take-off with all microphones installed 4 ft (1.2 m) above the ground. As can be seen in Figure 4.2, the Approach certification point

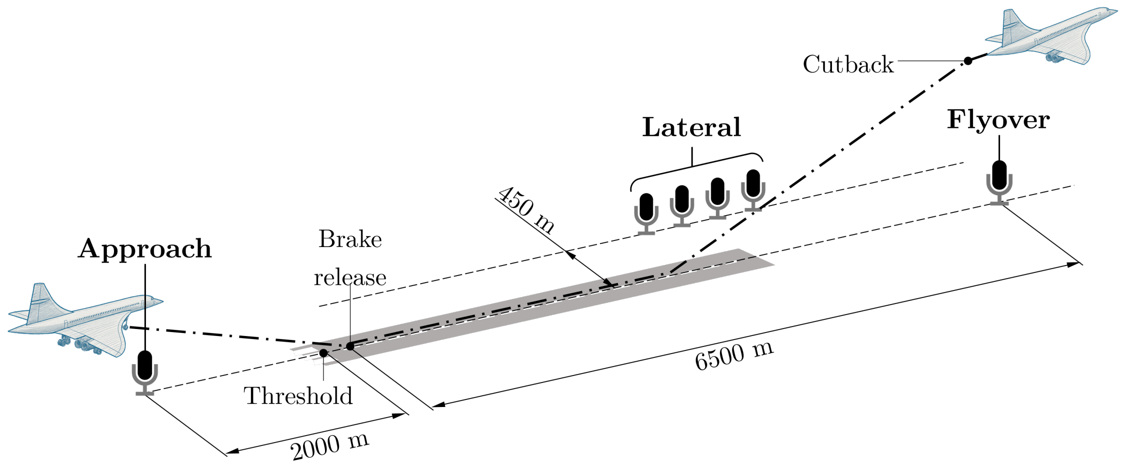

Figure 4.2: Certification points on take-off and landing according to ICAO with relevant operational points

is located on the centerline, 2000 m downwind of the runway threshold. Since the certification regulations specify a 3° glide slope approach, the altitude of the aircraft at that point is fixed at $h = 120\,m$.

On take-off, there are two certification points. The Flyover certification point is located on the centerline, 6500 m from break release. The Lateral certification point is defined as the point on a line parallel to the runway on which the highest PNLT value is recorded. It is 450 m removed laterally from the centerline.

There are restrictions to the trajectories flown for certification:

- Both landing and take-off are to be flown along the runway centerline, reducing the problem from a 3D trajectory to a 2D profile.
- Minimum climb: during the entire take-off, a minimum climb gradient of 4% ($\approx$ 2.3°) must be maintained.
- Minimum cutback altitude: for any operation, including certification, a minimum altitude must be reached before a manual cutback can be performed. The minimum altitude is 300 m for 2 engine aircraft, 260 m for 3 engine aircraft, 210 m for 4 engine aircraft.
- Maximum speed: Flying in excess of 250 kts is not permitted below 10,000 ft.
- No change to the engine setting and aircraft configuration is allowed below the obstacle avoidance height of 35 ft.

- Spool rate: to avoid discomfort or even injuries to passengers, the maximum spool rate during thrust reductions will be 4% n_{rel} per second. This limit is not set in regulations but was chosen ensure only realistic profiles would be considered for certification.
- No change to the engine setting and aircraft configuration is permitted during the 10 dB-down time.

Since the last point is not relevant to safety but severely limits the use of VNRS and may be subject to change for this reason, it will be ignored in the studies presented in this thesis. This means that changes to the aircraft configuration and engine settings can be made at any time in order to minimize take-off certification noise.

In practice, the flybys are usually conducted at constant thrust, altitude and speed equivalent to the actual take-off or landing to simplify the process. This practice will not be investigated in this thesis.

4.1.3 Evolution of certification limits

The limits for noise certification of transport aircraft first became applicable with the so-called *Chapter 2*, or *Stage 1* in 1972. The procedure to determine certification noise levels has been unchanged, but there has been a continuous reduction of permitted levels ever since: *Chapter 3* (or *Stage 2*) followed in 1977, setting calculable limits for the individual measurement points and their cumulative noise levels. It is still used as a reference today. The current limits [23] at relevant take-off weights, depending on engine number can be found in Fig. 4.3.

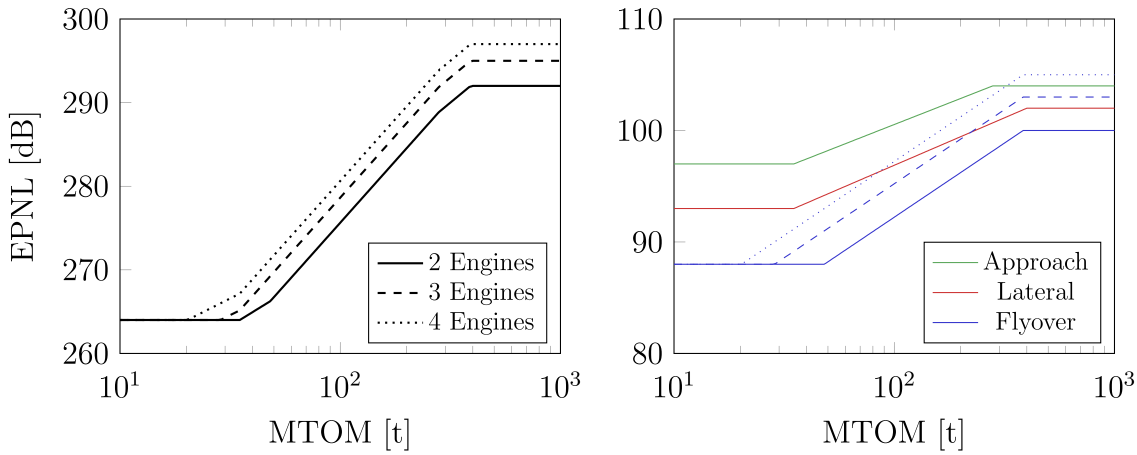

Figure 4.3: Maximum certification noise levels according to *Chapter 14*, cumulative on the left and individual certification points on the right

As of this writing (2026), the limits that were set in 2014 as *Chapter 14* by ICAO or *Stage 5* by the FAA are still in force and it is expected that SST will have to abide by these same limits. They stipulate a margin of 1 EPNdB at the Approach, Lateral and Flyover certification points as well as a 17 EPNdB margin in cumulative level to the limits set in *Chapter 3*. This set of rules is applicable to new transport aircraft types submitted for certification after December 30th of the year 2017, or for aircraft with an MTOM of less than 55 tonnes, 2020.

They will be used as a noise target or reference in the certification noise studies presented in this thesis.

4.2 Noise propagation to observer position

To obtain the receiver signal at the certification microphone positions, the propagation of sound from the engine to the observer on the ground must me predicted. In this thesis, a flyby simulation process using noise propagation models implemented in the DLR in-house tool *VIOLIN* (Virtual acOustic fLyover sImulatioN) was applied. It will be covered in this section.

4.2.1 Modeling approach

The engine noise source models were discussed in the previous chapter: fan noise is simulated analytically using a meanline approach and jet noise is predicted with a semi-empirical model assuming a perfectly mixed single stream.

The focus on analytical models is maintained for the prediction of noise propagation to the observer. The radial and azimuthal modes of all fan noise sources are superposed to create the directivity characteristic. Broadband noise is assumed to be non-correlated. Tonal noise information is stored in complex pressure values to ensure the phase information is maintained. When calculating the interaction of tonal noise sources from multiple engines or the effects of ground reflection, this information is needed to accurately determine interference effects. Reflection and scattering by the fuselage and the wings are not resolved in detail but can be neglected as proposed later in this section.

The details of this approach are described by Moreau [173]. For the sake of brevity, only the modelled propagation phenomena and their general impact will be explained here.

4.2.2 Modelled phenomena

The free-field noise propagation effects have different impacts on the signal received at the observer position. These impacts will be briefly covered here to give a better understanding of how they can be exploited to reduce noise at certification points. Their respective modeling approaches will be explained as well. Figure 4.4 is showing the relevant geometric parameters.

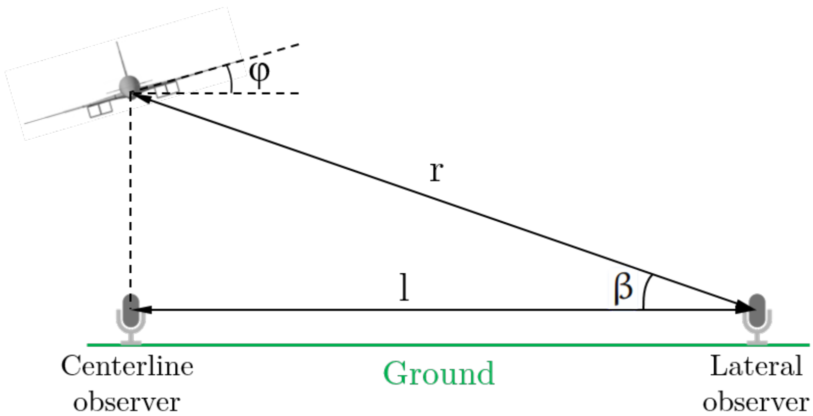

Figure 4.4: Measurements relevant to attenuating effects: roll angle φ, elevation angle β, observer distance r and lateral distance l

Radial spread

In the atmosphere, sound propagates in a spherical spread. The sound power level PWL is distributed over this spherical surface, which means that the SPL at an observer position reduces with increased distance r from the source:

$$SPL \sim \frac{1}{r^2} \tag{4.4}$$

This correction can simply be calculated based on the observer distance r.

Ground reflection

Since the microphones are installed in an elevated position (4 ft), they are not only reached by the direct wave from the noise source, but also the wave reflected off the ground. This amplifies the received noise signal, depending on the ground impedance which is modelled after Delany and Bazley [174]. For certification, a grass ground is dictated and is assumed to have a flow resistivity of 200,000 Pa·s·m^{-2}. The effect of ground reflection is modelled as the reflection of 2D wave on a flat plane.

Doppler shift

The Doppler shit denotes the change in the frequency of engine noise induced by the motion of the engine relative to the observer position. It can be analytically calculated:

$$f_{\mathrm{Doppler}} = \frac{1}{1 - M_{\mathrm{rel}}} \cdot f_0 \tag{4.5}$$

f_0 denotes the source frequencies and M_{rel} the Mach number of the motion of the engine relative to the observer. The impact of this effect cannot be generalized and depends on each individual case but is unlikely to be significant for certification noise levels.

Atmospheric jitter

Atmospheric jitter denotes the interaction effects of sound with atmospheric turbulence. The non-uniform propagation leads to amplitude and phase fluctuations of the sound waves, i.e. scattering and modulations. It is modelled using an enhanced Rietdijk Method as developed by Prescher [175]. The impact of those stochastic fluctuations on EPNL can be neglected.

Atmospheric absorption

Sound is attenuated when propagating through air, with the level of attenuation depending on temperature and humidity. SPL are reduced proportionally with distance, but higher frequencies are dampened stronger than lower frequencies, as can be seen in Figure 4.5. In this thesis, the atmospheric absorption is calculated in accordance to ISO 6913-1 [176].

Installation effect

The fuselage and wings of the aircraft impact engine noise propagation significantly by either shielding it or reflecting sound waves off their hard surfaces. These effects are combined in the SAE AIR 5662 model [177] as an engine noise directivity characteristic. This characteristic depends on the aircraft's roll angle ϕ and the engine installation configuration. AIR 5662 provides correlations for engines mounted under the wing, propeller engines, and rear fuselage mounted engines. For level flight, as is demanded for certification, the installation effect can be neglected for underwing engine configurations such as the SENECA M1.8 airliner.

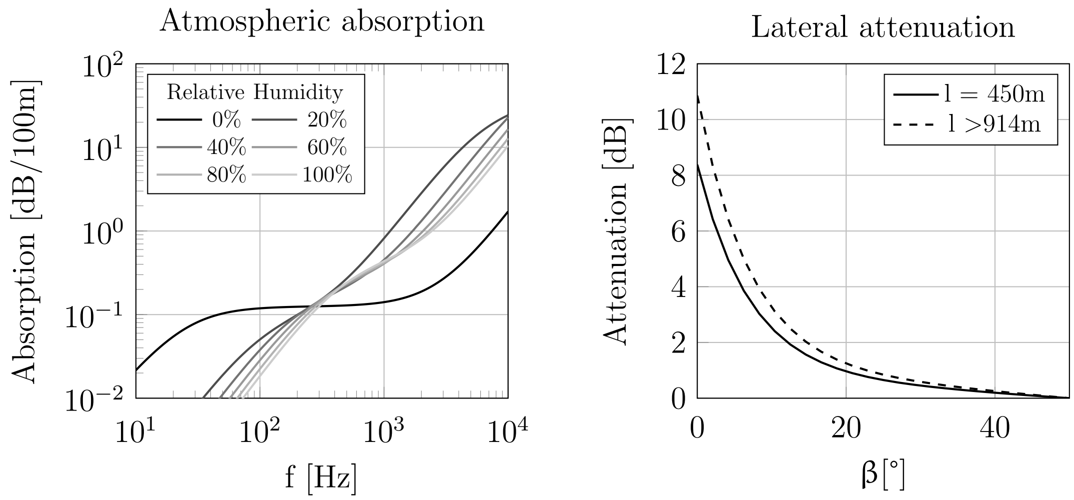

Figure 4.5: The effects of atmospheric absorption at 25°C and lateral attenuation

Lateral attenuation

Close to the ground, sound propagation is significantly impacted by ground reflection, refraction-scattering and other ground effects in superposition. The SAE AIR 5662 model offers an empirical correlation for all these effects. It is based on measurement data which inherently comprises all propagation effects between aircraft and observer. Only radial spread and atmospheric absorption (which can be solved reliably) are compensated for in the model. This means that the SAE AIR 5662 model includes Doppler shift, atmospheric jitter, ground reflection, and all other effects which will be summarized as "lateral attenuation". To avoid a book-keeping error, as described by Berton [178], by including Doppler effect, jitter, and ground reflection twice[1], their impact must be corrected for the SAE AIR 5662 model across all frequencies. Since neither Doppler shift nor atmospheric jitter (being a stochastic phenomenon) change the time-averaged sound pressure level $\overline{SPL}$ even over short time intervals, their application does not require correction. A correction for ground reflection is applied using the strategy proposed by Berton [178]. By removing the impact of ground reflection, only effects not modelled separately are included in the lateral attenuation. They result in a strong attenuation at low elevation angles β, especially at large lateral distances l as shown in Figure 4.5.

[1]Meaning once as individual effects and once as part of the SAE AIR 5662 model.

Chapter 5

Fan Design for Supersonic Aircraft

The fan of a supersonic aircraft engine needs to provide high FPRs at high efficiency in cruise and reliably cover a large envelope of operations. This entails significant constraints during its design process and thus limits its design space. LTO noise minimization as a secondary design aspect often conflicts with the other design goals, making this process even more challenging.

The methods used to design the fan concepts for the SENECA M1.8 airliner engines will be explained in this chapter and the resulting fan designs presented. The aircraft and all its systems are only developed at a pre-design level, so the fan designs will be limited to this development level as well. A highly detailed fan design would not be guaranteed to match a final, converged engine design and thus does not increase the reliability of LTO noise predictions when neither aircraft nor engines are provided at the same level of detail. 3D design elements such as lean and sweep will thus be neglected, reducing the design parameters and subsequently the design process complexity.

The fan pre-design will include:

- Hub and tip contour
- Blade numbers
- Stagger angles of leading and trailing edge
- Chord lengths
- Blade chord taper
- Blade thickness

The SENECA M1.8 airliner has a design FPR≈2.1, which is low enough to be provided by a single-stage fan but high enough to make a two-stage fan a viable design. Both concepts will be designed and their acoustic and aerodynamic properties compared.

5.1 Fan design process

The engine cycle was developed by Plohr [103] to correspond to the SENECA M1.8 airliner's mission. Consequently, the operating conditions of the fan such as mass flow and pressure ratio are fixed and the fan must match the cycle across the entire envelope.

To design an aeroacoustically optimized fan for minimum certification noise levels, multiple goals have to be met. From a manufacturers perspective, safety and fuel consumption remain paramount and are not sacrificed in favor of a low-noise design. Hence, realistic fan designs must operate with high stability and isentropic efficiency in cruise. At the same time, the fan noise in LTO operation needs to be evaluated. Since the goal is to minimize certification noise levels, studying the source power levels is not sufficient. Certification noise must be calculated at the predetermined observer positions or with an equivalent setup.

Such a fan design process was developed by Gräbert et al. [179], wherein an initial fan design is produced using handbook fan design rules which is then optimized using an evolutionary algorithm. This algorithm weighs aerodynamic performance at the design point and certification noise levels while iterating certain fan design parameters within a predetermined design space. After convergence, this results in a fan design which has low certification noise levels and a high cruise efficiency while providing stable operation inside the engine envelope. This process is applied to the single- and two-stage fan concepts.

The Top of Climb of a preliminary mission profile is chosen as the design point as it puts the highest thrust demand and thermal load on the engine while marking the beginning of the cruise phase. This makes it both critical for stability and representative for cruise conditions.

Not all geometry parameters will be open to the optimization. Some will be fixed in the initial design because they either have little impact on fan noise and efficiency or significantly slow the optimization process:

- Hub and casing contours cannot be changed in a significant capacity without jeopardizing the flow stability and a reasonable Mach number evolution along the fan.

- Blade thickness and chord taper were adopted according to common modern blade designs and their variations are not expected to have an impact on fan noise if they are within reasonable limits.

5.1.1 Initial design

The initial fan design, which already determines some parameters of the final design, was conducted following the statistics, guidelines and rules formulated by Bräunling [102] and Grieb [180]. Grieb provides data on military multi-stage low-pressure compressors, which were considered the most relevant for this application. While these compressors usually provide a higher FPR, their stage pressure ratios and BPRs are closer to the engine in question than modern civil subsonic designs. The parameter studies performed by Moreau [45] on fan design were considered as well. Design parameters finalized in the initial design will be selected more rigorously than the parameters which will enter the optimization process based on the initial design.

For the fan to match the engine design geometrically and aerodynamically, several parameters are predetermined. These are fan diameter, fan inlet conditions, FPR and mass flow at ToC. Normally, the fan in *PropNoise* is modelled with an inlet in a free stream. For supersonic applications, another approach must be taken. In supersonic flight, the airflow is slowed and compressed in the inlet through a series of shocks. Since the inlet design and shock systems are complex, the scaled characteristic of a supersonic inlet [181][1] is used during the engine cycle design to model the fan inflow conditions. Here, these are set in front of the fan, eliminating the inlet from the cruise case entirely, instead of simply modeling it as a diffuser with small losses.

The first step in developing the initial design is to find the rotor pressure ratio(s). For a two-stage design, the FPR is built up between the two stages of the fan. According to private communications by an experienced fan designer, a reasonable ratio is $\frac{FPR_1}{FPR_2} = 1.12$. The front stage produces a higher pressure ratio, because it experiences higher tip Mach numbers and thus stronger compression through shocks. Although both fan rotors share the same tip speed with equal diameter, the inflow into the second stage is hotter than into the first stage. This increases the speed of sound and subsequently reduces the tip Mach number.

Based on the pressure ratios, an appropriate hub and casing contour can be determined. These are not open to optimization, so they need to be selected carefully. The contours must satisfy two conflicting goals. To reduce losses in the rear rows and compressor and avoid choking in off-design operation, the axial Mach number should be as low as possible. However, a strong deceleration also reduces stability: if the meridional velocity density ratio (MVDR), with $MVDR = (\rho v_{\text{mer}})_{\text{inflow}}/(\rho v_{\text{mer}})_{\text{outflow}}$ (v_{mer} being the meridional velocity), is too small, the axial speed decreases too much and the DeHaller stability criterion is violated. Thus, the compression along the rotor rows must be stabi-

[1]Configuration NVSTOL (Section 4.2.1.11) was used

lized through a contracting flow area. Hub and casing contours are selected for a trade-off between high flow stability and low Mach numbers.

Next, a target rotor relative tip Mach number $M_{tip,rel}$ is chosen, depending on the stage pressure ratio. A higher tip Mach number means more pressure is being built up by the rotor-attached shocks which reduces isentropic efficiency but also blade loading. It is chosen based on an internal data collection, which can be observed in Figure 5.1 and the data provided by Grieb. The fan speed (and thus tip Mach number) is open to optimization for the single-stage design but not the two-stage design, so it must be selected with more precision for the latter.

At its design point, the preliminary ToC, the engine of the SENECA M1.8 airliner has a bypass ratio $BPR = 2.67$ and a fan pressure ratio $FPR = 2.09$ [103]. Hence, the target stage FPRs and associated tip Mach numbers are:

Concept	**(Front) Rotor FPR**	$\mathbf{M_{tip,rel}}$
Single-Stage	2.09	1.56
Two-Stage	1.53	1.28

This puts the single-stage design tip Mach number slightly lower than that of an older reference design [110], but within a realistic range.

When designing the blade rows, both the geometry of the individual blade and design aspects of the row (such as the number of blades) must be considered. The maximum aspect ratios of the individual blades are limited by mechanical and aeroelastic considerations, with higher loads and fan speed requiring lower aspect ratios. The aspect ratios selected here are based on existing fan design data. These maxima will be maintained during the optimization step. Low aspect-ratio fans, necessary for designs with a high stage pressure ratio, eliminate the need for additional dampening such as span damper, despite incurring a lower isentropic efficiency, as demonstrated by Urasek et al. [182]. This sets the relevant boundary for chord lengths for all blade rows.

Blade row solidity σ is a highly relevant parameter for both noise and stability, and is defined as the ratio of chord length c and blade spacing s: $\sigma = \frac{c}{s}$. While a low solidity means less wetted surface, generally lowering broadband noise and increasing the isentropic efficiency, a reasonably high solidity must be maintained for a stable flow. It is particularly important for blade loading in off-design operation. Higher solidity generally allows the fan to cope better with inflow distortion according to Valentine et al. [183] and delay stall onset at high incidences as demonstrated by Sane et al. [184]. In general, a higher solidity is required to achieve higher FPRs [185] which is particularly relevant to high-pressure fans. For increased FPRs, increased solidity has been shown by Metzger et al. [186] to reduce noise in low pressure fans, but the same trend can be expected in high-pressure fans. The solidity is determined by the blade number and chord length. Since the channel geometry and approximate Mach number distribution are known, blade numbers can be selected to exploit cut-off effects. Through an iterative process, blade numbers and chords lengths can be chosen to fulfill the cut-off criterion and provide a desirable solidity. All these parameters are open for optimization and for this reason, they do not have to be iterated intensely for the initial design.

Finally, the stagger angles of the rows at the meanline position are calculated to provide the desired incidence and flow turning to reach the target FPR of the design point. This is done in an iterative, analytical process described by Moreau in the non-public *PropNoise* manual [187]. This process has been able to reproduce the actual metal angles of existing fan designs with only small deviations.

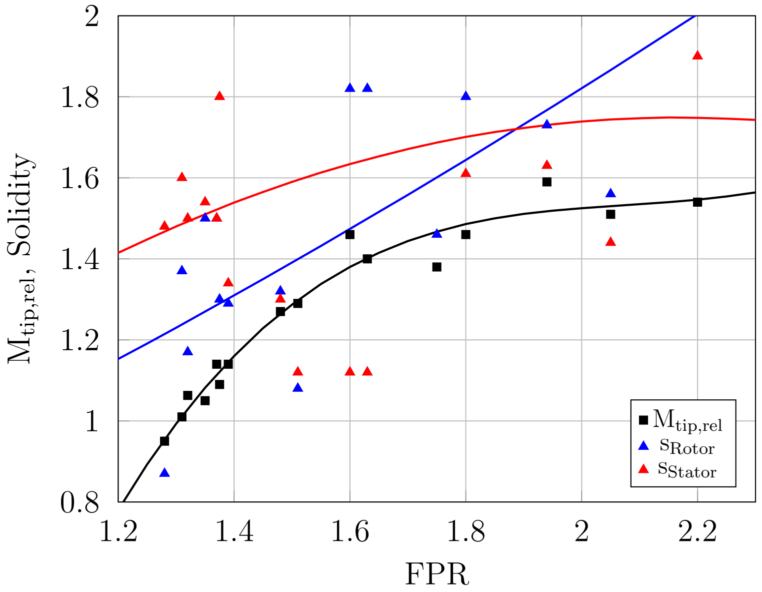

Figure 5.1: Turbofan design data from internal database with polynomial regression curves[3]

5.1.2 Optimization process

The goal is to develop a fan design which minimizes the aircraft certification noise levels while maintaining a high isentropic efficiency at the ToC. Since a meaningful optimization can only happen when both parameters are considered, both the aerodynamic performance and aeroacoustic prediction tools of *PropNoise* and the propagation effects and EPNL calculation tools of *VIOLIN* must be applied.

[3]Solidities: Second order regression; Tip Mach number: Third order regression

Optimization algorithm

The impact of changes to the fan design on noise and efficiency cannot be estimated using basic rules or highly simplified models with sufficient accuracy, so each iteration of the design must be fully evaluated individually. Since many parameters in the design can be changed, a manual modification and evaluation is impractical and time-consuming. To automate this process an evolutionary optimization algorithm based on a stochastic, population-based method suitable for finding an optimum in a continuous parameter space is used to evaluate fan design permutations.

The evolutionary algorithm used in this case is designed to minimize an arbitrary optimization target parameter $g(k)$ as described by Storn [188]. A set of previously defined parameters is required as the input value, which is then referred to as a candidate. The population K is a collection of candidates k, which is initially filled by candidates which can be predefined or a stochastic selection from the parameter space. A new candidate k_n is generated at each iteration from a mutated candidate k' and the best candidate k_0 in the population K. In this case, the best candidate means the fan design with the smallest optimization target parameter. To generate k', two random candidates $k_{\text{rand},1}$ and $k_{\text{rand},2}$ are selected from the population and the mutation is formed from their difference and a mutation factor m:

$$k' = k_0 + m \cdot (k_{\text{rand},1} - k_{\text{rand},2}) \tag{5.1}$$

In the following, a new candidate k_n is created. This is then filled with parameters from k_0 and k', whereby this is randomly selected for each parameter according to a previously selected weighting (recombination factor). This resulting candidate is then calculated. For $g(k_n) < max(g(K)) = g(k_{\text{max}})$, k_n is added to the population and k_{max} is removed. This procedure is also known as the *best1bin* method.

The convergence criterion compares the standard deviation S of the population's target parameters $g(K)$ with the absolute of its mean value, multiplied with a relative tolerance factor f_{tol}. The optimization is considered as converged when the following criterion is reached:

$$S(g(K)) \leq f_{\text{tol}} \cdot |\overline{g(K)}| \tag{5.2}$$

The disadvantage of this method is that it can only optimize for a single target parameter. Thus, all goals, specifically isentropic efficiency, certification noise levels, stability, and mechanical integrity must be unified into one target parameter or codified as a boundary condition.

Implementation

The following geometric parameters were open for optimization within their respective restricted parameter space:

- Meanline leading and trailing edge stagger angles: minimum and maximum boundaries are chosen around initial design to aid convergence
- Meanline chord lengths: minimum boundary set to not exceed maximum aspect ratio; very high maximum boundary set because longer chords generally lead to more interaction noise and more friction, so the algorithm will automatically select lower chord lengths
- Blade numbers: minimum boundary set not to fall below minimum solidity; very high maximum for identical reasons to chord length
- Fan speed: minimum and maximum around initial design to aid convergence

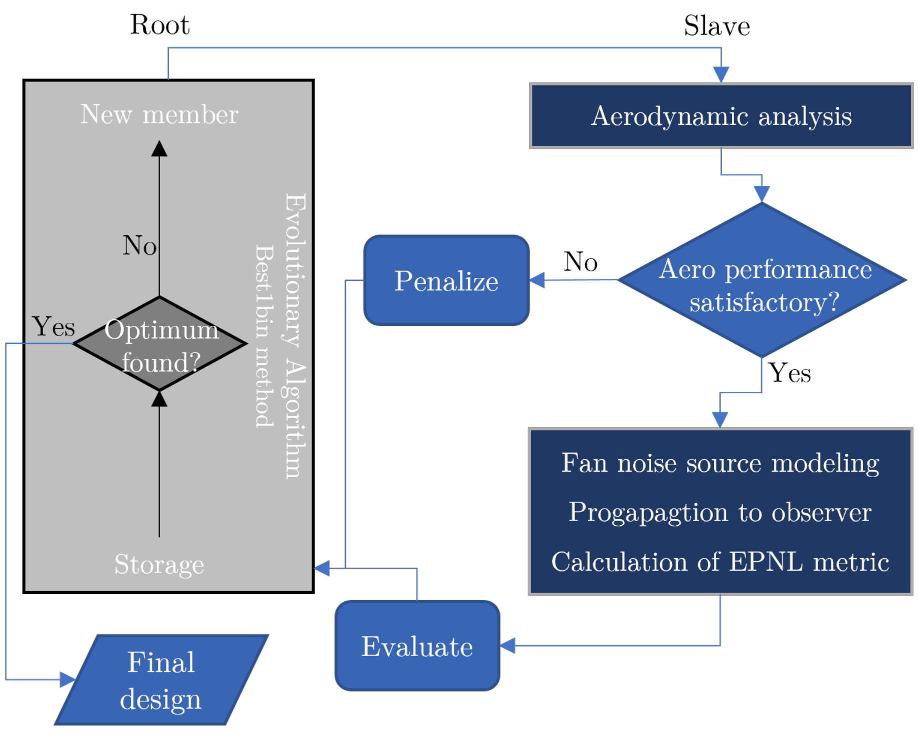

Figure 5.2: Schematic overview of the design optimization process

Figure 5.2 shows the design of the optimization process. For each new candidate, it must first be determined if they are viable or non-viable. For this decision, only the aerodynamics at the design point are considered. Penalties are applied for:

- Failure to produce the required FPR
- High aerodynamic loads and high incidences, which indicate low stability

This is necessary because *PropNoise* relies on physics-based models that rely on various assumptions. If these assumptions are violated, the results are not valid. Outside of this validity space, the results of these models can become unrealistically advantageous, so this must be prevented in the optimization process. Otherwise, an optimum is found that does not reflect reality and is of no use for the desired evaluation. Furthermore, the candidate must achieve the specified FPR. If the results of a candidate do not fall within the specified limits, it is considered invalid. A penalty value is then returned to the optimizer and the next candidate is processed.

The variables considered, their limits and penalties are listed below:

- FPR
  - Limit: $0.99 \cdot 2.094 < FPR < 1.01 \cdot 2.094$
  - Penalty: $pen_{\mathrm{FPR}} = f_1 \cdot (FPR - 2.094)^2$
- Maximum incidence inc_{max}
  - Limit: $inc_{\mathrm{max}} < 5°$
  - Penalty: $pen_{\mathrm{inc}} = f_2 \cdot rad(|inc_{\mathrm{max}}| - 5°)$
- Lieblein diffusion number D
  - Limit: $D < 0.55$
  - Penalty: $pen_{\mathrm{D}} = f_3 \cdot (D - 0.55)$

The penalty factors f_1, f_2 and f_3 were varied through an iterative process to accelerate the convergence of results. Their final values are:

- $f_1 = 2000 = 4188/2.094$
- $f_2 = 5.24 = 26.2/5$ for degrees and $f_1 = 300 \approx 26.2/0.087$ for radians
- $f_3 = 300 = 165/0.55$

If a candidate violates any of those limits, its acoustic properties are not evaluated and only the penalty scores are returned to the optimization algorithm. In that case the target parameter is:

$$f(k_n) = pen_{\text{FPR}} + pen_{\text{inc}} + pen_{\text{D}} \tag{5.3}$$

If a candidate fulfills all aforementioned conditions, it is considered valid. The corresponding design is then passed on to the acoustic evaluation, for which simplified flyby simulations with *VIOLIN* (see Section 4.2) are conducted to reduce computational cost. Only a single engine at a constant operating point is considered, so interference effects between the engines as well as transient operation are neglected. For this purpose, three representative operating points, corresponding to the three noise certification points are selected. The points chosen for the SENECA M1.8 airliner fans are listed in Table 5.1. Each flyby is simulated on a single linear trajectory segment, corresponding to the flight altitude, climb angle and pitch at the moment the certification point is passed on a full profile. The representative certification noise levels $EPNL_{\text{App}}$, $EPNL_{\text{Lat}}$ and $EPNL_{\text{FO}}$ are summed up to $EPNL_{\text{cum}}$, as one target characteristic.

Fan noise only needs to be reduced in scenarios where it is the dominant noise source. To establish if this is the case, jet noise is included for each operating point. However, no liner attenuation was assumed for the optimization process, so the impact of the fan noise sources in the acoustic evaluation is overestimated. Besides higher noise levels in general, it can lead to the fan being "overoptimized" for low noise in conditions where it will not be the dominant engine noise source. This is particularly relevant at the high thrust operating point corresponding to the Lateral position, where jet noise would be expected to be dominant over fan noise.

The isentropic efficiency of the fan is the other target characteristic, which is defined as:

$$\eta_{\text{ise}} = \frac{T_{\text{inlet}}(c_{\text{opt}} - 1)}{T_{\text{exhaust}} - T_{\text{inlet}}} \quad with \quad c_{\text{opt}} = FPR^{\frac{\gamma-1}{\gamma}} \tag{5.4}$$

These two target characteristics are then combined into a target parameter:

$$f(k_n) = EPNL_{\text{cum}} + (1 - \eta_{\text{ise}}) \cdot 100 \tag{5.5}$$

This effectively translates to a trade-off of 1 EPNdB $EPNL_{\text{cum}}$ to 1% η_{ise}. While isentropic efficiency is generally valued over certification noise levels by engine manufacturers, this is considered an acceptable trade-off considering cost and fuel burn. The specific ratio was chosen after a discussion with an expert of an engine manufacturer [189].

The relative convergence tolerance was set to $f_{\text{tol}} = 0.01$, i.e. the optimization will stop when no more than a $0.01 \cdot f(k_n)$ improvement over the population was achieved, corresponding to $0.01\%\eta_{\text{ise}}/0.01EPNL_{\text{cum}}$.

	ToC	**Approach**	**Lateral**	**Flyover**
h [m]	10668	120	89	261
M_∞	1.54	0.25	0.28	0.29
FPR	2.09	1.17	1.53	1.45
Q [kgs^{-1}]	337.6	220.7	351.3	330.4

Table 5.1: Fan operating points for optimization (not ISA-corrected); ToC is considered for cruise efficiency evaluation; Approach, Lateral and Flyover for certification noise estimation

5.1.3 Single-stage optimization

For the single-stage design, the following parameters were varied as part of the optimization process:

	Rotor	**Stator**
LE stagger angle	×	×
TE stagger angle	×	-
Chord length	×	×
Blade number	×	×
Rotational speed	×	-

Table 5.2: Optimization parameters for the single-stage design

The trailing edge (TE) stagger angle of the stator was fixed at 0° to ensure a purely axial outflow. This leaves 8 parameters to be optimized.

The results of the optimization with regards to the optimization are shown in Figure 5.3. On the left, the evolution of the target parameter $g(k_n)$ can be seen. With a total of 91,242 iterations, 1,404 valid candidates were produced until an optimum was found. New minima were found with more iterations, but also the density of valid, low scoring candidates increased significantly, as is evidenced by the point cloud on the bottom right. As can be seen in Figure, 5.3 the optimization had to be restarted multiple times due to limitations in run-time. For each run a population of the best candidates was provided to maintain the optimization progress. This led to phases without new minima after each restart. The optimization took 19 days in total to finish.

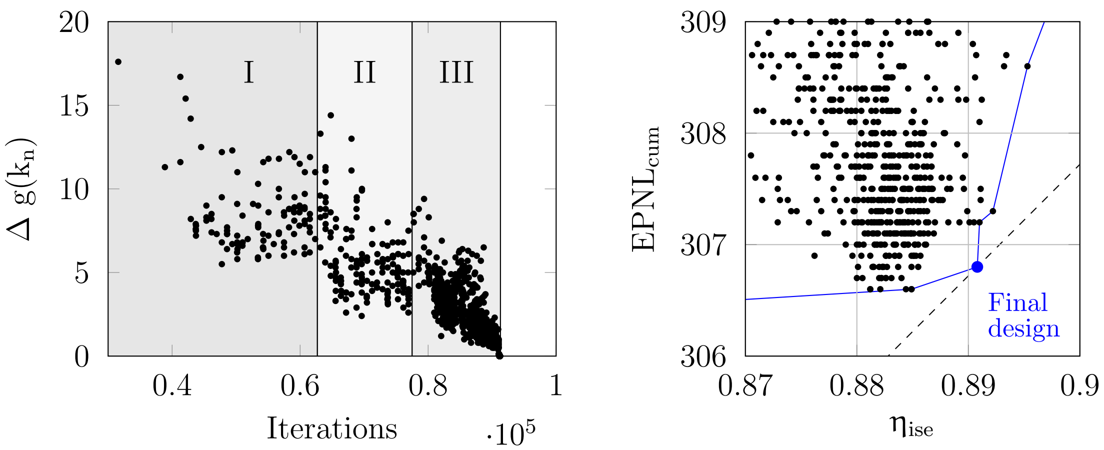

Figure 5.3: Single-stage optimization results; left: optimization progress with individual optimizer runs (I, II, II); right: best candidates with Pareto front

In the right plot, the Pareto front of the two target characteristics, isentropic efficiency η_{ise} and cumulative certification noise level $EPNL_{\text{cum}}$ is shown. As can be seen in the Pareto plot, the final design is the candidate with the best compromise of isentropic efficiency and cumulative noise level, with more efficient designs being much noisier. The "ragged" progress of the minima and shape of the Pareto front is due to the specific fan operation: the operating point representative for the Lateral certification is close to choking conditions, so many candidates failed that operating point and are thus missing from the graphics displayed here. This unsteady behavior is problematic for the evolutionary algorithm and makes the optimization progress less smooth.

Geometric parameters of the initial and final single-stage fan designs can be found in Table 5.3; a schematic meridional view of the final design is displayed in Figure 5.4. The rotor-stator spacing (RSS) is defined as the ratio of axial distance between the rows over axial chord of the upstream row (rotor or stator). The final blade numbers produce a cut-off design for tonal interaction noise. A diverging channel geometry between rotor and stator is chosen to combat the extreme negative incidences that the stator experiences during low power settings, when the rotor row acts as nozzle due to low compression ratios.

	Initial Design	**Final Design**
Rotor $M_{tip,rel}$	1.59	1.62
Rotor chord [m]	0.495	0.406
Stator chord [m]	0.284	0.217
$RSS_{Intrastage}$	0.89	0.53
Rotor blades	17	16
Stator blades	40	47
Rotor solidity	1.96	1.53
Stator solidity	2.56	2.33
Rotor MVDR	1.24	1.26
Stator MVDR	1.02	1.03

Table 5.3: Single-stage fan geometry parameters at 70% channel height

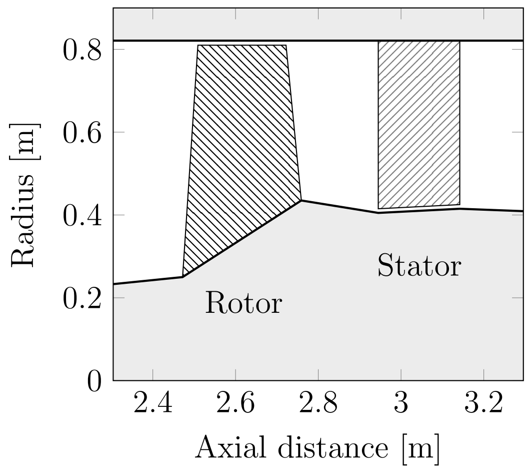

Figure 5.4: Single-stage fan schematic in meridional view

To confirm the optimization was successful, a brief look at the characteristics of the initial and final design listed in Table 5.4 is sufficient. The acoustic properties of the final design will be evaluated in detail later in this chapter.

	Initial Design	**Final Design**
η_{ise} (ToC)	0.817	0.891
Approach EPNdB	94.6	93.5
Lateral EPNdB	101.9	101.6
Flyover EPNdB	112.2	112.7
Cumulative EPNdB	308.7	307.8

Table 5.4: Optimization target comparison of single-stage designs

The final design is predicted to be less noisy than the original design, and has a much higher isentropic efficiency. This is due to lower solidities, reducing the wetted surface and leading to a reduction in friction loss. The shorter rotor chords also cause smaller, less turbulent wakes, in on-design operation reducing wake interaction noise. The higher blade loading makes broadband wake interaction noise stronger, which is most relevant in low power settings, where neither jet nor buzzsaw noise are dominant and rotor loading is high. This causes the small increase in Approach levels. In high power settings, buzzsaw noise is dominant, so there is only a small difference between both designs which is due to a slightly higher fan speed in the final design. The individual noise sources of the final design will be discussed in detail in the ensuing section.

During the initial design step, it became clear that there is only a small design space where the fan can deliver the high FPR with sufficient stability and not be choked at any point. The small improvement in $g(k_n)$ over the design process and the small differences between initial and final design are caused by this small design space.

5.1.4 Two-stage optimization

The design process for the two-stage design was adjusted according to knowledge obtained from the single-stage design process: The chord length of the rear stator did not impact fan noise significantly, furthermore it is usually located in the bypass where the spatial restrictions are not as strict. It was thus set to a fixed chord length which produces a low diffusion number in all operating conditions. Rotational speed has a big impact on the fan aerodynamics and its variation slows convergence significantly, which is even more relevant since the aerodynamic and aeroacoustic calculations of the two-stage design take significantly longer than the single-stage calculations. Fan speed was not optimized, because the relation of lower fan speeds reducing noise is simple and the low but reasonable fan speed of the initial design could be maintained.

For the two-stage design, the following parameters were open for optimization:

	Rotor 1	**Stator 1**	**Rotor 2**	**Stator 2**
LE stagger angle	×	×	×	×
TE stagger angle	×	×	×	-
Chord length	×	×	×	-
Blade number	×	×	×	×

Table 5.5: Optimization parameters for two-stage design

The trailing edge (TE) stagger angle of the stator was again fixed at 0°. This amounts to 14 parameters to optimize, so a significantly slower convergence than for the single-stage design was expected. To maintain a reasonable time frame, the optimization tolerance was relaxed to $f_{\text{tol}} = 0.05$.

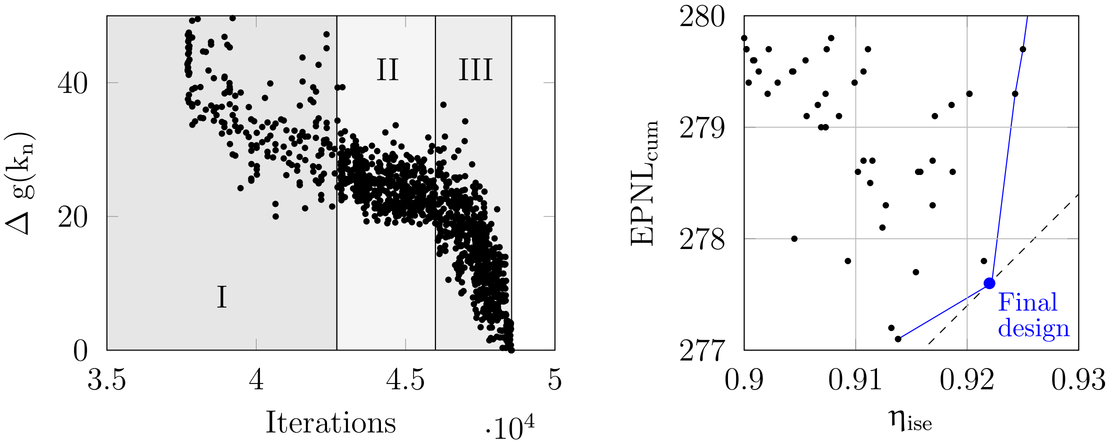

Figure 5.5: Two-stage optimization results; left: optimization progress with individual optimizer runs (I, II, II); right: best candidates with Pareto front

The results of the optimization are shown in Figure 5.5. On the left, the evolution of the target parameter $g(k_n)$ can be seen. Through 48,549 iterations, 1,363 valid candidates were produced. At the start of optimization run II, the parameter spaces were refined which led to more valid candidates being produced. However, the fan's isentropic efficiency was limited due to the minimum solidity, caused by the minima set for the chord length and blade numbers. The optimization algorithm produced the best candidates around these limits constantly, while providing a relatively low diffusion number at all operating points. Consequently, the parameter ranges were widened to allow a lower solidity on run III, leading to the ensuing drop in $g(k_n)$.

In the plot of the right, the Pareto front of the two target characteristics, isentropic efficiency η_{ise} and cumulative certification noise level $EPNL_{\text{cum}}$ is shown. The much lower density of candidates compared to the single-stage optimization is due to the relaxed optimization tolerance and generally lower number of iterations.

Geometric parameters of the initial and final two-stage fan designs can be found in Table 5.6, a schematic meridional view of the final design is displayed in Figure 5.6. Like for the single-stage fan, the diverging channel geometry between second stage rotor and stator is chosen to combat the high negative incidences that the stator experiences during low power settings, when the rotor row acts as nozzle due to low compression ratios. All inter- and intrastage distances are very large since the fan was only optimized with regards to noise and both potential field and wake interaction noise benefit from increased axial distances between rows. A realistic design would likely be more compact because of the significant weight penalties attached and the diminishing acoustic benefits of vastly increased axial distances between rows. An improved design which takes this into account was developed in a follow-up project STORMIE and the improvements made will be presented in the final section of this chapter. A cut-off design was not achievable between the first stage stator and second stage rotor.

	Initial Design	Final Design
Rotor 1 chord [m]	0.189	0.230
Stator 1 chord [m]	0.169	0.141
Rotor 1 blades	25	19
Stator 1 blades	41	37
Rotor 1 solidity	1.15	1.06
Stator 1 solidity	1.63	1.23
Rotor 1 MVDR	1.09	1.10
Stator 1 MVDR	1.01	1.01
$\mathbf{RSS_{intrastage\ 1}}$	1.41	1.30
$\mathbf{RSS_{interstage}}$	1.12	1.34

	Initial Design	Final Design
Rotor 2 chord [m]	0.162	0.178
Stator 2 chord [m]	0.137	0.141
Rotor 2 blades	36	29
Stator 2 blades	64	57
Rotor 2 solidity	1.34	1.18
Stator 2 solidity	2.00	1.84
Rotor 2 MVDR	1.12	1.12
Stator 2 MVDR	1.02	1.02
$\mathbf{RSS_{intrastage\ 2}}$	1.88	1.83

Table 5.6: Two-stage fan geometry parameters at 70% channel height

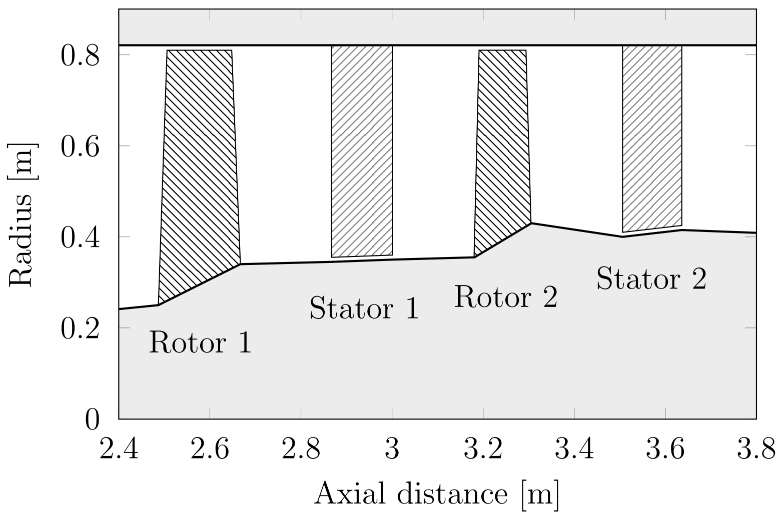

Figure 5.6: Two-stage fan schematic in meridional view

The optimization was successful as the characteristics of the initial and final design listed in Table 5.7 confirm.

The optimized fan has a higher isentropic efficiency and a lower cumulative certification noise level. Fewer blades and shorter chords reduce friction losses and thus increase the isentropic efficiency. Furthermore, interaction noise was reduced with a lower the front stage pressure ratio and higher the second stage pressure ratio. As will be shown in the ensuing section, the dominant interaction noise sources depend on the front stage wakes. The effect is stronger with lower thrust levels, where neither buzzsaw nor jet noise are dominant over interaction noise and the loading of the front stage is particularly high.

	Initial Design	Final Design
η_{ise} (ToC)	0.870	0.922
Approach EPNdB	99.1	97.4
Lateral EPNdB	85.5	85.6
Flyover EPNdB	95.2	94.6
Cumulative EPNdB	279.8	277.6

Table 5.7: Optimization target comparison of two-stage designs

5.2 Aeroacoustic properties of Single and Two-Stage Designs

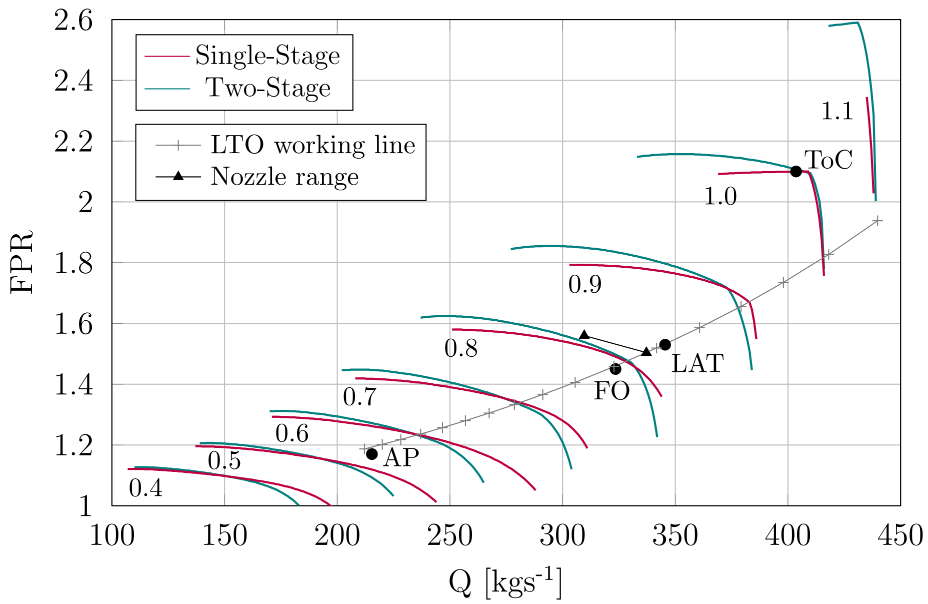

Figure 5.7: Fan maps of single- and two-stage final designs with representative operating points; working line with open nozzle and thrust equivalent throttle line with changing nozzle settings shown

To better understand the final fan designs' impact on certification noise as well as noise optimized operation on landing and take-off, their acoustic properties are now evaluated in more detail.

The fan maps of the resulting single- and two-stage design can be seen in Figure 5.7 with the optimization operating points. It is easy to see that due to the open nozzle throat, the fans are close to choking at high thrust on the LTO working line. This means they operate in off-design conditions for medium to high thrust LTO scenarios.

5.2.1 Single-stage fan

To comprehensively evaluate the acoustic properties of the fan, its entire operating range during LTO operation must be considered. Figure 5.8 shows the sound power level (PWL) of the relevant noise sources radiated into the free-field over the relative thrust $\mathrm{T_{rel}}$ along the open nozzle LTO working line. The aerodynamic parameters relevant to these sources are shown as well. The noise generation mechanisms were explained in Section 3.2 and will only be recapitulated in brief. Acoustic liners are not considered, so tonal noise would be much weaker in real-life applications, while broadband noises will not be attenuated as effectively. Non-ideal blades (see Section 3.2.1) are assumed for the prediction of buzzsaw noise.

Jet noise increases with higher thrust due to higher jet velocities. As can be seen by the straight trend line on the logarithmic plot, it is scaling with thrust approximately to the fifth power $PWL_{\mathrm{jet}} \sim T^5$. This is expected, since $T \sim v_{\mathrm{jet}} \cdot Q$ and $PWL_{\mathrm{jet}} \sim v_{\mathrm{jet}}^8$. It does however not become dominant due to the strong fan noise sources. With the application of acoustic liners, jet noise will be dominant for high power settings.

Broadband wake interaction noise is the dominant broadband fan noise source. It correlates with the local flow Mach number, in this case the stator relative Mach number $\mathrm{M_{rel}}$, and would be expected to display a third power thrust-PWL scaling. However, it also depends on the rotor wake turbulence which is signified by its turbulent kinetic energy (TKE). The rotor wake TKE is very high but shows a negative correlation with thrust. This is due to the wide-chord rotor which inherently produces thick and turbulent boundary layers and experiences high incidence angles at low power, since the fan is designed for high thrust operation. In these conditions, the rotor cannot provide the compression dictated by the contracting flow channel. At high thrust, the incidence is reduced significantly but higher blade loading leads to a higher negative pressure gradient along the chord, causing thick, highly turbulent wakes. This negates the effect of the decreasing incidence on TKE. The decreasing TKE and increasing local Mach number cause only small variations in noise level over the LTO operating range.

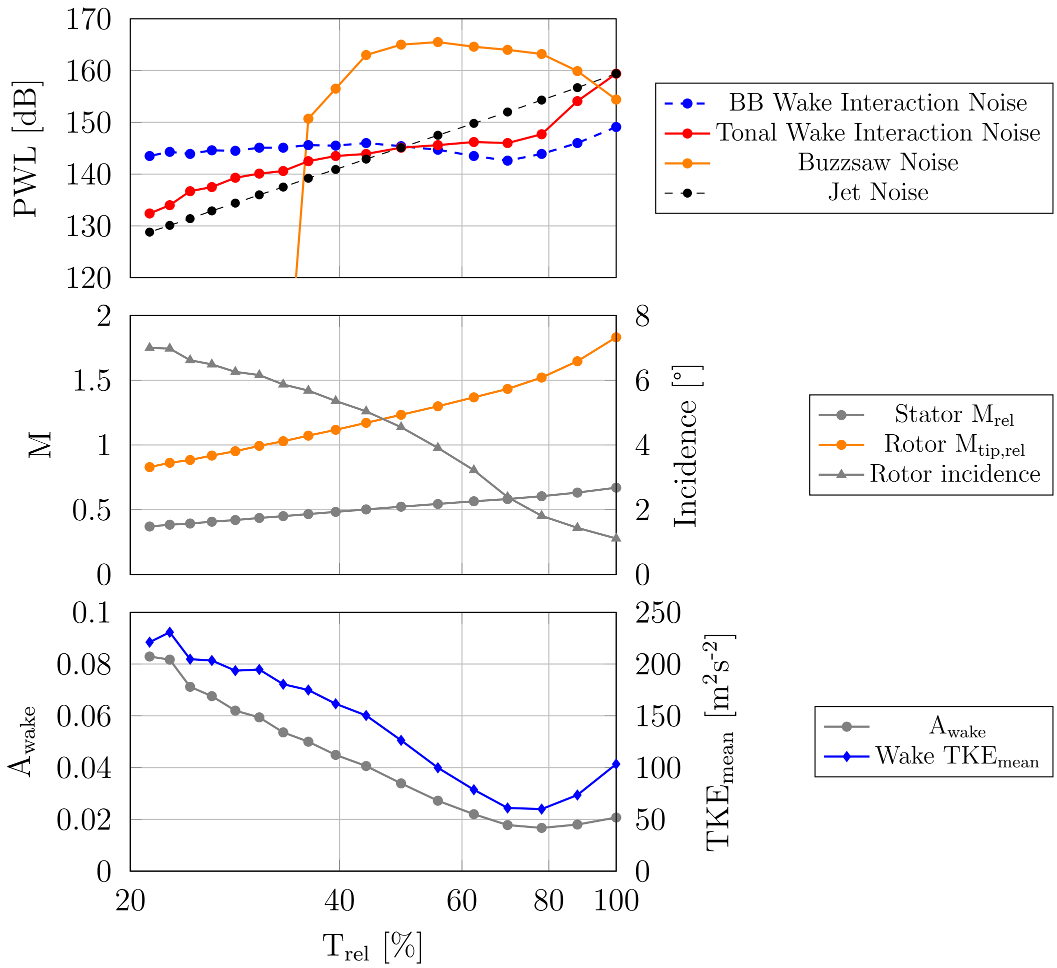

Figure 5.8: Radiated noise source ranking along engine thrust range for single-stage fan design

Tonal wake interaction noise shows a similar trend, but the impact of the decreasing wake area A_{wake} is much lower. This leads to a steeper increase in PWL with a higher thrust and thus relative Mach number. The sharp increase in sound power at high thrust operation above 70% T_{rel} is due to the reduced effectiveness of the cut-off design: a strong mode of the 2.BPF (mode orders: m=32, n=0) and 1.BPF (mode orders: m=16, n=0) respectively become cut-on in the intrastage domain and cause a significant rise in tonal wake interaction noise.

Buzzsaw noise depends on the tip Mach number $\mathrm{M}_{\mathrm{tip,rel}}$ and only becomes relevant once a minimum section of the span is supersonic, which only happens beyond an $\mathrm{M}_{\mathrm{tip,rel}}$ of 1.1. The shock strength decreases with higher supersonic tip Mach numbers and the propagation angle gets shallower, meaning the shock travels longer distances before reaching the inlet plane, leading to stronger decay. However, the part of the blade with a shock extends radially towards the hub with increasing tip Mach numbers. The combination of these effects lead to the maximum of buzzsaw noise at $M_{\mathrm{tip,rel}} \approx 1.2$ in medium power settings. NASA conducted acoustic wind tunnel tests with three high pressure ratio fans for SST applications in their Glenn Research Center 9x15 LSWT [82]. When comparing the prediction results presented in this section to the single-stage fan measurements, absolute noise levels are not as relevant since they depend heavily on the specific application of acoustic liners. The difference between tonal and broadband noise levels agreeing well indicates that the noise predictions for this SST fan design are in line with experimental findings. However, this is a single point comparison.

5.2.2 Two-stage fan

Figure 5.9 shows the relevant noise sources for the two-stage design. As for the single-stage design, weak noise sources are excluded. No attenuation by acoustic liners is included in the results shown here.

The broadband wake interaction noise between first stage rotor and stator is the strongest broadband interaction noise source. It is driven by the high incidences of the first stage rotor, in particular at low thrust, when front rotor in multi-stage compressors is commonly highly loaded. Consequently, the rotor wakes are very pronounced and highly turbulent. The broadband wake interaction noise of this design displays a trend very similar to the single-stage design for identical reasons: decreasing TKE and increasing local Mach number with increasing thrust. The chord of the front rotor is much shorter than for the single-stage design, which reduces both wake area and wake TKE and consequently the source's sound power level. The local Mach number is also slightly lower than for the single-stage stator, amplifying this reduction.

The tonal wake interaction noise between first stage stator and second stage rotor is the dominant tonal interaction noise source. Since inverse cut-off effects[4] cannot be exploited in high-speed fans, the downstream row needs to have a significantly higher blade count than the respective upstream row for a cut-off design. This is impossible for four consecutive rows without choking the fan through blockage. Consequently, the second stage rotor has fewer blades than the first stage stator. Without a cut-off design, all acoustic energy at source is transmitted throughout the entire duct, making it the dominant tonal source in lower thrust operation until R1 $M_{tip,rel} \approx 1.1$ is reached and buzzsaw becomes dominant.

Despite the long distance between all rows, the unsteady pressure signature upstream of the second stage rotor excites the trailing edge of the first stage stator significantly at high thrust settings. This happens when the second stage rotor enters the transonic domain and creates a set of blade-attached shocks, which effectively replace the rotor's

[4] As proven effective for low-speed fans by Schade et al. [190]

potential field. These shocks do not exit the inlet as buzzsaw noise but cause strong interaction noise. The shock system also interacts with wakes, causing broadband noise, but this interaction is not modelled and will thus be ignored.

Due to the lower design tip Mach number, buzzsaw noise becomes dominant at higher power settings than for the single-stage fan. It peaks at Rotor 1 a tip Mach number R1 $M_{tip,rel} \approx 1.2$. Non-ideal blades are assumed for the prediction of buzzsaw noise.

Jet noise is identical to the single-stage design, since the fan concept has no impact on the exhaust flow. It becomes the dominant broadband noise source starting at medium thrust.

When comparing these noise predictions to the two-stage fan data measured in NASA's 9x15 LSWT [82], a similar difference between tonal and broadband noise is found. This is, again, a single point comparison but demonstrates that the predictions here are in line with experimental findings.

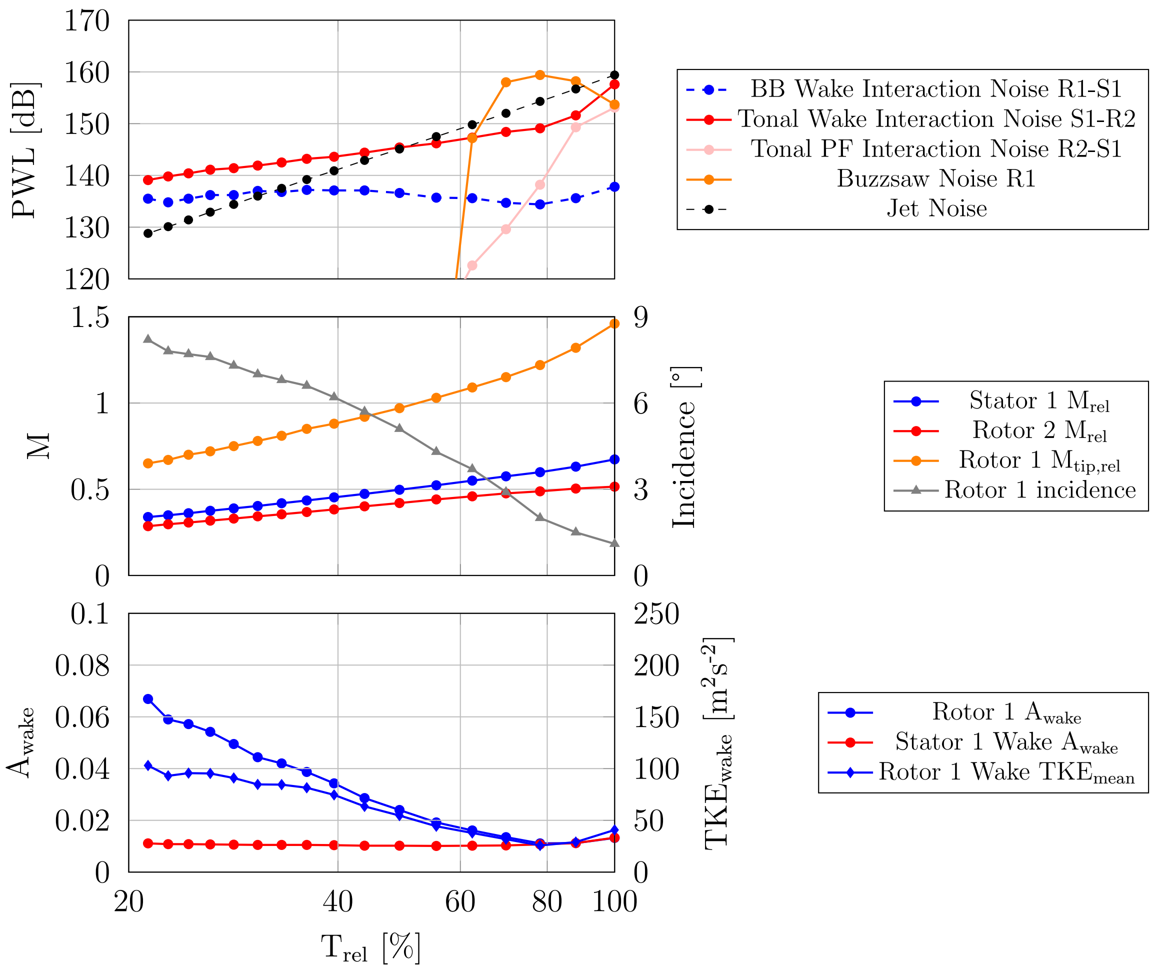

Figure 5.9: Radiated source ranking among dominant sources along engine thrust range for two-stage fan design

To evaluate the impact of the rotor-stator spacing (RSS), i.e. axial distances between rows, on engine weight, a retrospective study was conducted by the designers of the engine, AT-TWK (Engine department) of DLR. Using a geometric model of the engine which allows a rough engine weight prediction, RSSs in the fan were varied. Both front stage intrastage and interstage RSS were varied and the relative change of the engine weight with the results shown in Figure 5.10. To evaluate the trade-off with fan noise, the overall power level (OAPWL) of the fan noise in landing operation is provided as well. The landing operating point was chosen because it is most sensitive to changes in interaction noise due to weak buzzsaw and jet noise. With an intra- and interstage RSS of 1.30 and 1.34 respectively, a weight increase of 3.3-3.5% and OAPWL reduction of 5.3-5.6 dB on landing over a more common, low RSS design can be assumed. Engines usually make up about 10% of the total aircraft MTOM (≈ 13.3% for the Georgia Tech M1.7 airliner [59], 10.4% for the SENECA M1.8 airliner [75]), so the increase in engine weight is significant. Consequently, rotor-stator spacings must be optimized and trade-offs with fan noise be studied for individual applications.

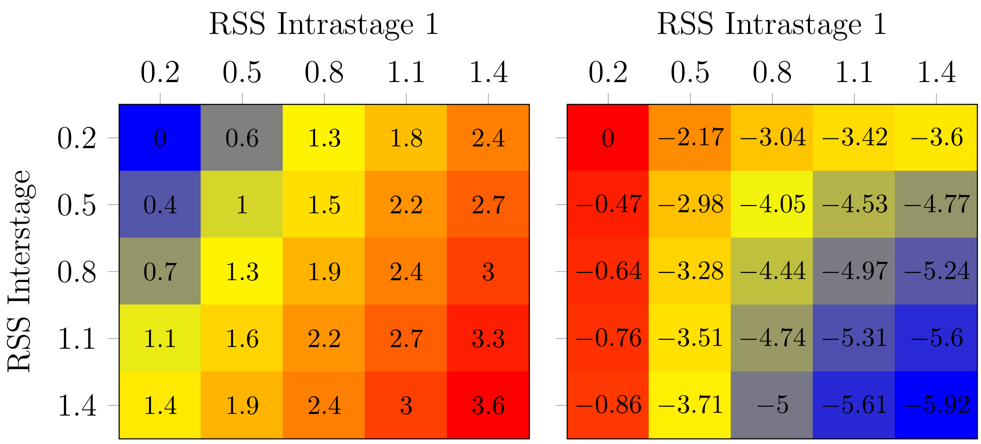

Figure 5.10: Relative engine weight gain in percent (left) and relative OAPWL in dB in landing operation (right) depending on axial spacing in inter- and intrastage

5.2.3 Impact of nozzle setting

With the final fan designs available, the impact of the nozzle setting on engine noise can be evaluated. To achieve this goal, the nozzle throat area was varied at a constant thrust representative for LTO operations. The resulting throttle line is denoted "Nozzle range" in the fan maps (Figure 5.7). The resulting changes in both fan and jet noise for both fan designs can be seen in Figure 5.11. Opening the nozzle increases mass flow and reduces jet velocity and fan loading.

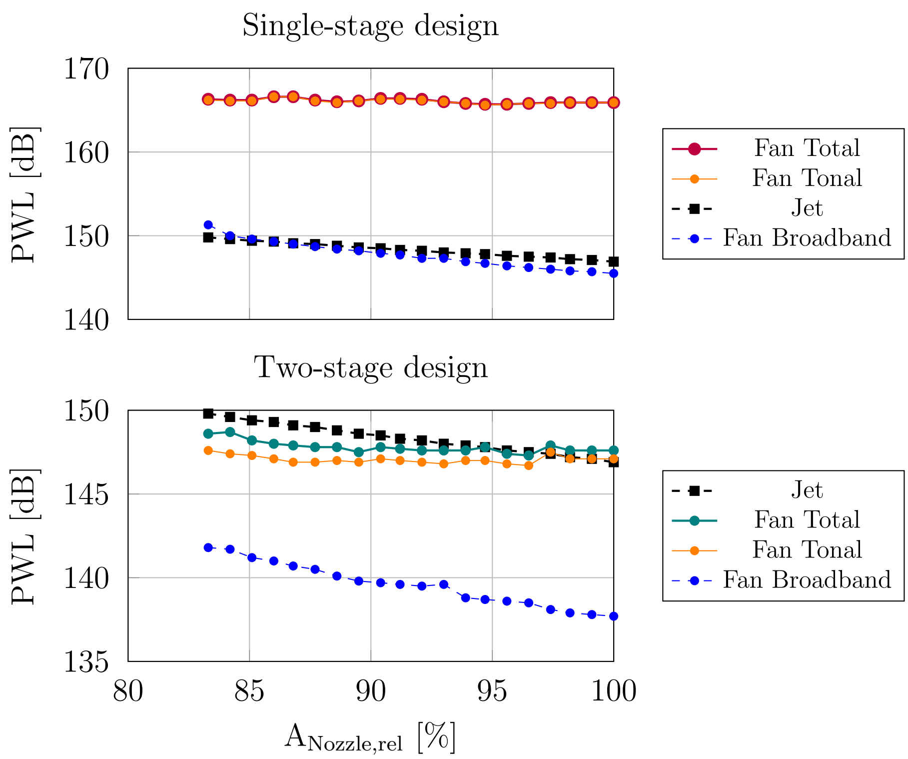

Figure 5.11: Fan and jet noise power levels over relative nozzle throat area

The lower jet velocity causes an approximately linear reduction in jet noise. The lower aerodynamic loading on the fan reduces broadband noise because the lower blade loading and lower incidences cause smaller, less turbulent wakes.

Tonal noise for both fans at this operating point is dominated by buzzsaw noise and exceeds the broadband fan noise significantly. Buzzsaw noise is not as sensitive to fan speed and blade loading, as was shown in the preceding subsections. This causes tonal noise to remain nearly constant for all nozzle positions.

Increasing the nozzle throat area A_{Nozzle} from 83.3% to its maximum reduces the jet noise PWL by 2.9 dB, the single-stage fan noise PWL by 0.4 dB and the two-stage fan noise PWL by 1.0 dB. At lower power settings, where buzzsaw noise is not dominant, an even bigger fan noise reduction can be expected. This is due to interaction noise being more sensitive to the nozzle setting, as is evident in the strong reduction in broadband noise for both fans.

An effect on flow stability is observed: Opening the nozzle reduced the maximum diffusion number on the rotors from 0.61 to 0.53 for the single-stage fan and from 0.58 to 0.48 for the two-stage fan. Rotor incidences were reduced from 6.4° to 4.2° and from 6.8° to 4.3° respectively. With a closed nozzle, neither fan has a significant surge margin. At lower power settings, where the surge margin is decreased even further, operating the fan with a closed nozzle would not be safe.

5.3 Process improvement through lessons learned

For the DLR project STORMIE, more supersonic aircraft fan concepts were designed. The lessons learned during the design process implemented in SENECA were applied.

Since the single-stage fan design proved to be less efficient and produces significantly higher sound power levels than the two-stage design, only a two-stage fan was developed.

To avoid a design too close to choking at the design point, each valid candidate's neighboring points on the throttle line were calculated and compared to the candidate. If a maximum FPR gradient was surpassed, choking as assumed, the candidate was automatically discarded.

The solidity of R1 of the SENECA design is very low. While it is enough to provide stable flow throughout the operating envelope in ideal conditions, it is not a realistic design: in real operating conditions a higher solidity would be required due to inflow distortions. They are expected to be significant due to the sharp inlet lip and high AoAs on landing and take-off. For the STORMIE design, more stringent solidity minima were set for the optimizer.

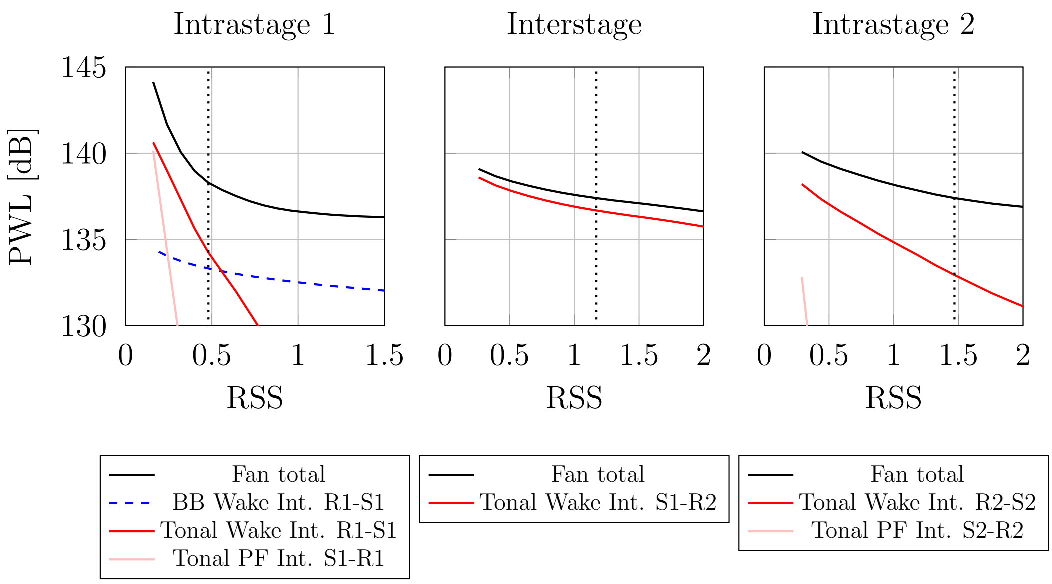

Figure 5.12: The sound power of interaction noise sources and total fan noise over axial distances, vertical lines mark the axial distance chosen for the final design

In line with the learnings presented in Section 5.2.2, the long axial distances between the rows were reduced based on an exploratory acoustic study. For the fan in landing operation, these rotor-stator spacings were varied individually (keeping the other RSSs constant at high values) and chosen to be as small as possible without incurring significantly higher interaction noise. The free-field sound power levels can be seen in Figure 5.12.

For both intrastage distances, there is a strong decline in tonal interaction noise, leading to a kink in the fan noise characteristic when other sources become dominant. The RSS corresponding to this kink was chosen in the final design. Due to a lack of cut-off effects for the interstage interaction noise, the reduction in sound power with increasing distance is more consistent. The axial distance selected in this case corresponds to the point at which the intrastage interaction noise sources with the final, reduced RSSs are at similar levels. The resulting rotor-stator spacings are: $\text{RSS}_{\text{intrastage 1}} = 0.48$, $\text{RSS}_{\text{interstage}} = 1.17$, $\text{RSS}_{\text{intrastage 2}} = 1.47$.

Chapter 6

Landing and Take-Off Noise Optimization

In this chapter, the certification noise levels of the of the SENECA M1.8 airliner are predicted. The methods and designs described in previous chapters are applied for this purpose. It is demonstrated that the airliner can achieve the *Chapter 14* limits.

After acoustic optimization was performed on a component level, the potential of advanced take-off procedures in the reduction of certification noise levels is investigated. To find their minimum, a take-off profile variation study exploring the individual aspects of variable noise reduction systems is performed.

A significant advantage of the two-stage over the single-stage fan design in acoustic performance was found in the preceding chapter. The two-stage fan will thus be used in the take-off profile variation study. To quantify impact of both fan designs on certification noise levels, a comparative study using two different take-off profiles is conducted as well.

The acoustic liner assumptions made in Section 3.2.4 are applied throughout this chapter. Their impact is investigated as part of an uncertainty study. This study addresses uncertainties inherent to the prediction of certification noise of an aircraft concept. Besides the impact of acoustic liners, the effects of airframe weight and aerodynamics modeling on certification noise levels are investigated.

6.1 Variable Noise Reduction Systems

Take-off procedures for subsonic aircraft are relatively simple but rigid: maximum thrust is applied until the rotation speed V_R is reached, the aircraft must climb with a speed exceeding the take-off safety speed V_2 by 10 to 20 kts and beyond the minimum cutback altitude, the pilot can manually cut back thrust, usually by approximately 25%. This will be referred to as a "standard take-off".

As explained in Chapter 2, supersonic aircraft have the highest thrust demand at the ToC or during cruise. Their engines can produce more thrust than necessary for a safe take-off. Due to this thrust surplus, the adjustment of take-off procedures with the goal of reducing environmental impact in a safe manner is possible. A take-off using these alternative procedures is referred to as an "advanced take-off". An adjustment of landing procedures, as was done for Concorde, is also feasible.

Since take-off and landing are critical phases of the flight with a high workload for the pilots, it was proposed to implement these adjustments without requiring pilot action as a variable noise reduction system. As defined by ICAO in its *Environmental Technical Manual* [191]: "A VNRS is an integral design feature, or subsystem, of an aircraft that automatically changes the configuration or operating condition of the aircraft to reduce noise." The system is intended to engage automatically with every operation and without the need of flight crew activation.

VNRS can be used during take-off, but also landing. *Concorde*, for example, started the landing sequence at high speed ($\approx$ 190 kts), slowing down to the landing speed of 160 kts only at 500 ft altitude (=152.4 m) [3]. This exploits the region of reverse command and allowed it to fly most of the landing sequence at lower thrust than on touchdown. The usefulness of VNRS in reducing certification noise at the Approach position is debatable due to time constraints: it is located only 2000 m from the threshold, where the flight altitude is only approximately 120 m (=394 ft). Supersonic aircraft are expected to have a high landing speed, so the time between passing the certification point and touchdown will not exceed 30 s. In this short time, the change from low-noise to landing configuration must be made, the aircraft trajectory stabilized and touchdown prepared. Because this does not appear to be achievable without jeopardizing safety, the use of VNRS during landing will not be discussed any further.

During take-off the use of VNRS can be separated into two categories: reducing engine noise through thrust management and adjusting the climb profile, and reducing airframe noise by optimized deployment of the landing gear and high-lift devices such as flaps and slats. Since no high-lift devices or landing gear were designed for the aircraft considered in this study[1] and the focus of this thesis is on engine noise, only thrust and climb management will be considered.

[1]Due to its conceptual design level

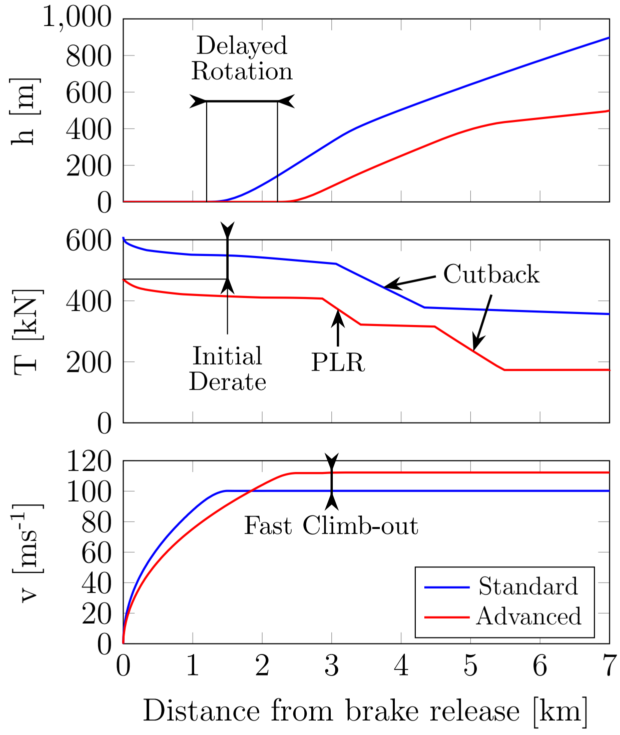

Figure 6.1: The elements of VNRS investigated in this thesis on take-off shown by comparing generic standard and advanced take-off profiles

The following measures can be implemented as part of a VNRS to reduce take-off engine noise, as depicted in Figure 6.1:

- Programmed lapse rate (PLR): after take-off, an automatic thrust reduction is triggered at a preset altitude. This happens before the manual cutback which must adhere to a minimum altitude. This measure of LTO noise reduction was first proposed by Grantham and Smith [25] and later described as PLR or auto-throttle take-off [192]. PLR usage can vary in activation altitude, thrust reduction, and spool rate. Here, it is applied as a thrust reduction relative to the thrust immediately before activation. While variations of the spool rate have been shown to affect certification noise levels by Berton [64], it will be fixed at 4%/s in this study for simplicity. It is the maximum rate as discussed in Chapter 4 and thus allows the quickest change between thrust settings. Berton found the optimum spool rate during PLR application for the *STCA* take-off profile to be only 2%/s.

- Fast Climb-out: to exploit the lower lift-dependent drag at higher speeds in the region of reverse command, a higher climb-out speed can be useful for SST. Higher speed also reduces jet noise by decreasing the speed difference between jet and ambient air. Climb-out speed is measured in surplus of the aircraft's take-off safety speed V_2. The advantages of this change in take-off procedures were first described by Berton [63].

- Delayed rotation: to more effectively exploit lateral attenuation, more thrust should be applied at low altitude. An extreme case is to continue the acceleration on the runway before a delayed rotation beyond the required lift-off speed. It will be defined as the difference between the aircraft's speed at the moment of rotation and the minimum rotation speed V_R. As for the fast climb-out, the delayed rotation take-off was first described by Berton [63].

- Initial derate: an engine derate for the entire take-off is beneficial. This is because the low BPR engines produce very high jet noise at full thrust. The available thrust with an open variable throat nozzle is limited due to the fan's choking margin which must be maintained. But without a further reduction, Lateral noise levels would be higher than necessary. Here, the derate is normalized as $\hat{T}_{rel}$ with the maximum thrust achievable with the engine at 100% fan speed, i.e. with a closed nozzle and the same fan speed as during ToC. Derated take-offs are also common for subsonic airliner and have been covered by regulations for decades [193].

- Closing fan inlet: if possible, all auxiliary openings in the inlet should be closed to provide better fan noise reduction through shielding and liners. No detailed inlet was available for this engine, so this aspect cannot be explored here.

The pilot-activated cutback should occur just before the Flyover point is reached to maximize its effectiveness. After that, the climb angle is reduced to the minimum 4% to reduce thrust demand. This aspect is identical for all profiles, so the thrust required after the cutback only depends on the drag incurred by the aircraft at a 4% climb.

Similar procedures were already applied to take-offs and landings of *Concorde*: at a predefined altitude, the afterburners were shut off to reduce community noise which leads to a thrust reduction similar to PLR. The manual activation however makes it closer in nature to a regular pilot-activated cutback. *Concorde* also reduced its speed very late during the landing sequence to reduce LTO noise, as described above.

6.2 Take-off variation study

To investigate the impact of VNRS on take-off certification levels, a series of take-off profiles of the SENECA M1.8 airliner were investigated. The results of such a study have already been published by Gräbert et al. [73], but the calculation have been redone with improved models, the results of which are shown here.

Five parameters were varied:

- PLR level: an automatic thrust reduction by 10, 20 and 30% compared to the thrust level immediately before PLR activation
- PLR activation altitude: 35 ft (minimum altitude) and 200 ft
- Climb-out speed: V_2+20 kts (current maximum permitted), V_2+40 kts, V_2+55 kts and V_2+72 kts. The last value corresponds to 250 kts, the absolute speed limit below 10,000 ft.
- Delayed rotation: acceleration on the runway past V_L, the minimum speed required for a safe lift-off. The maximum speed in excess of V_L depends on the individual take-off profile, so no no values could be predefined.
- Initial derate: three initial thrust levels, at 70, 59 and 53% of the maximum thrust were investigated. Thrust above 70% caused Lateral noise levels at break release which were too high, negating all optimization potential, an observation also made by Berton [64]. The reference maximum thrust is defined as the thrust of the engine at 100% fan speed with a perfectly expanded jet in sea-level static conditions. For this engine design, it cannot be achieved with an open nozzle position without choking the fan.

There are discussions in the community to limit the application of a delayed rotation to 205 kts due to tire design constraints [93]. For this study, only the 250 kts absolute speed limit was applied for multiple reasons:

- Even with limited applicability, the investigation of a wider parameter space in an academic study can show potential for LTO noise minimization in the future
- When entirely new aircraft are being developed, it is not improbable that a custom tire can be designed to withstand higher speeds
- The zero-growth tire design of *Concorde* still exists which is rated to 250 kts; it took off at approximately 220 kts [3]

The variation of five parameters normally entails the evaluation of a large number of different profiles. However, not all combinations allow a take-off that abides the certification trajectory restrictions: Thrust determines how much energy is available during take-off and can be converted into speed or climb performance. When reduced thrust is applied the minimum climb angle cannot always be maintained or the minimum cutback altitude not reached before the Flyover certification point, making the profile unusable for this study. In total, 58 profiles were investigated.

To evaluate the impact of the individual parameters, the cumulative, Lateral and Flyover margins to the certification noise limits are considered. The impact of the individual parameters on the take-off profile and thus certification noise levels are interdependent, but an attempt is made to isolate the effects of each parameter. The full results of this study can be found in Appendix I.

6.2.1 PLR

The impact of PLR on certification levels is shown in Figure 6.2. It is clear that there is a trade-off between Lateral and Flyover certification noise when applying PLR: the lower thrust with increasing PLR levels reduces Lateral noise significantly, but also impacts climb performance negatively. This leads to a lower altitude at the Flyover point and higher noise levels as a consequence.

The advantages for Lateral levels are higher for earlier activation: 35 ft activation height produce higher margins than 200 ft. Because of the maximum spool rate, the thrust reduction is not instant, so the noise benefits of PLR cannot be fully exploited with late activation. Stronger engine noise while the engine is still spooling down causes higher Lateral levels, especially for higher PLR levels for which the spool-down takes longer. This can be seen by the widening gap with increasing PLR levels between the Lateral certification noise levels of 35 ft and 200 ft activation height.

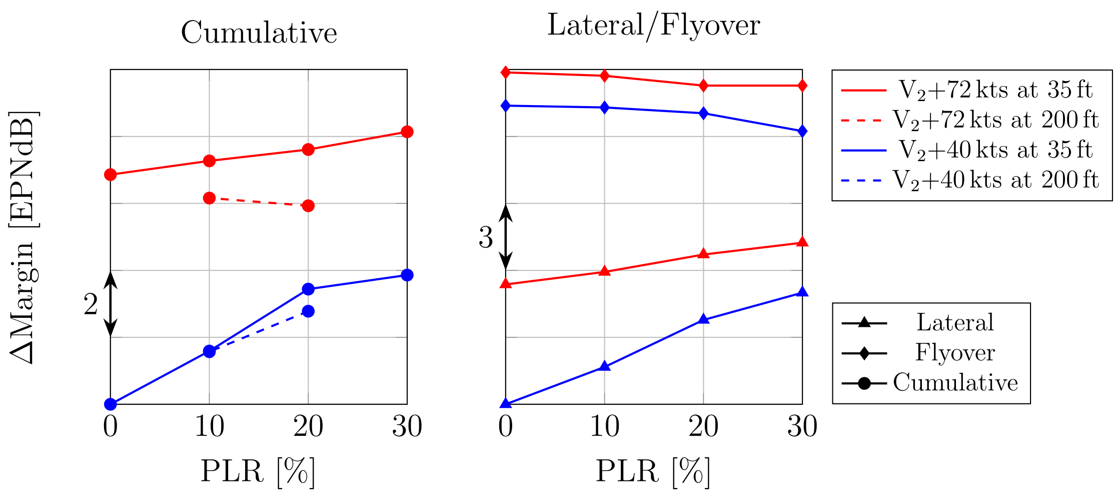

Figure 6.2: Impact of PLR variation for several profiles with the maximum derated take-off thrust (70% $\hat{T}_{rel}$)

The certification noise of take-off profiles with higher climb-out speeds is more thrust sensitive, since their climb is already shallower than for lower speeds. Any reduction in thrust reduces the altitude at the Flyover point (and thus distance to it) even more. For this reason, the benefit of PLR is not as significant for the V_2+72 kts profiles when compared to V_2+40 kts. For the profiles with V_2+72 kts and PLR activation at 200 ft, the benefit in Lateral levels is even smaller than the cost at Flyover, leading to a slightly reduced cumulative margin with higher PLR levels.

Overall, PLR has a positive impact on cumulative certification noise levels, especially when activated at low altitude. The impact is stronger for slower climb-outs.

6.2.2 Fast climb-out

The climb-out speed variation presents another energy trade-off between speed and altitude: to achieve higher speeds, the climb angle must be reduced, especially when thrust lower thrust is applied. This means that only profiles with the highest thrust at break release can achieve a climb-out speed of 250 kts without violating the minimum climb angle or cutback altitude.

As can be seen in Figure 6.3, the shallower climb does not negatively affect Lateral noise levels, because these levels are achieved around a similar altitude, independent of the longitudinal position and thus the climb angle. Higher speed leads to an improved glide ratio, reducing the thrust demand. Furthermore, jet noise is reduced, because there is a smaller velocity gradient between jet and ambient air. Consequently, Lateral certification noise margins increase almost linearly with higher climb-out speed.

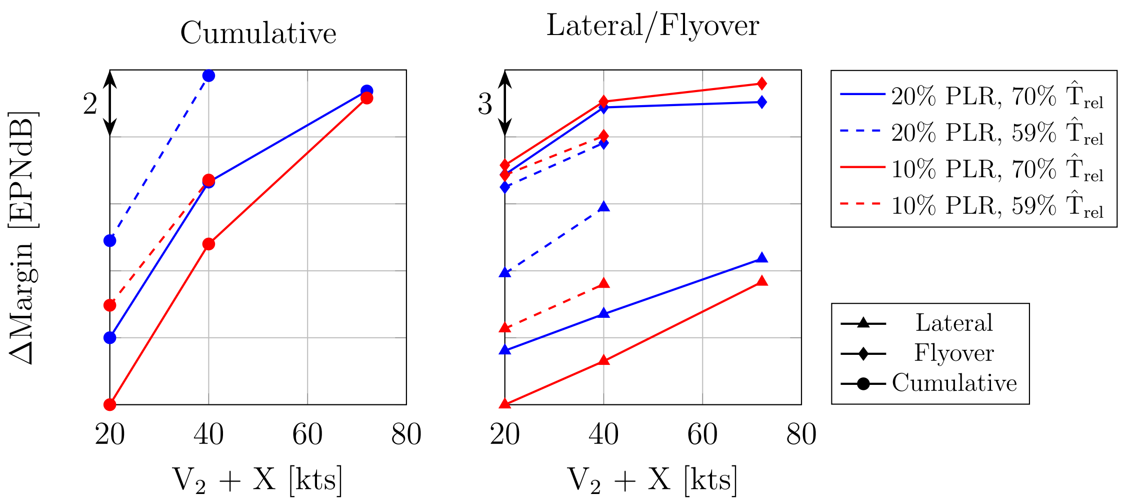

Figure 6.3: Impact of climb-out speed variation for several profiles with PLR activation at 35 ft

While less thrust is required for the 4% climb after cutback at the Flyover location with higher speed, the shallower climb also leads to a reduced altitude. This trade-off is decreasingly favorable with increasing climb-out speeds, leading to plateauing Flyover certification levels past 40 kts V_2 excess.

Overall higher climb-out speeds up until the speed limit of 250 kts increase cumulative certification margins, but the advantage diminishes with higher climb-out speeds.

6.2.3 Delayed rotation

A delayed rotation is implemented to further exploit both the region of reverse command and lateral attenuation by accelerating on the runway. Accelerating to a higher speed improves the glide ratio at lift-off. Higher altitude or speed can be reached through the longer application of high thrust before the activation of PLR and climbing out of the strongest lateral attenuation effects.

As can be seen in Figure 6.4, the advantage of a delayed rotation is minimal for lower climb-out speeds: the climb angle is steeper, a higher altitude is reached at the Flyover point and the additional altitude advantage gained by applying high thrust for a longer time is less significant. Furthermore, less in-air acceleration is required, so the aerodynamic advantage is only exploited briefly. Therefore, neither Lateral nor Flyover levels are impacted in a meaningful capacity.

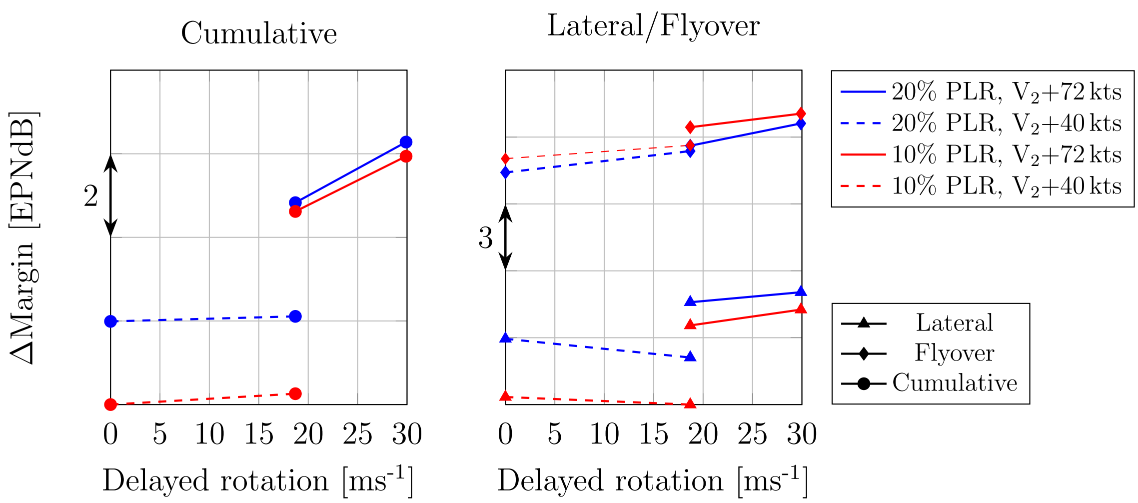

Figure 6.4: Impact of delayed rotation for several profiles with the maximum derated take-off thrust (70% $\hat{T}_{rel}$)

For high climb-out speeds, the increase in Flyover altitude through better thrust management is significant and helps increase the margins there. It also increases Lateral margins, because the aircraft passes the Lateral certification points at higher speed, reducing jet noise and thrust demand. To reach the maximum climb-out speed while applying PLR, a delayed rotation becomes necessary, since otherwise climb and acceleration could not be maintained.

6.2.4 Derate

As shown in the previous sections, thrust reduction and higher speeds increase cumulative certification margins. To achieve both the minimum climb requirements, a high speed and a PLR level at low altitude, higher initial thrust is necessary. All aspects of VNRS are interdependent, in particular with derated take-off thrust. Hence, a parametric study as those shown in the preceding sections is not practical. Higher initial thrust causes more noise but allows a better exploitation of other VNRS effects and vice-versa. For this reason, the take-off profiles with the highest cumulative margins are compared for the three selected derate settings. The results can be seen in Figure 6.5.

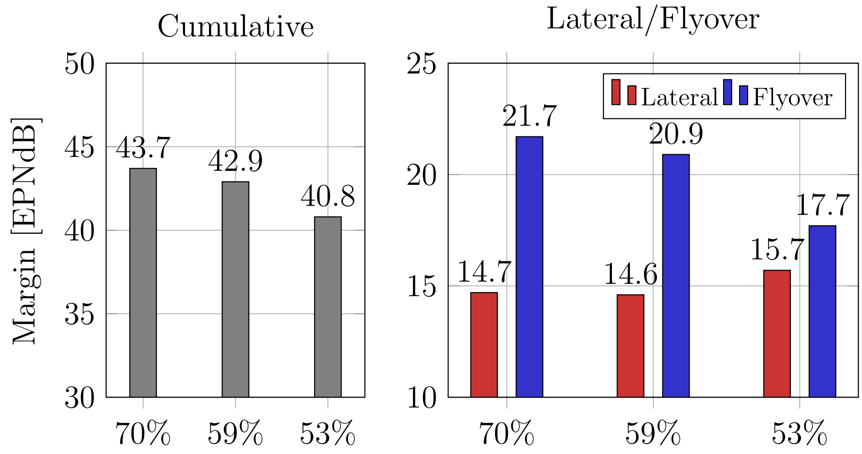

Figure 6.5: Lateral, Flyover and cumulative certification noise levels and margins of the best profiles for each derated thrust setting:
70% $\hat{T}_{rel}$, 30% PLR at 35 ft, V_2+72 kts, max. delayed rotation
59% $\hat{T}_{rel}$, 0% PLR, V_2+55 kts, max. delayed rotation and
53% $\hat{T}_{rel}$, 0% PLR, V_2+40 kts, max. delayed rotation

Despite the different parameters of the profiles, a general trend can be observed: the lower initial thrust and thus lower thrust after PLR application leads to higher Lateral margins, but reduces the margin at Flyover due to the worse climb performance. This trade-off favors higher initial thrust, leading to lower cumulative certification noise levels. The highest cumulative margins are achieved when the effects of PLR, fast climb-out and delayed rotation are fully exploited.

6.2.5 Conclusion

The profile with the lowest cumulative certification level is the profile with: 70% $\hat{T}_{rel}$, 30% PLR activated at 35 ft with a climb-out speed of V_2+72 kts. It produces a cumulative certification margin of 43.7 EPNdB. Figure 6.6 shows a significantly reduced noise footprint associated with this take-off profile when compared to that of a standard take-off.

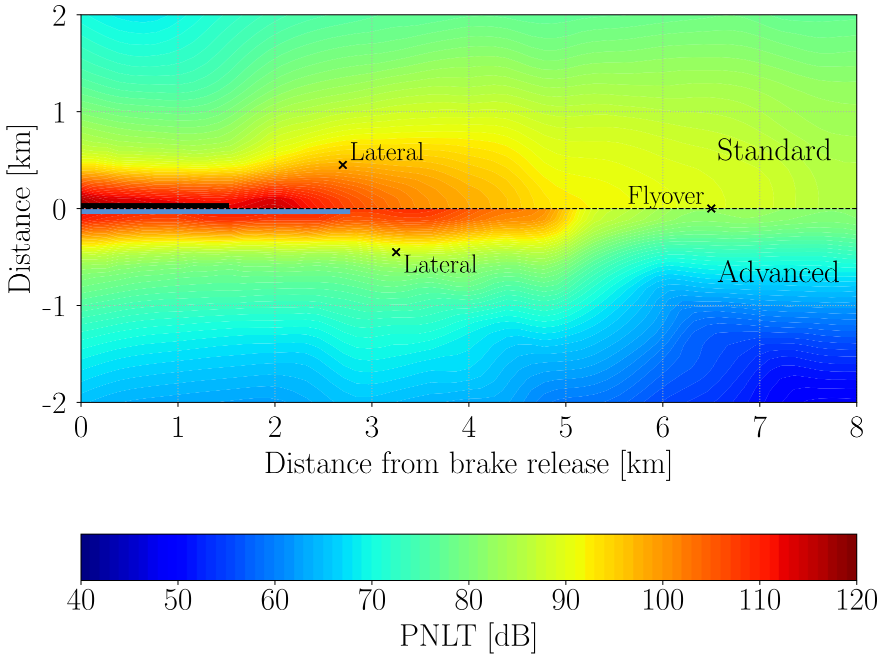

Figure 6.6: Map showing the noise footprint of the 100% $\hat{T}_{rel}$ standard take-off and optimal advanced take-off, used runway length and certification points included

While it is difficult to compare these results to supersonic aircraft certification noise studies using different aircraft and engine designs, a general agreement in trends and overall results should be sought. The studies conducted by NASA, DLR and JAXA are using supersonic business jet designs [56, 57, 58, 62, 63, 64, 65, 66, 67], so they are not fully comparable, but because noise limits scale with weight, no enormous differences in margins are to be expected. Studies with other supersonic airliner designs are more relevant, such as those conducted by Georgia Tech [59], Blue Ridge Research [60] and Cranfield University [76].

The trends found in both business jet and airliner profile variation studies generally agree well with those found here. They confirm the trade-off between Lateral and Flyover certification noise levels and the effectiveness of VNRS. The Georgia Tech study, which fields the aircraft with the most comparable mission to the SENECA M1.8 airliner, shows different trends with regards to climb-out speed, finding that an increase reduces the cumulative margins. However, the aircraft is much heavier which is a possible explanation for the lower certification noise margins and has much larger wings than the M1.8 airliner, which likely reduce the minimum drag speed and thus effectiveness of a fast climb-out.

The absolute margins at all three certification points, as well as the cumulative margins are very high for the SENECA M1.8 airliner. This is particularly obvious when comparing them to the much smaller margins predicted by other researchers. The cumulative margins for other airliner designs are 6.1 and 4.1 EPNdB for the Georgia Tech Mach 1.7 and Northrop Grumman Mach 2.0 airliner designs respectively. While no cumulative margin was calculated for the Cranfield Mach 2.2 airliner[2], the take-off certification levels indicate a similarly low cumulative margin. High cruise Mach numbers aggravate the effects of design constraints discussed in Chapter 2, so lower margins can be expected for designs with a higher cruise Mach number, but this does not fully explain the difference in certification noise margins. Design differences offer possible explanations: The engine cycle of the SENECA M1.8 airliner was designed to minimize take-off noise, which is not explicitly stated about the other designs. Furthermore, no other study states the consideration of a two-stage fan design; NASA and DLR explicitly assume a single-stage fan. Furthermore, design assumptions for the SENECA M1.8 airliner and their impact on LTO noise must be examined.

For this reason, the impact of fan design, aircraft weight and aerodynamic performance on certification noise levels were investigated. The results of these studies are shown in the following sections.

6.3 Single- and two-stage fan designs

As shown in the previous chapter, the fan concept has a significant impact on engine noise emissions. To evaluate the impact on certification noise levels, flyby simulations were conducted with both the single- and a two-stage fan concept. Lateral and Flyover certification points on a standard and an advanced take-off profile and the Approach point were investigated. The final fan designs presented in the previous chapter were used in this study. Jet noise is included in all calculations to show the realistic impact of fan designs on LTO noise instead of isolated fan noise emissions. The results of a similar study have been published by Gräbert et al. [194] but calculations have been rerun with improved models and a more realistic standard take-off profile was chosen. The fan and jet noise calculations are conducted on a discretized profile with discrete operating points,

[2] The Approach certification point was not investigated

so artifacts of this discretization remain in the results. Preliminary studies with smaller time steps show that this only has a negligible impact on certification noise levels.

The resulting certification levels and their differences are shown in Table 6.1. The impact of the fan concepts on certification noise levels is investigated in more detail in the following sections. The engine operating points are provided. The time series of sound pressure levels (SPL) of fan noise sources for both designs and jet noise as well as the respective resulting tone corrected perceived noise levels (PNLT) are also shown and discussed.

	Two-Stage	**Single-Stage**	**Difference**
Approach	80.2	86.2	6.0
Standard Lateral	90.8	91.2	0.4
Standard Flyover	88.8	89.2	0.4
Standard Cumulative	259.8	266.6	6.8
Advanced Lateral	83.4	83.5	0.1
Advanced Flyover	77.3	86.0	8.7
Advanced Cumulative	240.8	255.7	14.9

Table 6.1: Certification noise level predictions for both fan concepts in EPNdB

6.3.1 Approach

	Single-Stage	**Two-Stage**
$\mathbf{T_{rel}}$ [%]	14.4	
FPR	1.17	
$\mathbf{M_{jet}}$	0.45	
$\mathbf{n_{rel}}$ [%]	50.9	52.0
Rotor (1) $\mathbf{M_{tip,rel}}$	0.82	0.64
Rotor inc [°]	6.3	7.1
Rotor $\mathbf{A_{wake}}$	0.063	0.047
Wake $\mathbf{TKE_{mean}}$ [$\mathbf{m^2s^{-2}}$]	161.7	67.1

Table 6.2: Approach operating point parameters

The landing profile is fixed at a 3° descent angle with a quasi-static engine operating point. The relevant engine and fan operation parameters representative of the Approach certification point are listed in Table 6.2. The relative LTO thrust[3] is very low, with

[3]Meaning relative to the maximum thrust available with a fully open nozzle

the engine operating in idle conditions. As discussed earlier, this entails high front rotor incidences which lead to very pronounced, turbulent wakes, making wake interaction noise the dominant engine noise source.

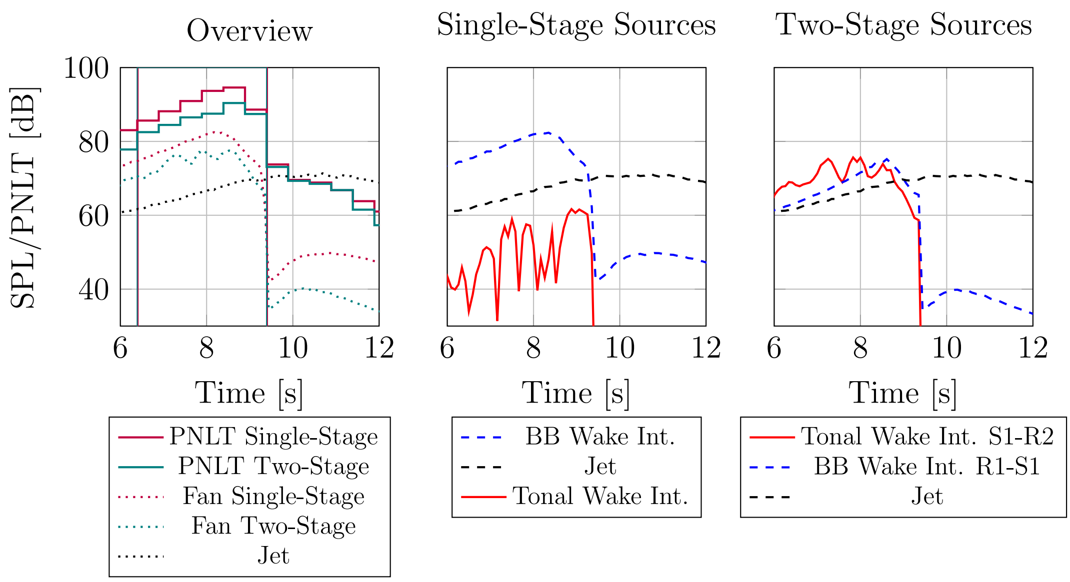

Figure 6.7: SPL on Approach, with 10 dB-down time indicated

The time series of SPL and PNLT of both fans can be seen in the left-hand plot of Figure 6.7. The vertical lines frame the 10 dB-down time, inside which PNLT is integrated to EPNL. The individual noise sources for both fan designs are analyzed in the center and right-hand plots.

The difference in liners attenuation between up- and downstream radiating fan noise is immediately obvious: fan noise arriving at the observer position after the moment the aircraft passes over it, i.e. the downstream radiated fan noise, is attenuated much more effectively due to the long bypass. The directivity characteristic of fan noise is strongly shifted towards upstream radiation as a consequence.

It can easily be seen that PNLT is driven by fan noise, since jet noise is a low-frequency broadband noise source which is penalized much less in the PNLT metric than higher frequency fan noise with tonal aspects. This leads to a significant difference in certification noise between both fan designs.

As discussed in Chapter 5, the single-stage fan's longer rotor chord length causes stronger turbulence, as evidenced by the higher TKE_{mean}, which leads to stronger broadband wake interaction noise. At low thrust, the cut-off design of the single-stage fan is effective. Since a cut-off design could not be achieved between the stages of the two-stage fan, the interstage tonal wake interaction noise remains strong even at low thrust. The tonal noise of both fans shows a strong oscillation pattern due to lobes in the directivity characteristic and interference of direct and reflected noise signals at the observer position. Overall, the single-stage fan noise is significantly stronger, causing the higher Approach certification noise level.

6.3.2 Take-off

To evaluate the impact of fan concepts on take-off certification noise, both a high thrust standard take-off and an advanced take-off using VNRS are investigated.

Standard take-off

A take-off with a constant 80% T_{rel} was chosen as a standard take-off profile. It is representative of current take-off procedures, where the maximum available thrust is applied and maintained until well into the climb segment of the flight. While the engine can produce more thrust in principle, this is considered unrealistic, because the open nozzle causes the fan to be choked under maximum power as was shown in Figure 5.7.

	Lateral		Flyover	
	Single-Stage	**Two-Stage**	**Single-Stage**	**Two-Stage**
$\mathbf{T_{rel}}$ [%]	80.0			
FPR	1.78		1.83	
$\mathbf{M_{jet}}$	0.91		0.94	
$\mathbf{n_{rel}}$ [%]	93.3	94.1	90.8	92.7
$\mathbf{M_{tip,rel}}$	1.60	1.27	1.55	1.23

Table 6.3: Parameters of standard take-off operating points

Aerodynamic parameters at operating points representative for the Lateral and Flyover certification points are listed in Table 6.3. In high thrust operation, the dominant noise sources are buzzsaw and jet noise. Buzzsaw noise is tonal and is heavily attenuated by the liners, making jet noise dominant over fan noise. This can be seen in Figures 6.8 and 6.9. Since the operating points and qualitative trends are very similar for Lateral and Flyover certification points, they are not discussed separately.

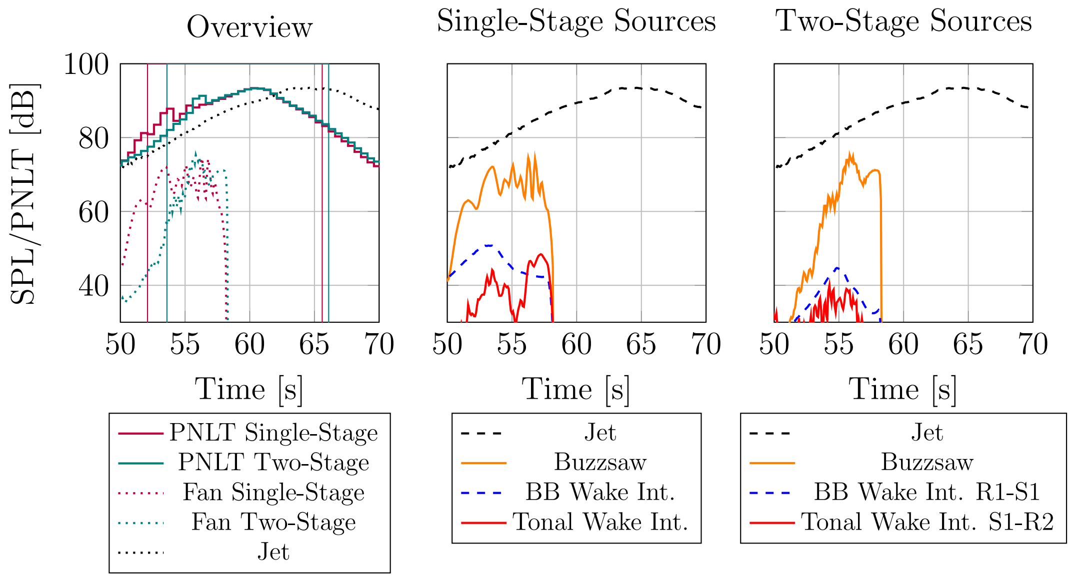

Figure 6.8: SPL on standard take-off at Lateral point with 10 dB-down time indicated

There is a time difference between the peaks of jet and fan noise due to jet noise radiating primarily downstream and fan noise radiating primarily upstream. Consequently, PNLT is only affected by fan noise in the first segment of the 10 dB-down time and the impact of fan noise on EPNL is very small. Fan noise for both designs is completely dominated by buzzsaw noise which displays an interference pattern. Because jet noise is dominant, the buzzsaw noise has a minor impact on PNLT and there is only a small difference in Lateral and Flyover certification noise between the single- and two-stage fan concept.

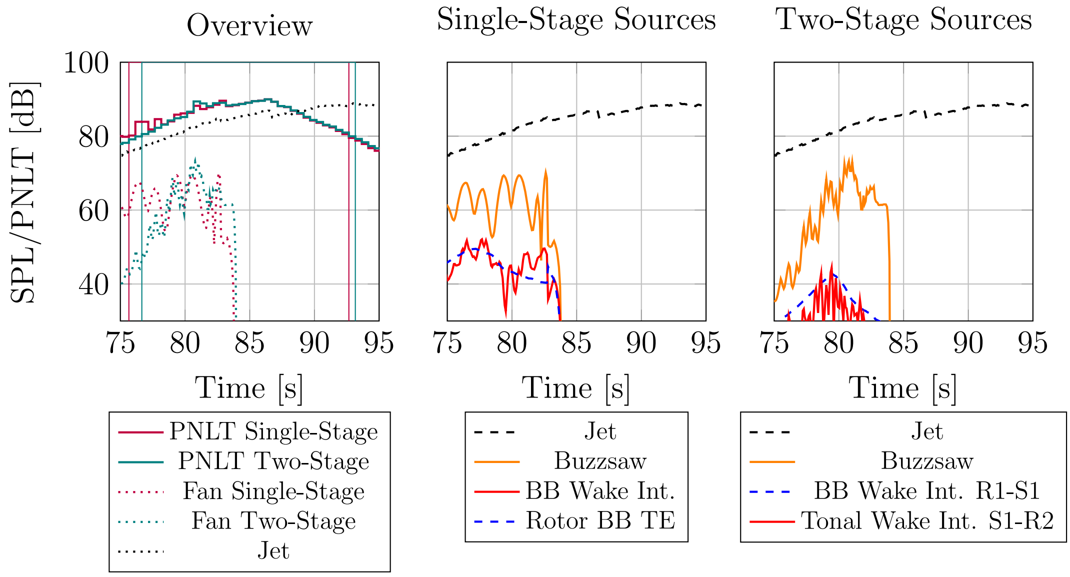

Figure 6.9: SPL on standard take-off at Flyover point with 10 dB-down time indicated

Advanced take-off

The optimum profile found in the VNRS study (see previous section) using the two-stage fan is used as the advanced take-off profile. Thus, a larger advantage of that design is to be expected. The advanced take-off is much shallower and at lower thrust than the standard take-off. The acoustic benefit of this profile relies on weaker noise level at source when passing the certification points, since the distance between engines and observer is reduced. The lower thrust makes fan noise more relevant to certification noise levels. As explained in Chapter 4, the position of the Lateral certification point is variable and depends on the position of the PNLT peak. This is relevant here, because the two fan designs have different Lateral certification points due to their different noise characteristics. The Lateral certification point of the two-stage fan is 1150 m beyond that of the single-stage design. Aerodynamic parameters at representative operating points are listed in Table 6.4.

	Lateral		Flyover	
	Single-Stage	**Two-Stage**	**Single-Stage**	**Two-Stage**
$\mathbf{T_{rel}}$ [%]	49.6	76.3	31.4	
FPR	1.52	1.75	1.37	
$\mathbf{M_{Jet}}$	0.79	0.92	0.68	
$\mathbf{n_{rel}}$ [%]	81.2	93.6	71.3	72.2
$\mathbf{M_{tip,rel}}$	1.34	1.25	1.16	0.92

Table 6.4: Parameters of representative operating points at certification points on the optimized take-off profile

The relative thrust when passing the Lateral points is different for both fan concepts. PLR thrust reduction is in effect for the single-stage concept, while the spool-down has just started for the two-stage concept. The medium and high thrust operation respectively means that buzzsaw noise is at peak power for both designs, as shown in Chapter 5.

As can be seen in Figure 6.10, fan noise influences PNLT significantly for both designs. For a short period, fan noise is even dominant over jet noise in SPL for the single-stage design, i.e. before frequency weighting and tone correction are applied.

Jet noise is the dominant broadband noise source throughout the entire flyby. The dominant fan noise source for both designs is the tonal buzzsaw noise, which is heavily penalized in PNLT. The buzzsaw noise of the single-stage design has a marginally higher sound power and causes higher SPLs than of the two-stage design. The different evolution of jet noise favors the single-stage fan and negates the difference in Lateral certification noise levels between the fan concepts.

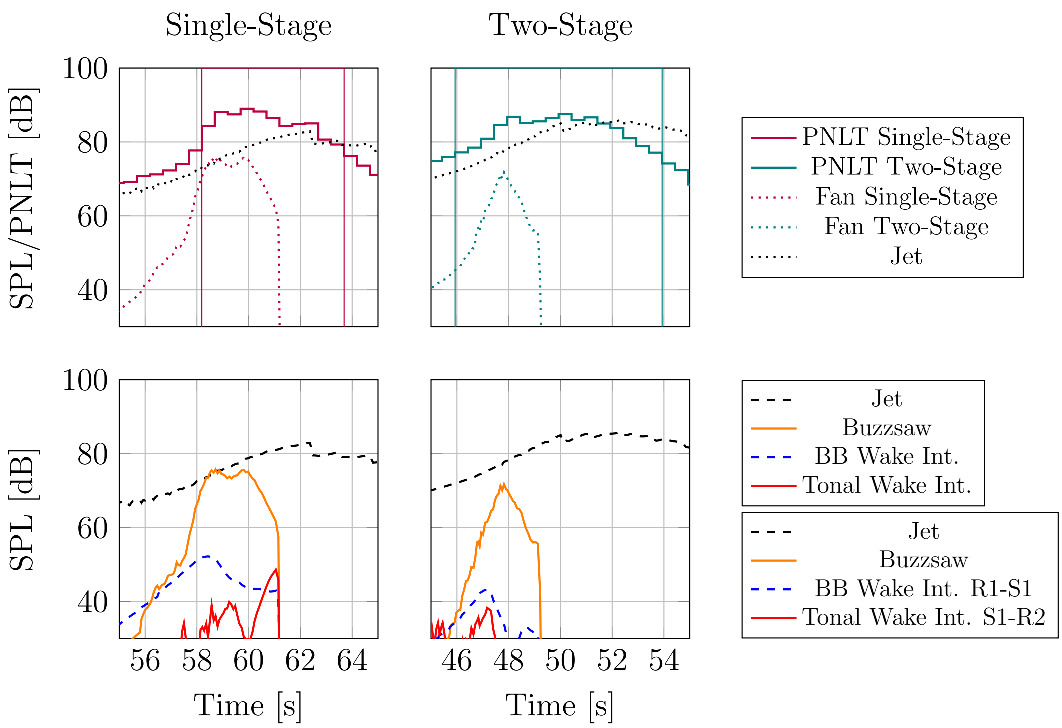

Figure 6.10: SPL on advanced take-off at Lateral point with 10 dB-down time indicated

The rotors are transonic, so interaction noise would experience significant rotor shielding and would not be able to propagate towards the inlet plane in reality. For the two-stage design rotor 2 is transonic as well, so even noise sources in the interstage domain which propagate downstream would be shielded. Since interaction noise is not dominant here, the lack of a rotor shielding model has no effect on the certification noise levels.

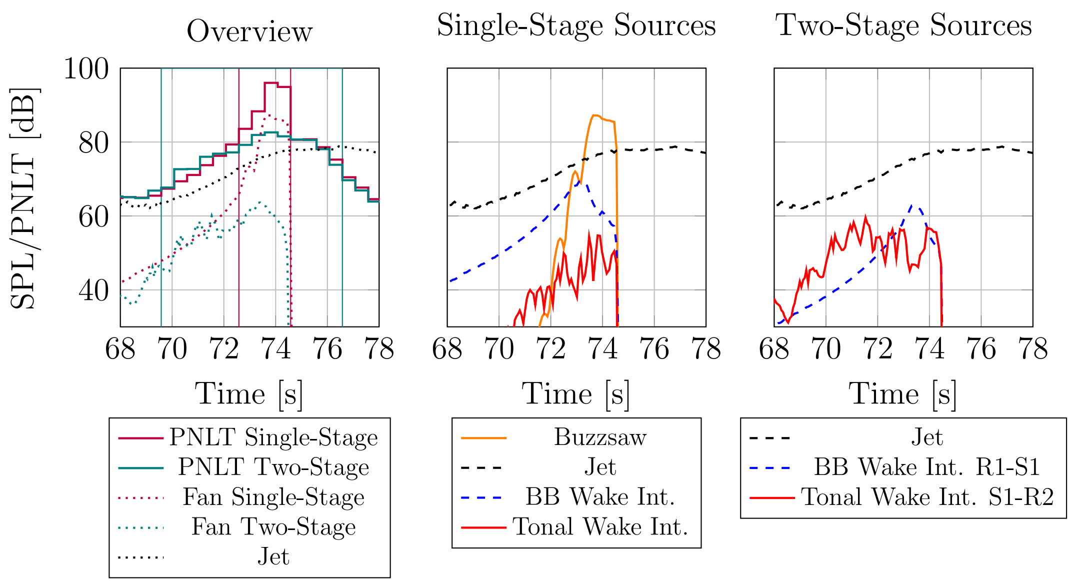

Figure 6.11: SPL on advanced take-off at Flyover point with 10 dB-down time indicated

Due to the high speed of 250 kts and shallow climb angle of 4%, the thrust when passing the Flyover point is low. Jet noise is the dominant broadband noise source for both concepts. The tip Mach number of the single-stage concept is just high enough to make buzzsaw noise the dominant noise source. Due to a pronounced lobe in directivity characteristic, it causes a short peak inside the 10 dB down time as illustrated in Figure 6.11. Buzzsaw noise for the two-stage design is non-existent as both rotors are subsonic (see Table 6.4). The two-stage fan PNLT at the Flyover point is dominated by jet noise and tonal wake interaction noise. Due to the absence of buzzsaw noise, the Flyover certification noise levels of the two-stage fan are significantly lower.

6.3.3 Conclusion

The choice between a single- and a two-stage fan concept has a significant impact on certification noise levels. The magnitude of this impact depends on the thrust level: at high thrust, jet noise is dominant and both fans produce buzzsaw noise, which leads to small differences between the concepts. At lower thrust levels, the differences are more significant, because the impact of fan noise increases. At medium thrust, the single-stage design causes buzzsaw noise, while the two-stage rotors are fully subsonic. This causes much higher certification noise for the single-stage concept. At low thrust, the wake interaction noise of the two-stage design is significantly weaker, causing reduced certification noise levels when compared to the single-stage concept. With the advanced take-off procedure, an advantage of almost 15 EPNdB was predicted for the two-stage design.

6.4 Uncertainties

The prediction of certification levels relies purely on models, from the design of the airframe over the engine models to the noise generation and propagation simulation. Especially on this early concept or pre-design level, the results of these models have significant uncertainties. This could be a cause of the surprisingly low certification levels[4] predicted for the SENECA M1.8 airliner in this chapter.

To explore the impact of different noise models, a comparative study within SENECA was conducted. The certification noise results of the 58 profiles presented in the preceding section were compared to those obtained by researchers of the National University Kyiv

[4]Even when considering the noise-focused aircraft and engine design.

Aviation Institute (NAU) and Royal Netherlands Aerospace Centre (NLR) with their respective models [195]. The different models used are listed in Table 6.5:

	DLR	NAU	NLR
Jet Noise	Stone '83 [152]	Stone '04 [155]	Stone '83
Fan Noise	PropNoise	Kontos [37]	Kontos
Airframe Noise	-	Fink [98]	-
Installation Effect	AIR 5662 [177]	-	AIR 5662
Atmospheric Absorption	ISO 9613-1 [176]	ARP866-A [196]	ARP866-A
Lateral Attenuation	AIR 5662	Soroka [197]	Soroka

Table 6.5: Noise source and propagation models used by SENECA partners

A detailed comparison of the models is out of scope for this thesis, so the differences will only be summarized and explained in brief. The trends shown in the preceding section were confirmed by NAU and NLR, showing a good agreement when comparing the certification noise level differences from profile to profile. The absolute predicted Flyover certification noise levels are very similar, with NAU predicting 0.45 EPNdB lower levels on average and NLR predicting 1.18 EPNdB higher levels on average. There are larger differences in Lateral certification levels, which were found to be caused by differences in lateral attenuation modeling. NAU predicting 5.08 EPNdB and NLR predicting 3.69 EPNdB higher Lateral levels on average.

While these differences are not insignificant and mean that the impact of lateral attenuation modeling must be investigated in more detail, they do not explain the large margins to Chapter 14 limits found in the VNRS study. This points to causes in the input data which NAU, NLR and DLR shared. Three parameters were identified which may have been modelled too advantageously when compared to other SST LTO research:

- Weight: Predicting the weight of an aircraft in a new design space is inherently difficult, since it is unclear which materials and technologies can be applied. Comparing the M1.8 airliner's weight to designs with similar missions, its weight is relatively low (see Table 1.1).

- Aerodynamic efficiency: The maximum glide ratio of the airliner in question during take-off varies between 9 and 14 depending on the profile. These glide ratios can theoretically be reached by a delta wing design with high lift devices but only in low lift operation. For take-off, glide ratios of 5-6 are more realistic, as demonstrated by Kirz et al. [93]

- Liner effectiveness: While the effectiveness of the liners of reducing tones by 20 and broadband noise by 10 dB/(l/d) is possible in principle, it is likely not realistic for the application chosen here. Attenuating all tones and broadband noise across the entire frequency spectrum is impossible in real-life applications. Furthermore, the long intake causes a thick boundary layer, which deviates sound energy away from the wall and reduces liner effectiveness on upstream propagating noise significantly, as demonstrated by Gabard [198]. The shallow nacelles limit liner depth and the area where they can be applied. Liners are less effective in attenuating noise propagating downstream, which was also neglected in the initial liner assumptions. This all means that a realistic attenuation is likely much lower, particularly in the bypass and does not scale linearly with inlet and bypass length. As demonstrated by Page et al. [60], liners have a big impact on predicted certification noise levels.

For this reason, penalties were applied to these parameters in realistic ranges and their impact on certification levels studied. Only the two-stage fan design was considered here. For significantly different aircraft weight or glide ratio, the engines including the fans would have to be re-designed. Since this is out of scope for the thesis, weight and glide ratio were only manipulated for LTO operations and no other possible consequences considered.

Predicting the LTO noise impact of an engine re-design, making it more powerful, is difficult since it depends on the specific cycle design. If a higher mass flow can be provided at identical thrust, both FPR and jet velocity are reduced. This is generally beneficial to fan and jet noise. If the engine diameter is unchanged, the design FPR will be higher, meaning the fan operates at lower relative thrust, likely making it noisier than the current design: At high thrust with an open nozzle the current fan operates close to the choking line, which is not desirable for stability and efficiency, but advantageous for fan noise as shown in Chapter 5.

6.4.1 Weight and aerodynamic penalties

The penalties were applied in two different fashions: reducing climb performance while maintaining the same thrust, and increasing thrust to follow the same flight profile.

For the first case, a profile with a steep initial climb angle is required to not violate the 4% minimum climb rate. For this reason, the standard take-off at a constant 80% relative LTO thrust was chosen.

To evaluate the impact of adjusted power settings to compensate for reduced aerodynamic performance and increased weight, a profile with low initial thrust is required.

Otherwise, the engine's operating envelope is exceeded. The optimal profile found in the VNRS study was chosen as the advanced take-off profile for this purpose. For the Approach point, the landing profile is fixed, so only the thrust can be adjusted.

For quasi-static operation, such as the landing sequence and the 4% climb after cut-back, both weight and glide ratio penalties require an identical increase in thrust to provide sufficient lift. For dynamic operation during take-off, the thrust increase will be higher for the weight penalty, because in addition to providing higher lift to maintain steady flight, lateral and horizontal acceleration must be provided.

Degraded climb

As discussed before, the Lateral certification level depends mostly on the engine operation and much less on the geometric flight profile. The certification point will move to where the aircraft reaches the critical altitude where radial spread, atmospheric dampening and lateral attenuation provide a minimum in overall attenuation. Even with a reduced climb performance, no significant changes in the Lateral certification levels can be expected for this reason.

At the fixed Flyover point, the different flight altitudes play a significant role, so higher certification levels are expected with the application of penalties.

These trends can clearly be seen in Figure 6.12.

The reduced certification margins are only due to a shorter propagation distance between aircraft and certification point, with engine noise at source being unaffected. Since the propagation attenuation effects have already been covered in Chapter 4, these results are neither interesting from an aeroacoustic point of view nor unexpected and will not be elaborated on.

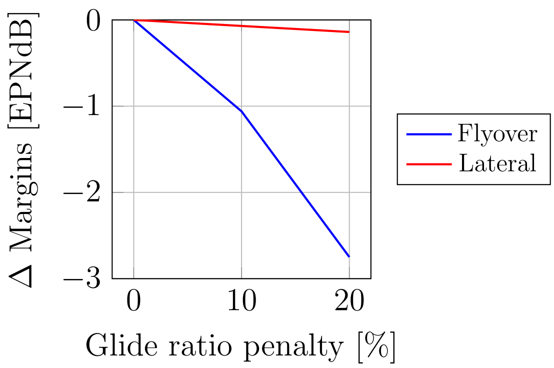

Figure 6.12: Change in certification margins for a degraded glide ratio on a standard take-off profile

Increased thrust

Changing the thrust along the optimized take-off profile warrants a more detailed investigation, since it directly impacts engine noise at source. As shown in Section 3.2, the increased thrust leads to higher fan and jet noise in principle. To evaluate the impact on certification noise, a study of the changes to the individual sources is necessary.

For the **Lateral certification point**, Figure 6.13 shows the time series of engine PNLT and the SPL of the relevant noise sources, buzzsaw and jet, at the observer position within the 10 dB-down time.

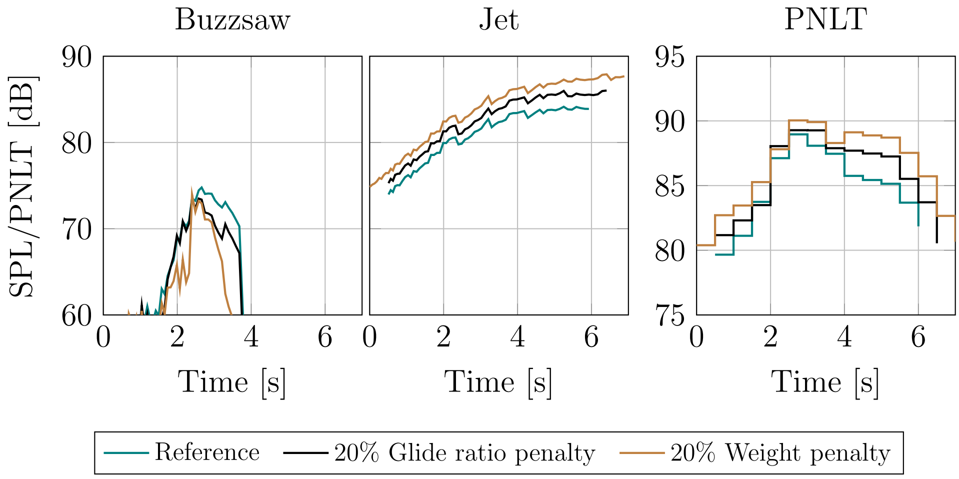

Figure 6.13: Dominant noise sources and PNLT at the Lateral point inside the 10 dB-down time, 20% glide ratio, and weight penalties applied

As shown in the preceding section, the fan noise of the two-stage design only has a small impact on Lateral certification noise. Buzzsaw noise displays a different evolution over time for each scenario, due to small changes in its directivity, but the peak pressures are not very different. This leads to only small changes in PNLT between 2 and 4 seconds which do not significantly impact the resulting EPNL.

As previously established, jet noise increases with higher thrust. Since the thrust increase is higher with the 20% weight penalty, there is an even larger increase observed for this scenario when compared to the reduced glide ratio. This drives an offset in PNLT which leads to a reduction in Lateral margins.

For the **Flyover point**, times series of PNLT and SPLs inside the 10 dB-down time are shown in Figure 6.14. After cutback, at a constant climb angle, there is a much smaller difference in thrust between the weight and glide ratio penalty scenario.

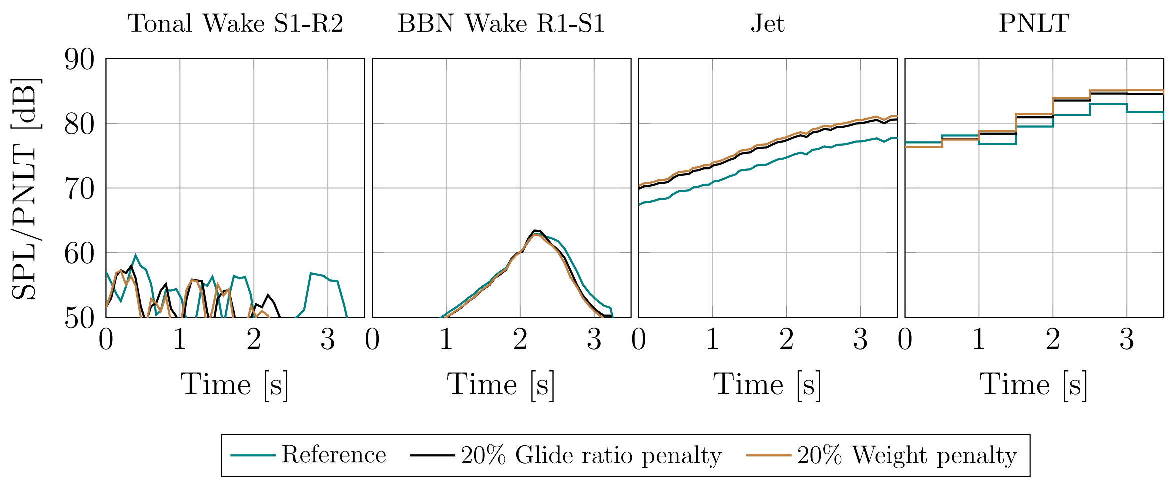

Figure 6.14: Dominant noise sources and PNLT at the Flyover point inside the 10 dB-down time 20% glide ratio and weight penalties applied

The fan noise sources have little impact on certification noise levels, so while there are some differences in the tonal noise, they have no significant impact on PNLT. These differences are mostly due to different interference and directivity patterns which are caused by the differences in fan speed between all scenarios.

Jet noise is increased for the penalized scenarios, but there is only a small difference between the weight and glide ratio penalty scenario. This causes a reduced Flyover margin when compared to the reference case, but no significant difference between the penalties.

For the quasi-static operating point at the **Approach certification point** there is no acceleration, so both weight and glide ratio penalties translate directly to increased thrust.

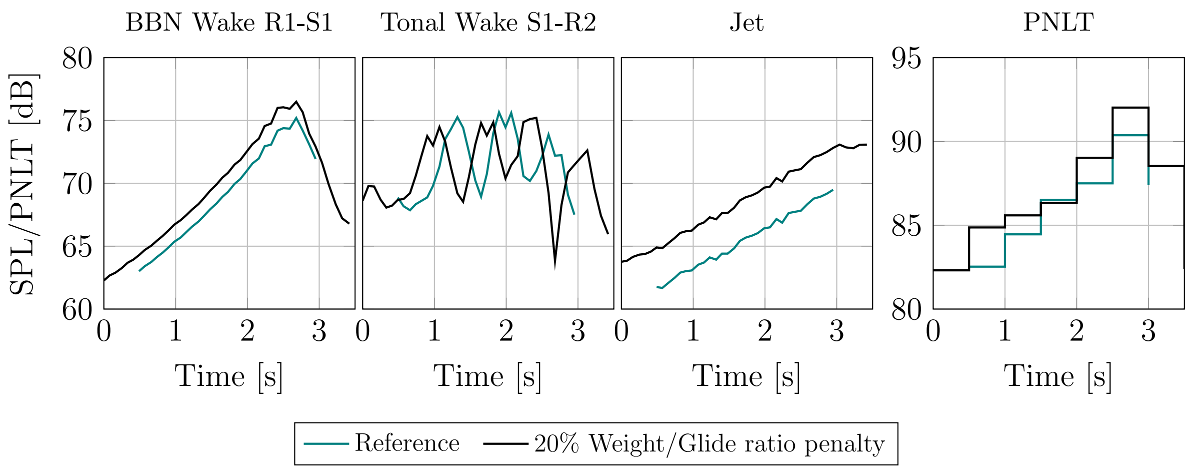

Figure 6.15: Dominant noise sources and PNLT at the Approach point inside the 10 dB-down time, 20% penalty applied

In Figure 6.15, it can easily be seen that even with increased jet noise, fan noise drives PNLT. Broadband wake interaction noise gets stronger, leading to higher PNLT levels. The peak SPL of tonal wake interaction noise does not change significantly, but the different interference patterns due to the different fan speeds change their impact on the discretized PNLT values. These semi-random discretization effects of the tonal noise impact PNLT and thus EPNL more than noise levels at source.

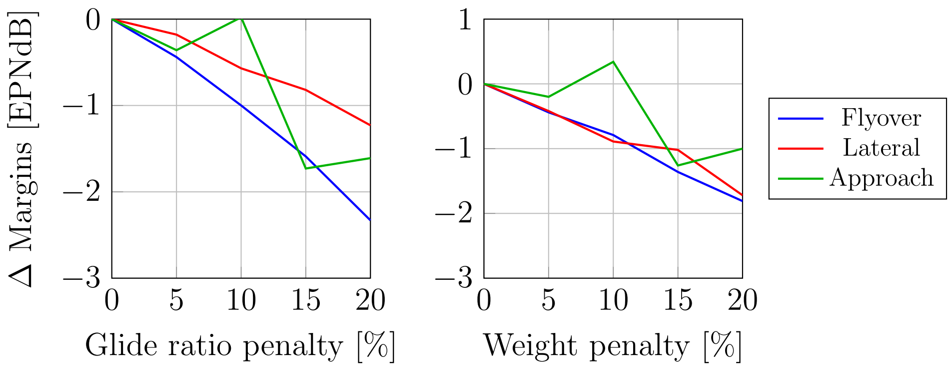

Figure 6.16: Variation in LTO certification levels when glide ratio and weight penalties are applied on the advanced take-off and landing

Consequently, the trends in EPNL margins are less clear for the Approach point than for the take-off certification points, as can be seen in Figure 6.16. In general, the expected trend towards lower margins at all certification points can be observed. Certification noise limits increase with aircraft weight, which partially offsets the increase in certification noise levels for all cases with a weight penalty. In total, a 20% reduction in glide ratio reduces the cumulative margin by 5.2 EPNdB and a 20% weight increase reduced it by 4.7 EPNdB. While these deviations are significant, the very high certification margins of the SENECA M1.8 airliner cannot be fully explained by optimistic or even unrealistic glide ratio or weight assumptions.

6.4.2 Liner penalties

The liner effect is modelled by simply subtracting a fixed number of dB from any source's sound pressure levels, depending on whether they radiate downstream through the bypass or upstream through the inlet and whether they are a broadband or tonal source (see Section 3.2.4). This allows for a simple linear scaling of liner effectiveness. The liner efficiency is reduced from the original -10/-20 dB/(l/d) to -5/-10 dB/(l/d), i.e. from 100% to 50%.

As was shown in the preceding sections, even with the full liner attenuation, fan noise impacts certification levels on the advanced take-off trajectory. Any reduction in liner effectiveness will lead to a further increase in these levels. Since the characteristics of noise generation and propagation to the observer are not altered, an in-depth analysis of the time signal at the observer positions would not yield any scientifically relevant insights.

The impact of a reduced liner effectiveness can be seen in Figure 6.17.

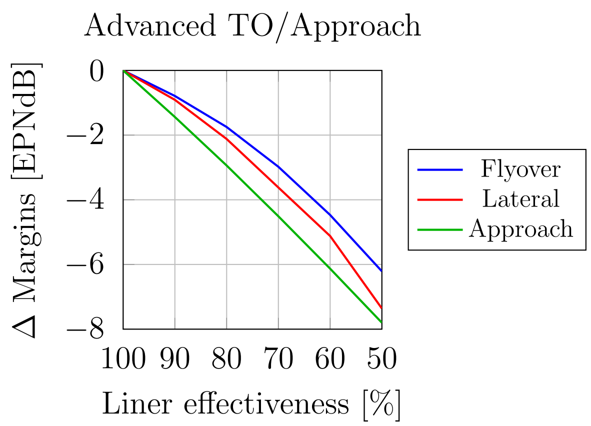

Figure 6.17: Variation in LTO certification levels when liner effectiveness is reduced

As can be seen, certification noise levels display a high sensitivity to liner effectiveness, amounting to a total reduction in cumulative margins of 21.4 EPNdB when reducing liner effectiveness by 50%. This indicates that a more refined approach to liner simulation is crucial for more accurate certification noise prediction.

6.4.3 Effects on cumulative noise levels

After examining the changes in certification noise margins for weight, glide ratio and liner effectiveness penalties individually, their combined effect on the SENECA M1.8 airliner's cumulative margin will be explored.

The realistic 20% weight increase and a still optimistic 20% glide ratio penalty cannot simultaneously be applied to the advanced take-off profile without exceeding the fan envelope[5], so their combined impact on certification noise cannot be predicted accurately. However, simply summing up their impact on its margins can be considered a reasonable approximation. Thus, a reduction in cumulative margin of ≈10 EPNdB can be expected.

[5]To avoid this, a new take-off profile with reduced aircraft performance needs to be simulated

Assuming a reduced acoustic liner performance of half the originally estimated attenuation can be considered realistic, resulting in a reduction of the cumulative margin by ≈21 EPNdB.

When combining the effects of increased weight, reduced glide ratio and scaled down liner performance, the total cumulative margin is decreased by ≈31 EPNdB. This shows that more conservative modeling and assumptions made in the conceptual design stage of the SENECA M1.8 airliner shift its certification levels into a more realistic range, as the resulting cumulative margin is ≈12 EPNdB. This is much closer to the cumulative margins found for other supersonic airliners of 4-6 EPNdB [59, 60].

Chapter 7

Conclusion

The goal of this thesis was to conduct an aeroacoustic analysis and optimization of supersonic aircraft engine noise and the engine components as well as to predict and minimize certification noise levels. The methods employed for certification noise prediction in this work are an improvement over the status quo, which will be discussed first. Then the findings about supersonic aircraft engine design and operation with the goal of certification noise reduction are discussed, which are a product of the application of these methods. Finally, an outlook at potential improvements and further studies in this field of research is laid out.

7.1 Relevance of engine components

In this thesis it was shown that supersonic aircraft need to abide by specific design constraints to be economically feasible and avoid high drag penalties in cruise: because of high friction and wave drag, the airframe and engines need to be very slender with a minimal cross-section. Low diameter engines limit the BPR, which entails a high jet velocity and a high FPR. This leads to an increase in both fan and jet noise which were considered to be the dominant engine noise sources and dominant overall in all take-off scenarios. This makes the fan and jet noise prediction most relevant for the prediction of supersonic aircraft landing- and take-off (LTO) and certification noise levels.

7.2 Improved methods over the state of the art

The certification noise level prediction for supersonic aircraft previously leaned heavily on empirical models which exhibit two significant shortcomings: their scope is limited to designs similar to their calibration domain and they lack supporting aerodynamic and thermodynamic modeling. Applying the analytical fan noise models of *PropNoise* in this thesis addressed these shortcomings with regards to the fan and allowed a more complete understanding of the impact of supersonic aircraft fan design and operations on LTO noise. The implementation of noise propagation modeling process with a focus on analytical models allowed for a more reliable prediction of certification noise of supersonic transport (SST) and a high-quality receiver signal.

Expanding the scope of fan noise modeling

The empirical fan noise models employed in earlier studies can only be considered accurate for single-stage designs since they were calibrated using single-stage fans operating on their working line. The analytical models applied in this thesis are only limited by the scope of their models and not a database used for calibration. They are thus able to process multi-stage fan designs by modeling the aerodynamics and thermodynamics, the aerodynamic excitation and solve for the resulting noise source terms instead of relying on correlations. This allowed studying all turbomachinery noise sources of multi-stage fans, not all of which can be modelled appropriately by empirical models. Off-design operation of the fan could be modelled more realistically. Since the variable throat nozzle design of the engine primarily investigated in this thesis moves the fan off the classic working line in LTO operations, this is highly relevant. Investigations of dominant noise sources, noise generation mechanisms, and noise mitigation effects in multi-stage fans throughout the entire fan envelope became possible this way.

Deepened understanding of fan noise for design-to-noise approach

The inclusion of aerodynamic and thermodynamic modeling yielded the ability to model both the relevant sources and noise generation mechanisms behind them, so insight into the impact of fan design and operation specific to SST on their noise emissions was gained. This enabled the author to implement a design-to-noise approach, i.e. the development of a low-noise fan design in early concept stages. It also permits an improved understanding on how LTO noise of a fixed fan design can be reduced in operation. With the ability to design noise-optimized multi-stage fan concepts as well as single-stage concepts, the set of fan concepts to design for a given aircraft and engine became much larger. These abilities were applied when designing single- and two-stage fan concepts for the SENECA M1.8 airliner. By incorporating the analytical fan noise models into a framework based on an evolutionary algorithm, an iterative design process was automated allowing for a large number of design variations to be evaluated. With this automated design-to-noise process, fan design optimization for minimum LTO noise while maintaining a high efficiency was made possible. The effectiveness of this optimization process was proven.

Improving modeling quality

The acoustic output produced by *PropNoise* is more refined than that of the empirical methods. Instead of producing a spectrum on discrete frequency bands and directivities, the simulation and superposition of acoustic modes allowed the calculation of a more accurate spectral and directivity characteristic. Furthermore, the narrow-band spectra were carried throughout the entire propagation simulation process, so most propagation effects could be simulated with physics-based models. In particular tonal signal and their interference are calculated more accurately this way. This leads to a highly detailed receiver signal and more reliable certification noise prediction.

7.3 Impact of results

Applying these improved methods to landing and take-off noise predictions yielded new findings about supersonic engine and fan design as well as the minimization of SST certification noise levels using variable noise reduction systems. Assumptions pertaining to noise, namely the inlet having no auxiliary inlets, the liner efficiency, airframe noise being negligible, and to the aircraft design, such as the effect of high lift devices, technology factors in weight estimation, etc., were made, so the absolute certification noise levels cannot be considered fully reliable. To quantify the impact of some of these assumptions, the sensitivity of certification noise level predictions to these input uncertainties were investigated as well.

7.3.1 Fan and engine design

Different fan designs were developed for an airliner cruising at Mach 1.8. In evaluation of those designs, it was shown that the fan design of supersonic aircraft engines has a significant impact on the aircraft's landing and take-off noise and thus certification noise levels. Traditional fan noise mitigation through cut-off design and blade loading management was proven to be effective, but for the high-FPR applications of SST, two other design aspects have major importance: variable features and the use of multi-stage concepts.

Variable features

Variable inlet guide vanes and variable throat nozzles are specific to SST engines, since their fans have to provide a very high FPR during supersonic climb and cruise, but very low relative thrust on approach and during taxi. The SENECA M1.8 airliner engine was designed with variable throat nozzle, which provides stability throughout the entire mission but also serves as a measure of LTO noise reduction. By opening the nozzle throat during LTO operation, the fan mass flow is increased. It was demonstrated that the decreased incidence and fan loading reduced fan noise to a significant extent. At an operating point representative for take-off, opening the nozzle reduces fan noise by 0.4 and 1.0 dB at source for the single- and two-stage designs respectively.

Multi-stage fan design

For the supersonic airliner fan designs covered in this thesis, it was found that a two-stage fan design with significantly lower individual stage pressure ratios will yield much lower fan noise levels when compared to a single-stage design. These findings are in line with previous studies, which showed that fan noise scales with the stage pressure ratio. The biggest effect was found to be the lower fan speeds of the two-stage design which reduces buzzsaw noise. At low and medium take-off power settings, buzzsaw noise could be eliminated entirely by keeping the two-stage rotors entirely subsonic. This was not possible for the single-stage rotor which is only subsonic at idle power during landing. The aerodynamic load management in a two-stage design is not as critical, allowing for blades with smaller chords which reduce wake area and turbulence and thus broadband interaction noise. However, there is an aeroacoustic disadvantage of two-stage fan designs: classic cut-off design does not work between all blade pairings. This leads to strong tonal interaction noise generated in the interstage segment. However, the realistic impact of this source is hard to predict without modeling through other rows transmission.

When comparing the airliner's cumulative certification noise levels with both fan designs, a 6.9 EPNdB difference was found with a standard take-off profile and a 14.9 EPNdB difference with an advanced take-off profile.

7.3.2 Jet noise mitigation

With current technology, jet noise can only realistically be reduced by perfectly mixing the core and bypass streams and reducing the jet velocities. It was demonstrated that a variable throat nozzle allows for over-expansion on the jet at take-off, thus reducing the jet velocities and consequently the jet noise at landing and take-off. At an operating point representative for take-off, opening the nozzle reduces jet sound power by 2.9 dB. Mixer and ejector technology were not covered in this thesis but can realistically reduce jet noise while incurring complexity and weight penalties.

7.3.3 Optimized take-off procedures

Using the SENECA M1.8 airliner, a profile variation study was conducted to investigate the impact of variable noise reduction systems in optimizing take-off procedures and the resulting trade-offs. It was shown that LTO noise of SST can be significantly reduced by varying their take-off procedures. The take-off profiles are varied by applying PLR, adjusting the rotation and climb-out speed, and using derated thrust. Two main objectives were accomplished:

- Minimizing the thrust applied around the certification noise monitoring points, reducing engine noise at the source
- Exploiting propagation effects to reduce noise immission to the observer

It was shown that there is a trade-off between thrust reduction and flight altitude. Higher altitude translates into increased distance between the aircraft and the Flyover observer position and exploits atmospheric absorption and radial spread while lower thrust translates to lower noise levels at source. Because jet noise and less significantly fan noise scale with thrust, the benefits of thrust reduction can outweigh the penalty of a reduced distance to the measurement point. Furthermore, lateral attenuation is exploited most effectively by applying high thrust at low altitude and reducing thrust as the angle of elevation of immission to the Lateral point increases.

Climbing out at a shallow angle, low thrust and high speed has been shown to be beneficial for minimizing certification noise for the M 1.8 supersonic airliner. A delayed rotation and the application of PLR help match the application of thrust to the angle of elevation for the Lateral certification point. The ideal PLR activation altitude has been found to be the 35 ft minimum. It was shown that increased airspeed has the largest impact in reducing certification noise levels for two reasons: jet noise is decreased because the speed differential between jet and ambient air is lower and furthermore, increased speed improves the aerodynamic efficiency in the region of reverse command which reduces the thrust demand.

The certification noise levels found in this study were very low, which is likely a result of highly optimistic assumptions about the airliner's weight, aerodynamic efficiency, and liner effectiveness. For that reason, their impact on certification noise levels was investigated.

7.3.4 Uncertainties

Certification noise prediction for aircraft at a pre-design level relies on many models which are used in sequence, which introduces uncertainties. For this reason, the noise models have been cross-checked and validated by multiple European partners in the scope of the trajectory variation study. A good agreement between the results was found, with the only notable difference being explained by absence of lateral attenuation modeling for some partners.

Uncertainties in airframe and aerodynamic design and liner modeling were investigated and their impact on certification noise quantified. Investigating the impact of glide ratio in a wide range was particularly relevant because common pre-design methods fail to predict the low-speed aerodynamic efficiency with reasonable accuracy. Numerical methods and a complete 3D wing design are necessary to improve the prediction quality. The impact of glide ratio and weight penalties on margins to Chapter 14 are significant with 20% penalties causing a 5.2 and 4.7 EPNdB lower cumulative margin respectively. They do however not fully explain the high margins found in the trajectory study.

The assumptions about liner effectiveness were shown to be very optimistic. Their impact on certification noise was proven to be very strong, with a reduction in liner effectiveness by 50% resulting in a 21.4 EPNdB lower cumulative margin.

7.4 Outlook

Several aspects of civil supersonic LTO and certification noise could not be explored in this thesis. The scope of the studies can be expanded and the methods used in LTO noise prediction can be refined.

Noise sources besides the engine noise were neglected in this thesis. While this appears to be a valid simplification for take-off, it might not be for landing. The long landing gear of supersonic aircraft at their high approach speeds might be a dominant noise source, so including airframe noise into LTO noise predictions is worth considering.

The high-quality receiver signal obtained with the certification noise prediction process described in this thesis was auralized using the process described by Moreau et al. [173]. The synthesized audio files were deemed realistic by experts. Psychoacoustic studies can be conducted using these files, evaluating the LTO noise of SST in more detail than through the certification metric EPNL. This can be achieved by calculating psychoacoustic parameters such as loudness or sharpness. Listening studies with human subjects are made possible as well, so that the actual human reaction to the LTO noise of SST can be assessed. Such studies are run as part of DLR project STORMIE.

When modeling physics analytically, it is effectively impossible to match reality perfectly. Simplifications are made and several effects are not modelled in the certification noise prediction routine. Future work to include additional effects could improve the accuracy of the LTO noise predictions, especially in SST applications:

- Transmission modeling: the propagation of noise within the engine is heavily influenced by the interaction of noise with the blade rows it traverses. Neither scattering into different mode orders nor transonic rotor shielding are modelled within *PropNoise* as of this writing.
- Liner modeling: The inlet section, which is particularly long for SST engines, can house liners which reduce fan noise significantly. The prediction of the effects of modern single degree of freedom and double degree of freedom liners is complicated enough to warrant its own field of research and is thus outside of the scope of this work. Modeling the impact of liners more accurately would significantly improve the quality of the LTO noise prediction however. A high sensitivity of the certification noise levels of the SENECA M1.8 airliner to liner modeling has been proven.
- Engine noise-airframe interaction: The propagation from engine to observer was simplified and did not include the interaction of engine noise with the airframe. This means that both shielding and reflection of engine noise by the wings and fuselage were not modelled.
- Lateral attenuation modeling: The lateral (or ground) attenuation was modelled using an empirical model. A more sophisticated, physics-based model might improve both quantitative and qualitative accuracy.
- Improved ray tracing: The sound propagation was modelled using straight rays. In reality, sound waves are diffracted and the sound rays bent. Ignoring these effects does likely not cause a significant error, but is a simplification nonetheless.

There are several technologies which can further reduce the LTO noise of SST but they were not covered in this thesis: Jet noise mitigation strategies are not covered in depth, but CAA simulations can shed light on the effectiveness of more sophisticated jet noise reduction mechanisms. The most prominent examples are mixer-ejector technology, which increases the exhaust mass flow and reduces jet velocity by pulling ambient air into the exhaust stream, non-coaxial core and bypass jets which use the bypass jet to shield the core jet and jet-jet shielding between the engines which reduces the jet noise in certain azimuthal directivities.

Bibliography

[1] A. Scanlan. Boom Supersonic Begins Construction on Overture Superfactory. https://boom-press-assets.s3.us-west-2.amazonaws.com/Boom_Supersonic_Groundbreaking.pdf, 2023.

[2] K. Petronis. Memorandum. https://www.faa.gov/media/11081, 2018.

[3] C. Orlebar. *The Concorde story*. Osprey Aerospace, 1997.

[4] BBC UK. Concorde grounded for good: Concorde flights are to end after more than three decades of luxury travel. *BBC News*, 2003.

[5] Federal Aviation Administration, Department of Transportation. §91.817 Civil aircraft sonic boom. 14 CFR 91.817. https://www.ecfr.gov/current/title-14/chapter-I/subchapter-F/part-91/subpart-I/section-91.817, 1973.

[6] D. J. Trump. Leading the World in Supersonic Flight. https://www.whitehouse.gov/presidential-actions/2025/06/leading-the-world-in-supersonic-flight/, 2025.

[7] L. B. Jones. Lower Bounds for Sonic Bangs. *The Journal of the Royal Aeronautical Society*, 65(606):433–436, 1961.

[8] W. Carlson. *The Lower Bound of Attainable Sonic-boom Overpressure and Design Methods of Approaching this Limit*. National Aeronautics and Space Administration, 1962.

[9] C. M. Darden. Progress in Sonic-Boom Understanding: Lessons Learned and Next Steps. In *High-Speed Research: 1994 Sonic Boom Workshop*, page 269, 1999.

[10] J. Alonso, A. Jameson, and I. Kroo. Advanced algorithms for design and optimization of Quiet Supersonic Platforms. In *40th AIAA Aerospace Sciences Meeting & Exhibit*, Reston, USA, 2002. American Institute of Aeronautics and Astronautics (AIAA).

[11] J. Pawlowski, D. Graham, C. Boccadoro, P. Coen, and D. Maglieri. Origins and Overview of the Shaped Sonic Boom Demonstration Program. In *43rd AIAA Aerospace Sciences Meeting and Exhibit*, Reston, USA, 2005. American Institute of Aeronautics and Astronautics (AIAA).

[12] Publications Office of the European Union. Fact Sheet - SOBER (Sonic boom european research programme : numerical and laboratory-scale experimental simulation). https://cordis.europa.eu/project/id/G4RD-CT-2000-00398?format=pdf, 2004.

[13] Publications Office of the European Union. Fact Sheet - RUMBLE (Sonic boom european research programme : numerical and laboratory-scale experimental simulation). https://cordis.europa.eu/project/id/769896?format=pdf, 2020.

[14] K. Yoshida. Supersonic drag reduction technology in the scaled supersonic experimental airplane project by JAXA. *Progress in Aerospace Sciences*, 45(4):124–146, 2009.

[15] A. Ueno and Y. Makino. Low-Boom and Low-Drag Design of Small Supersonic Transport Considering Propulsion Airframe Integration: JAXA Research and Devel. Memorandum, 2018.

[16] Y. Makino, Y. Naka, J. Akatsuka, A. Ueno, and H. Ishikawa. R&d of quiet supersonic aircraft technology to open up new markets for supersonic aircraft. *Aeronautical and Space Sciences Japan*, 72(2):49–55, 2024.

[17] B. Liebhardt, L. Lütjens, A. Ueno, and H. Ishikawa. JAXA's S4 supersonic low-boom airliner–a collaborative study on aircraft design, sonic boom simulation, and market prospects. In *AIAA AVIATION 2020 Forum*, page 2731, Reston, USA, 2020. American Institute of Aeronautics and Astronautics (AIAA).

[18] K. Hatfield. NASA's Quesst Mission Marks X-59's Historic First Flight. https://www.nasa.gov/image-article/nasas-quesst-mission-marks-x-59s-historic-first-flight-2/, 2025.

[19] L. Weber, P. Bertram, T. Dietl, S. Schnell, M. Plohr, and B. Liebhardt. Conceptual Design of Supersonic Transport Configurations. In *AIAA AVIATION 2025 Forum*, Reston, USA, 2025. American Institute of Aeronautics and Astronautics (AIAA).

[20] S. Schnell, A. Tidow, and J. Kirz. Multi-Fidelity Aerodynamic Data Set Generation and Analysis of the FSTB-L Supersonic Business Jet. In *AIAA AVIATION 2025*

Forum, Reston, USA, 2025. American Institute of Aeronautics and Astronautics (AIAA).

[21] Federal Aviation Administration, Department of Transportation. §36.301 Noise limits: Concorde. 14 CFR 36.301. https://www.ecfr.gov/current/title-14/chapter-I/subchapter-C/part-36/subpart-D/section-36.301, 1978.

[22] Federal Aviation Administration, Department of Transportation. Part 36 - Noise Standards: Aircraft Type and Airworthiness Certification: 14 CFR 36. https://www.ecfr.gov/current/title-14/chapter-I/subchapter-C/part-36, 2025.

[23] ICAO. Annex 16 - Environmental Protection - Vol.I: International Standards and Recommended Practices, 2017.

[24] P. de Saint Martin. Final Report - HISAC (Environmentally friendly high speed aircraft). https://cordis.europa.eu/docs/results/516/516132/hisac-t-6-26-1-d6-20-publishable-activity-report.pdf, 2009.

[25] W. D. Grantham and P. M. Smith. Development of SCR Aircraft Takeoff and Landing Procedures for Community Noise Abatement and their Impact on Flight Safety. *Supersonic Cruise Research*, pages 299–333, 1979.

[26] J. J. Berton. Optimum Climb to Cruise Noise Trajectories for the High Speed Civil Transport. https://ntrs.nasa.gov/api/citations/20040008601/downloads/20040008601.pdf, 1996.

[27] U. Herrmann. EPISTLE: High lift system design for low-noise applied to a supersonic aircraft. *The Aeronautical Journal*, 110(1107):327–331, 2006.

[28] T. Ohnuki, K. Hirako, and K. Sakata. National experimental supersonic transport project. In *25th ICAS PROCEEDINGS*, pages 2006–1. The International Council of the Aeronautical Sciences (ICAS), 2006.

[29] Publications Office of the European Union. Fact Sheet - EUROSUP (Reduction of Wave & lift-dependent drag for supersonic transport aircraft). https://cordis.europa.eu/article/id/80314-supersonic-transport-aircraft?format=pdf, 1998.

[30] O. Dessens, H. L. Rogers, J. A. Pyle, C. Marizy, M. Gauss, and G. Pitari. Results of the SCENIC project: impacts of supersonic aircraft emissions upon the atmosphere. In *TAC-Conference*, pages 141–146, Oxford, UK, 2006.

[31] D. Arnal. Final Report - SUPERTRAC (Supersonic transition control). https://cordis.europa.eu/docs/results/516/516100/supertrac-publishable-summary-report.pdf, 2008.

[32] U. Herrmann. CISAP: Cruise Speed Impact on Supersonic Aircraft Planform: A Project Overview. In *10th AIAA/ISSMO Multidisciplinary Analysis and Optimization Conference*, Reston, USA, 2004. American Institute of Aeronautics and Astronautics (AIAA).

[33] G. Norris. Aerion Unveils Major Updates To AS2 Supersonic Business Jet Design. *Aviation Week*, 2020.

[34] A. Scanlan. Boom Supersonic Reveals Refined Overture and Announces Landmark Market-Expanding Alliance with Northrop Grumman and New Tier One Suppliers. https://boomsupersonic.com/press-release/boom-supersonic-reveals-refined-overture-and-announces-landmark-market-expanding-alliance-with-northrop-grumman-and-new-tier-one-suppliers, 2022.

[35] A. Scanlan. Boom Supersonic Announces Significant Overture Program Advances. https://boomsupersonic.com/press-release/boom-supersonic-announces-significant-overture-program-advances, 2023.

[36] M. F. Heidmann. Interim prediction method for fan and compressor source noise: Technical Memorandum. Technical Report NASA TM-X-71763, NASA, Cincinnati, USA, 1979.

[37] K. B. Kontos, R. E. Kraft, and P. R. Gliebe. Improved NASA-ANOPP noise prediction computer code for advanced subsonic propulsion systems: Contractor Report. Technical Report NASA CR-202309, General Electric Co., Cincinnati, USA, 1996.

[38] E. A. Kresja and J. R. Stone. Enhanced Fan Noise Modeling for Turbofan Engines. Technical Report NASA CR-2014-218421, NASA Lewis Research Center, Cincinnati, USA, 2014.

[39] J. J. Berton. System Noise Prediction of the DGEN 380 Turbofan Engine. In *21st AIAA/CEAS Aeroacoustics Conference*, Reston, USA, 2015. American Institute of Aeronautics and Astronautics (AIAA).

[40] D. Stephens, A. A. Svetgoff, and E. Envia. Acoustic Simulations of Two-Stage Fans Behind a Supersonic Inlet. In *AIAA SCITECH 2025 Forum*, Reston, USA, 2025. American Institute of Aeronautics and Astronautics (AIAA).

[41] N. Hurm. GE's Affinity: The first civil supersonic engine in 55 years – launching a new era of efficient supersonic flight. https://www.geaerospace.com/news/press-releases/regional-business-engines/ges-affinity-first-civil-supersonic-engine-55-years, 2018.

[42] J. W. Rawls Jr. and J. C. Yeager. High Speed Research Noise Prediction Code(HSRNOISE) User's and Theoretical Manual. https://ntrs.nasa.gov/api/citations/20040200978/downloads/20040200978.pdf, 2004.

[43] W. R. Sears. Some Aspects of Non-Stationary Airfoil Theory and Its Practical Application. *Journal of the Aeronautical Sciences*, 8(3):104–108, January 1941.

[44] R. K. Amiet. High frequency thin-airfoil theory for subsonic flow. *AIAA Journal*, 14(8):1076–1082, 1976.

[45] A. Moreau. *A unified analytical approach for the acoustic conceptual design of fans of modern aero-engines*. PhD thesis, TU-Berlin, 2017.

[46] P. Joseph, K.E. Britchford, and P. Loheac. A model of fan broadband noise due to rotor-stator interaction. In *5th European Conference on Turbomachinery Fluid Dynamics and Thermodynamics (01/01/03 - 01/01/03)*, pages 45–54, 2003.

[47] F. R. Menter. Two-equation eddy-viscosity turbulence models for engineering applications. *AIAA Journal*, 32(8):1598–1605, August 1994.

[48] J. C. Kok. Resolving the Dependence on Freestream Values for the k-ω Turbulence Model. *AIAA Journal*, 38(7):1292–1295, July 2000.

[49] C. Wagner, T. Hüttl, and P. Sagaut. *Large-Eddy Simulation for Acoustics*. Cambridge University Press, January 2007.

[50] F. Menter, A. Hüppe, A. Matyushenko, and D. Kolmogorov. An Overview of Hybrid RANS–LES Models Developed for Industrial CFD. *Applied Sciences*, 11(6):2459, March 2021.

[51] C. Frey, G. Ashcroft, H.-P. Kersken, and C. Weckmüller. Advanced Numerical Methods for the Prediction of Tonal Noise in Turbomachinery: Part II—Time-Linearized Methods. In *Volume 8: Turbomachinery, Parts A, B, and C*, GT2012, pages 1779–1789. American Society of Mechanical Engineers, June 2012.

[52] H.-P. Kersken, C. Frey, C. Voigt, and G. Ashcroft. Time-Linearized and Time-Accurate 3D RANS Methods for Aeroelastic Analysis in Turbomachinery. *Journal of Turbomachinery*, 134(5), May 2012.

[53] C. Frey, G. Ashcroft, H.-P. Kersken, and C. Voigt. A Harmonic Balance Technique for Multistage Turbomachinery Applications. In *Volume 2B: Turbomachinery*, GT2014. American Society of Mechanical Engineers, June 2014.

[54] S. Chen and G. D. Doolen. Lattice Boltzmann Method for Fluid Flows. *Annual Review of Fluid Mechanics*, 30(1):329–364, January 1998.

[55] K. Kusano, M. Furukawa, K. Sakoda, K. Hatakenaka, and T. Fukui. Hybrid lattice Boltzmann method using Cartesian and body-fitted grids for turbomachinery aeroacoustic simulations. *Journal of Sound and Vibration*, 588:118516, October 2024.

[56] J. J. Berton. Aircraft Noise and Performance Data for a Notional Supersonic Business Jet. In *28th AIAA/CEAS Aeroacoustics 2022 Conference*, Reston, USA, 2022. American Institute of Aeronautics and Astronautics (AIAA).

[57] M. Nöding, L. Bertsch, J. Kirz, R. Ewert, and J. J. Berton. Application and comparison of proposed SST noise certification regulations to a conceptual business aircraft. In *AIAA AVIATION 2023 Forum*, Reston, USA, 2023. American Institute of Aeronautics and Astronautics (AIAA).

[58] J. Akatsuka and T. Ishii. System Noise Assessment and Uncertainty Analysis of a Conceptual Supersonic Aircraft. *Aerospace*, 9(4):212, 2022.

[59] D. Mavris, J. Tai, W. A. Crossley, and DeLaurentis D. ASCENT Project 010 2023 Annual Report. `https://s3.wp.wsu.edu/uploads/sites/2479/2024/05/ASCENT-Project-010-2023-Annual-Report.pdf`, 2023.

[60] J. A. Page, D. Rankin, and J. M. Gallman. Takeoff and Landing Analysis of Two Northrop Grumman Supersonic Conceptual Vehicle Designs. In *AIAA SCITECH 2025 Forum*, Reston, USA, 2025. American Institute of Aeronautics and Astronautics (AIAA).

[61] J. Morgenstern, N. Norstrud, J. Sokhey, S. Martens, and J. J. Alonso. Advanced Concept Studies for Supersonic Commercial Transports Entering Service in the 2018 to 2020 Period. Technical Report NASA CR-2013-217820, Lockheed Martin Aeronautics Co., Palmdale, USA, 2013.

[62] J. J. Berton, S. M. Jones, J. A. Seidel, and D. L. Huff. Noise predictions for a supersonic business jet using advanced take-off procedures. *The Aeronautical Journal*, 122(1250):556–571, 2018.

[63] J. J. Berton, D. L. Huff, K. Geiselhart, and J. A. Seidel. Supersonic technology concept aeroplanes for environmental studies. In *AIAA SCITECH 2020 Forum*, page 0263, Reston, USA, 2020. American Institute of Aeronautics and Astronautics (AIAA).

[64] J. J. Berton. Variable Noise Reduction Systems for a Notional Supersonic Business Jet. *Journal of Aircraft*, 60(3):688–701, 2023.

[65] J. Akatsuka and T. Ishii. System Noise Assessment of NASA Supersonic Technology Concept Aeroplane Using JAXA's Noise Prediction Tool. In *AIAA SCITECH 2020 Forum*, Reston, USA, 2020. American Institute of Aeronautics and Astronautics (AIAA).

[66] M. Nöding and L. Bertsch. Application of Noise Certification Regulations within Conceptual Aircraft Design. *Aerospace*, 8(8):210, 2021.

[67] M. Nöding, M. Schuermann, L. Bertsch, M. Koch, M. Plohr, R. Jaron, and J. J. Berton. Simulation of Landing and Take-Off Noise for Supersonic Transport Aircraft at a Conceptual Design Fidelity Level. *Aerospace*, 9(1):9, 2022.

[68] L. Bertsch, M. Plohr, and M. Nöding. PLR and take-off speed implications on noise contours and local gaseous emissions for SST business jet concept aircraft. *INTER-NOISE and NOISE-CON Congress and Conference Proceedings*, 270(4):7370–7381, 2024.

[69] D. Mavris, J. Tai, W. A. Crossley, and DeLaurentis D. ASCENT Project 010 2021 Annual Report. `https://s3.wp.wsu.edu/uploads/sites/2479/2022/10/ASCENT-Project-010-2021-Annual-Report.pdf`, 2022.

[70] R. Jaron and N. Viola. The Future of Civil Supersonic Transport in Europe: The SENECA and MORE&LESS Projects. In *34th ICAS PROCEEDINGS*. The International Council of the Aeronautical Sciences (ICAS), 2024.

[71] M. Schuermann. *Supersonic Business Jets in Preliminary Aircraft Design*. Phd thesis, TU Braunschweig, 2016.

[72] L. Bertsch, F. Loessle, M. Nöding, B. Schaeffer, and S. B. Mulani. Considerations Toward Uncertainty Quantification of Single Event Noise Predictions for Novel SST Concept Aircraft. In *AIAA SCITECH 2025 Forum*, Reston, USA, 2025. American Institute of Aeronautics and Astronautics (AIAA).

[73] M. Graebert, R. Jaron, M. Plohr, S. Zenkner, C. Richter, C. Stöhr, C. Villena Munoz, M.-J. van der Meulen, R. Habing, M. Huet, F. Petrosino, M. Barbarino, F. Fischer, and O. Zaporozhets. Landing and Take-Off Noise Prediciton of Conceptual Supersonic Aircraft. In *34th ICAS PROCEEDINGS*, Florence, Italy, 2024. The International Council of the Aeronautical Sciences (ICAS).

[74] H. Smith and Y. Sun. Design Case of the E-19 AEOLUS Supersonic Business Jet. In *AIAA AVIATION 2020 Forum*, Reston, USA, 2020. American Institute of Aeronautics and Astronautics (AIAA).

[75] C. Villena Munoz, C. Lawson, A. Riaz, and A. Sharma. Design of the SENECA Mach 1.8 Supersonic Airliner with Multi-Fidelity Aerodynamic Analysis for Noise-Optimized Take-Off Trajectories. In *34th ICAS PROCEEDINGS*, Florence, Italy, 2024. The International Council of the Aeronautical Sciences (ICAS).

[76] C. Villena Munoz, G. Bonavolontà, C. Lawson, and A. Riaz. Conceptual Design of a Next Generation Supersonic Airliner for Low Noise and Emissions. In *AIAA SCITECH 2023 Forum*, Reston, USA, 2023. American Institute of Aeronautics and Astronautics (AIAA).

[77] Junichi Akatsuka, Atsushi Ueno, and Yoshikazu Makino. System Noise Assessment and Prediction Methodology Uncertainty Analysis for JAXA's Supersonic Conceptual Aircraft With Variable Noise Reduction System. In *AIAA SCITECH 2025 Forum*, Reston, USA, 2025. American Institute of Aeronautics and Astronautics (AIAA).

[78] J. E. Bridges. Results of the NASA Prediction Uncertainty Reduction Tech Challenge. In *AIAA SCITECH 2025 Forum*, Reston, USA, 2025. American Institute of Aeronautics and Astronautics (AIAA).

[79] G. R. Busch and J. E. Bridges. Reduction of Aircraft Noise Uncertainty for a Notional Supersonic Business Jet. In *AIAA SCITECH 2025 Forum*, Reston, USA, 2025. American Institute of Aeronautics and Astronautics (AIAA).

[80] M. Graebert, R. Jaron, C. Villena Munoz, M. Plohr, and A. Moreau. Impact of airframe and aerodynamic design uncertainties on LTO noise of SST. *To be published*, 2025.

[81] L. V. Lopes and C. L. Burley. ANOPP2 User's Manual. `https://ntrs.nasa.gov/api/citations/20160014858/downloads/20160014858.pdf`, 2016.

[82] D. Stephens. Fan Noise for a Concept Commercial Supersonic Transport. In *53rd AIAA/SAE/ASEE Joint Propulsion Conference*, Reston, USA, 2017. American Institute of Aeronautics and Astronautics (AIAA).

[83] D. Stephens. Acoustic Simulations and Commercial Supersonic Flight. `https://ntrs.nasa.gov/api/citations/20210021219/downloads/Stephens_NASA_Acoustic%20Simulations%20and%20Commercial%20Supersonics.pdf`, October 2021.

[84] K. Yoshida. Supersonic drag reduction technology in the scaled supersonic experimental airplane project by JAXA. *Progress in Aerospace Sciences*, 45(4–5):124–146, May 2009.

[85] T. E. Blackall. *Concorde: the story, the facts and the figures*. G. T. Foulis & Co. Ltd., 1969.

[86] D. Hills. The Airbus Challenge. `https://conf.uni-obuda.hu/EADS2008/Hills.pdf`, 2008.

[87] Airbus Customer Service. *Getting to grips with aircraft performance*. Airbus, 2002.

[88] J. R. Spreiter. Aerodynamic Properties of Slender Wing-Body Combinations at Subsonic, Transonic and Supersonic Speeds, 1948.

[89] G. Erickson, J. Schreiner, and L. Rogers. On the structure, interaction, and breakdown characteristics of slender wing vortices at subsonic, transonic, and supersonic speeds. In *16th Atmospheric Flight Mechanics Conference*. American Institute of Aeronautics and Astronautics (AIAA), August 1989.

[90] R. P. Hallion. Lippisch, Gluhareff, and Jones: The Emergence of the Delta Planform and the Origins of the Sweptwing in the United States. *Aerospace Historian*, 26(1):1–10, 1979.

[91] M. Jarrah and H. Ashley. Impact of flow unsteadiness on maneuvers and loads of agile aircraft. In *30th Structures, Structural Dynamics and Materials Conference*, Reston, USA, 1989. American Institute of Aeronautics and Astronautics (AIAA).

[92] A. A. Sidorenko, A. D. Budovskiy, A. A. Maslov, B. V. Postnikov, B. Y. Zanin, I. D. Zverkov, and V. V. Kozlov. Plasma control of vortex flow on a delta wing at high angles of attack. *Experiments in Fluids*, 54(8), August 2013.

[93] Jochen Kirz, Samuel Schnell, and Michel Noeding. CFD-Based Design of a Supersonic Business Jet for Low Environmental Impacts Including Trim and Stability

Constraints. In *AIAA AVIATION FORUM AND ASCEND 2025*. American Institute of Aeronautics and Astronautics (AIAA), July 2025.

[94] J. J. Berton, S. M. Jones, J. A. Seidel, and D. L. Huff. Advanced Noise Abatement Procedures for a Supersonic Business Jet. In *International Symposium on Air Breathing Engines (ISABE 2017)*, Manchester, UK, 2017. International Society for Air Breathing Engines (ISABE).

[95] T. von Kármán and N. B. Moore. Resistance of Slender Bodies Moving With Supersonic Velocities, With Special Reference to Projectiles. *Journal of Fluids Engineering*, 54(2):303–310, 1932.

[96] W. Haack. Geschoßformen kleinsten wellenwiderstandes. `https://web.archive.org/web/20070927020313/http://www.lima-wiederladetechnik.de/Ballistik/Lilienthal-139-1-Haack.pdf`, 1941.

[97] T. T. Takahashi. Development of a Semi-Empirical Takeoff and Landing Method for Supersonic Commercial Aircraft. In *AIAA Scitech 2021 Forum*, Reston, USA, 2021. American Institute of Aeronautics and Astronautics (AIAA).

[98] M. R. Fink. Noise Component Method for Airframe Noise. *Journal of Aircraft*, 16(10):659–665, 1979.

[99] W. Herkes and R. Stoker. Wind tunnel measurements of the airframe noise of a high-speed civil transport. In *36th AIAA Aerospace Sciences Meeting and Exhibit*, page 030, Reston, USA, 1998. American Institute of Aeronautics and Astronautics (AIAA).

[100] S. Adamidis, D. D. Gatto, C. Mourouzidis, S. Brown, and V. Pachidis. Installation Effects of Supersonic Inlets on Next-Generation SST Turbofan Engines. In *EASN 2024*, page 50, Basel, Switzerland, 2024. MDPI.

[101] W. H Ball and R. A. Atkins Jr. Rapid Evaluation of Propulsion System Effects Volume II - PIPSI Users Manual, 1978.

[102] W. J.G. Bräunling. *Flugzeugtriebwerke*. Springer Vieweg Berlin, Heidelberg, 2015.

[103] M. Plohr, S. Zenkner, S. Bake, and D. Zeitz. Thermodynamic Design and Emissions Model of a Mach 1.8 Supersonic Airliner Engine. In *34th ICAS PROCEEDINGS*, Florence, Italy, 2024. The International Council of the Aeronautical Sciences (ICAS).

[104] D. Papamoschou and M. Debiasi. Conceptual Development of Quiet Turbofan Engines for Supersonic Aircraft. *Journal of Propulsion and Power*, 19(2):161–169, 2003.

[105] P. H. Calder and P. C. Gupta. Future SST engines with particular reference to Olympus 593 evolution and Concorde experience. *The Aeronautical Journal*, 80(786):235–252, June 1976.

[106] G. A. Ganley. Concorde Propulsion - Did We Get It Right? The Rolls-Royce/Snecma Olympus 593 Engine Reviewed. In *SAE Technical Paper Series*, volume 1 of *AEROTECH*. SAE International, September 1991.

[107] Forecast International. Aviation Gas Turbine Forecast - Pratt & Whitney F119. `https://www.forecastinternational.com/archive/disp_pdf.cfm?DACH_RECNO=901`, 2012.

[108] IAE. V2500 Engine Product Card. `https://prd-sc102-cdn.rtx.com/prattwhitney/-/media/pw/products/commercial-jet-engines/v2500/files/ce_v2500_pcard.pdf?rev=1fbb81a571404d49bbcab203125208a3&rid=56c45a5d1c97408aa54725b4ecea641c&hash=CD12DD07BD767F40F8DA878608E26344`, 2024.

[109] EASA. Type-Certificate Data Sheet for Engine V2500-A5, V2500-D5, V2500-E5 Series, 2022.

[110] N. T. Monsarrat, M. J. Keenan, and P. C. Tramm. Design Report: Single-Stage Evaluation of Highly-Loaded High-Mach-Number Compressor Stages, 1969.

[111] P. de Haller. Das Verhalten von Tragflügelgittern in Axialverdichtern und im Windkanal. *Brennstoff-Wärme-Kraft (BWK)*, 5(333):24, 1953.

[112] D. Stephens, A. A. Svetgoff, and E. Envia. Acoustics of a Supersonic Mach 1.4 Axisymmetric Spike Inlet. In *AIAA AVIATION 2023 Forum*. American Institute of Aeronautics and Astronautics (AIAA), June 2023.

[113] J. Morgenstern, M. Buonanno, J. Yao, M. Murugappan, U. Paliath, L. Cheung, I. Malcevic, K. Ramakrishnan, N. Pastouchenko, T. Wood, S. Martens, P. Viars, J. L. Tersmette, R. Simmons, D. Plybon, J. J. Alonso, F. Palacios, T. Lukaczyk, and G. Carrier. Advanced Concept Studies for Supersonic Commercial Transports Entering Service in the 2018 to 2020 Period. Technical Report NASA CR—2015-218719, Lockheed Martin Aeronautics Co., Palmdale, USA, 2015.

[114] W. E. Mallett and D. E. Groesbeck. Effects of compressor interstage bleed and adjustable inlet guide vanes on compressor stall characteristics of a high-pressure-ratio turbojet engine at altitude. Technical report, Lewis Flight Propulsion Laboratory, Cleveland, USA, 1956.

[115] A. Moreau, R. Schnell, and M. Mennicken. Acoustic preliminary design of a low-noise fan stage considering a variable-area nozzle and variable-pitch rotor blades. *CEAS Aeronautical Journal*, 14(2):325–341, March 2023.

[116] M. D. Guynn, J. J. Berton, M. J. Tong, and W. J. Haller. Advanced Single-Aisle Transport Propulsion Design Options Revisited. In *2013 Aviation Technology, Integration, and Operations Conference*. American Institute of Aeronautics and Astronautics (AIAA), August 2013.

[117] H. R. Welge, J. Bonet, T. Magee, D. Chen, S. Hollowell, A. Kutzmann, A. Mortlock, J. Stengle, C. Nelson, E. Adamson, S. Baughcum, R. T. Britt, G. Miller, and J. Tai. N+2 Supersonic Concept Development and Systems Integration. Technical Report NASA CR-2010-216842, Langley Research Center, Hampton, USA, 2010.

[118] Warren C. Strahle. Combustion noise. *Progress in Energy and Combustion Science*, 4(3):157–176, 1978.

[119] R. Meier zu Ummeln. *Aeroakustische Bewertung von Fanstufen im Rahmen des Vorentwurfs von Triebwerken*. PhD thesis, TU Berlin, 2023.

[120] M.S. Howe. A review of the theory of trailing edge noise. *Journal of Sound and Vibration*, 61(3):437–465, December 1978.

[121] C. L. Morfey and M. J. Fisher. Shock-Wave Radiation from a Supersonic Ducted Rotor. *The Aeronautical Journal*, 74(715):579–585, July 1970.

[122] D. Hawkings. Transonic Fan Noise. Technical Report ARC CP-1226, Aeronautical Research Council, 1973.

[123] F. F. Ehrich. Acoustic Resonances and Multiple Pure Tone Noise in Turbomachinery Inlets. *Journal of Engineering for Power*, 91(4):253–262, October 1969.

[124] S. Kaji and T. Okazaki. Generation of sound by rotor-stator interaction. *Journal of Sound and Vibration*, 13(3):281–307, November 1970.

[125] J. M. Tyler and T. G. Sofrin. Axial Flow Compressor Noise Studies. In *SAE Technical Paper Series*, volume 620532. SAE International, January 1962.

[126] U. Ganz, S. Glegg, and P. Joppa. Measurement and prediction of broadband fan noise. In *4th AIAA/CEAS Aeroacoustics Conference*. American Institute of Aeronautics and Astronautics (AIAA), June 1998.

[127] M. J. Lighthill. On sound generated aerodynamically I - General Theory. *Proceedings of the Royal Society of London. Series A. Mathematical and Physical Sciences*, 211(1107):564–587, March 1952.

[128] J. E. Ffwocs Williams and D. L. Hawkings. Sound generation by turbulence and surfaces in arbitrary motion. *Philosophical Transactions of the Royal Society of London. Series A, Mathematical and Physical Sciences*, 264(1151):321–342, May 1969.

[129] M. Goldstein. Unified approach to aerodynamic sound generation in the presence of solid boundaries. *Acoustical Society of America*, 1974.

[130] R. Meier zu Ummeln. *Gegenüberstellung zweier Prognoseverfahren zur Korrelation von Fanakustik mit lokalen Strömungsgrößen beziehungsweise globalen Leistungsparametern.* Bachelor's thesis, TU Berlin, Berlin, 2012.

[131] A. Moreau, M. Staggat, and C. Gscheidle. A Fast Prediction Method for Rotor Buzz-saw Noise based on an Analytical Approach. In *25th AIAA/CEAS Aeroacoustics Conference*, Reston, USA, 2019. American Institute of Aeronautics and Astronautics (AIAA).

[132] R. Jaron. *Aeroakustische Auslegung von Triebwerksfans mittels multidisziplinärer Optimierungen.* PhD thesis, TU Berlin, 2018.

[133] S. Guerin. Farfield Radiation of Induct-Cutoff Pressure Waves. In *23rd AIAA/CEAS Aeroacoustics Conference*, Reston, USA, 2017. American Institute of Aeronautics and Astronautics (AIAA).

[134] A. Ravindranath and B. Lakshminarayana. Mean Velocity and Decay Characteristics of the Near and Far-Wake of a Compressor Rotor Blade of Moderate Loading. *Journal of Engineering for Power*, 102(3):535–547, July 1980.

[135] R. B. Ginder and D. R. Newby. An Improved Correlation for the Broadband Noise of High-speed Fans. *Journal of Aircraft*, 14(9):844–849, September 1977.

[136] A. Moreau and S. Guérin. The Impact of Low-Speed Fan Design on Noise: An Exploratory Study. *Journal of Turbomachinery*, 138(8), March 2016.

[137] C.L. Morfey. Amplification of aerodynamic noise by convected flow inhomogeneities. *Journal of Sound and Vibration*, 31(4):391–397, December 1973.

[138] S. A. L. Glegg and C. Jochault. Broadband Self-Noise from a Ducted Fan. *AIAA Journal*, 36(8):1387–1395, August 1998.

[139] T. J. Trella and P. K. Kasper. Attenuation of a resonant dissipative silencer in a rigid duct. *Applied Acoustics*, 7(2):127–138, April 1974.

[140] Lord Rayleigh. The Theory of the Helmholtz Resonator. *Proceedings of the Royal Society of London. Series A, Containing Papers of a Mathematical and Physical Character*, 92(638):265–275, 1916.

[141] D.L. Lansing and W.E. Zorumski. Effects of wall admittance changes on duct transmission and radiation of sound. *Journal of Sound and Vibration*, 27(1):85–100, March 1973.

[142] G. W. Bielak, J. W. Premo, and A. S. Hersh. Advanced Turbofan Duct Liner Concepts. Technical Report NASA CR-1999-209002, Boeing Commercial Airplane Group, Hampton, USA, 1999.

[143] E. J. Rice. Propagation of Waves in an Acoustically Lined Duct with a Mean Flow. In *Basic Aerodynamic Noise Research: A Conference Held at NASA Headquarters, Washington, DC, July 14-15, 1969*, volume 207, page 345, 1969.

[144] E. J. Rice. Acoustic liner optimum impedance for spinning modes with mode cut-off ratio as the design criterion. In *3rd Aeroacoustics Conference*, Reston, USA, 1976. American Institute of Aeronautics and Astronautics (AIAA).

[145] E. J. Rice. Inlet noise suppressor design method based upon the distribution of acoustic power with mode cutoff ratio. *Advan. in Eng. Sci., Vol. 3*, 1976.

[146] E. J. Rice and D. T. Sawdy. A theoretical approach to sound propagation and radiation for ducts with suppressors. In *Meeting of the ASA*, 1981.

[147] L. Cremer. Theorie der Luftschall-Dämpfung im rechteckkanal mit schluckender wand und das sich dabei ergebende höchste dämpfungsmaß. *Acustica*, 3(2):249–263, 1953.

[148] J. F. Unruh. Finite length tuning for low frequency lining design. *Journal of Sound and Vibration*, 45(1):5–14, 1976.

[149] S. Rienstra. Impedance Models in Time Domain, Including the Extended Helmholtz Resonator Model. In *12th AIAA/CEAS Aeroacoustics Conference (27th AIAA Aeroacoustics Conference)*, Reston, USA, 2006. American Institute of Aeronautics and Astronautics (AIAA).

[150] J. Wong, E. Nesbitt, M. G. Jones, and D. M. Nark. Flight Test Methodology for NASA Advanced Inlet Liner on 737MAX-7 Test Bed (Quiet Technology Demonstrator 3). In *25th AIAA/CEAS Aeroacoustics Conference*. American Institute of Aeronautics and Astronautics (AIAA), May 2019.

[151] Michael J. T. Smith. *Aircraft noise*. Cambridge University Press, 1989.

[152] J. R. Stone, D. E. Groesbeck, and C. L. Zola. Conventional profile coaxial jet noise prediction. *AIAA Journal*, 21(3):336–342, 1983.

[153] W. Olsen and R. Friedman. Jet noise from coaxial nozzles over a wide range of geometric and flow parameters. In *12th Aerospace Sciences Meeting*, page 43, 1974.

[154] J. R. Stone, C. Zola, and B. Clark. An improved model for conventional and inverted-velocity-profile coannular jet noise. In *37th Aerospace Sciences Meeting and Exhibit*. American Institute of Aeronautics and Astronautics (AIAA), January 1999.

[155] J. R. Stone, E. A. Krejsa, and B. J. Clark. Jet noise modeling for supersonic business jet application. Technical Report NASA CR-2004-212984, Langley Research Center, Hampton, USA, 2004.

[156] M. Harper-Bourne and M. J. Fisher. The Noise from Shock Waves in Supersonic Jets. *AGARD-CP-131*, 11:1–13, 1973.

[157] R. Jaron, M. Graebert, R. Habing, M.-J. Meulen, M. Huet, I. Legriffon, F. Petrosino, M. Barbarino, K. Lefarth, and O. Zaporozhets. Jet Noise Prediction Benchmark for Landing and Takeoff Noise of Supersonic Aircraft. In *Internoise 2023*, 08 2023.

[158] R. Habing, M.-J. van der Meulen, M. Huet, R. Jaron, F. Petrosino, and O. Barbarino, M.and Zaporozhets. Dual-Stream Jet Noise Test with Internal Mixer Design Variations for LTO Noise of Supersonic Aircraft. In *34th ICAS PROCEEDINGS*, Florence, Italy, 2024. The International Council of the Aeronautical Sciences (ICAS).

[159] M. Huet, O. Atinault, F. Gand, and H. Demontis. Numerical Evaluation of Jet Noise with Flight Effect for Supersonic Civil Aircraft Using ZDES. In *AIAA AVIATION*

FORUM AND ASCEND 2025. American Institute of Aeronautics and Astronautics (AIAA), July 2025.

[160] B. J. Cocking. The effect of temperature on subsonic jet noise. Technical Report Reports and Memoranda No. 3771, National Gas Turbine Establishment, Aeronautical Research Council, 1974.

[161] A. Powell. On the Generation of Noise by Turbulent Jets. In *Aviation Conference of ASME*. The American Society of Mechanical Engineering, 1959.

[162] V. Mengle, W. Dalton, J. E. Bridges, and K. Boyd. Noise reduction with lobed mixers - Nozzle-length and free-jet speed effects. In *3rd AIAA/CEAS Aeroacoustics Conference*. American Institute of Aeronautics and Astronautics (AIAA), May 1997.

[163] N. Saiyed, J. E. Bridges, and K. Mikkelsen. Acoustics and thrust of separate-flow exhaust nozzles with mixing devices for high-bypass-ratio engines. In *6th Aeroacoustics Conference and Exhibit*, page 1961, 2000.

[164] K. Q. Zaman, J. E. Bridges, R. S. Castner, and A. F. Fagan. An investigation of a mixer-ejector nozzle for jet noise reduction. In *25th AIAA/CEAS Aeroacoustics Conference*. American Institute of Aeronautics and Astronautics (AIAA), May 2019.

[165] D. Rutherford. The International Civil Aviation Organization's CAEP/13 aircraft noise standards. `https://theicct.org/wp-content/uploads/2025/05/ID-358-%E2%80%93-Noise-standard_ICAO_final.pdf`, 2025.

[166] T. W. Reese, K. D. Kryter, and S. S. Stevens. The relative annoyance produced by various bands of noise. *Report No. PB 27*, 306, 1944.

[167] K. D. Kryter. Loudness and Annoyance-Value of Bands of Noise. In *Oralism and Autism: Transactions of the 30th Annual Meeting of the National Forum on Deafness and Speech Pathology*, pages 26–28, 1948.

[168] K. D. Kryter. The meaning and measurement of perceived noise level. *Noise Control*, 6(5):12–27, 1960.

[169] R.A. Pinker. Mathematical formulation of the noy tables. *Journal of Sound and Vibration*, 8(3):488–493, 1968.

[170] E. Terhardt and G. Stoll. Bewertung des Wohlklangs verschiedener Schalle. *Fortschritte der Akustik, DAGA'78*, pages 583–586, 1978.

[171] W. Aures. Berechnungsverfahren für den sensorischen Wohlklang beliebiger Schallsignale. *Acustica 59*, pages 130–141, 1985.

[172] K. D. Kryter and K. S. Pearsons. Some Effects of Spectral Content and Duration on Perceived Noise Level. *The Journal of the Acoustical Society of America*, 35(6):866–883, June 1963.

[173] A. Moreau, A. Prescher, S. Schade, M. Dang, R. Jaron, and S. Guérin. A framework to simulate and to auralize the sound emitted by aircraft engines. In *2023 InterNoise Conference*, Chiba, Japan, 2023.

[174] M. E. Delany and E. N. Bazley. Acoustical properties of fibrous absorbent materials. *Applied acoustics*, 3(2):105–116, 1970.

[175] A. Prescher. *Modellierung der Schallausbreitung in einer inhomogenen Atmosphäre und ihr Einfluss auf binaural synthetisierten Überfluglärm*. Master's thesis, TU Berlin, Berlin, 2023.

[176] International Organization for Standartization. Acoustics - Attenuation of sound during propagation outdoors: Part 1: Calculation of the absorption of sound by the atmosphere. `https://cdn.standards.iteh.ai/samples/17426/3a2d69b767024b74805b83b063a91445/ISO-9613-1-1993.pdf`, 1993.

[177] Society of Automotive Engineers. AIR5662 - Method for Predicting Lateral Attenuation of Airplane Noise, 2019.

[178] J. J. Berton. Simultaneous Use of Ground Reflection and Lateral Attenuation Noise Models. *Journal of Aircraft*, 59(2):536–543, March 2022.

[179] M. Graebert, R. Jaron, A. Moreau, and M. Plohr. Aeroakustischer Vergleich eines ein- und eines mehrstufigen Fan-Konzepts für zivile überschallfähige Triebwerke. In *DLRK 2023*, 2023.

[180] H. Grieb. *Verdichter für Turbo-Flugtriebwerke*. Springer Verlag, 2009.

[181] E. J. Kowalski and R. A. Atkins Jr. A Computer Code for Estimating Installed Performance of Aircraft Gas Turbine Engines – Vol.3 Library of Nozzle/Inlet Configurations and Performance Maps, 1979.

[182] D. C. Urasek, W. T. Gorrel, and W. S. Cunnan. Performance of two-stage fan having low-aspect-ratio first-stage rotor blading: NASA technical paper, 1979.

[183] H. H. Valentine and W. T. Beale. Experimental Investigation of Distortion Removal Characteristics of Several Free-Wheeling Fans. Technical report, Lewis Flight Propulsion Laboratory, Cleveland, USA, 1958.

[184] S. Sane and P. Tagade. Effect of Rotor Solidity on Stall Inception and Growth in Axial Flow Fan. In *40th AIAA/ASME/SAE/ASEE Joint Propulsion Conference and Exhibit*. American Institute of Aeronautics and Astronautics (AIAA), June 2004.

[185] B. B. Bell and L. J. DeKoster. The effect of solidity, blade section and contravane angle on the characteristics of an axial-flow fan. Technical report, Langley Memorial Aeronautical Laboratory, Langley Field, USA, 1942.

[186] F.B. Metzger, D. B. Hanson, R. W. Menthe, and G.B. Towle. Analytical parametric investigation of low pressure ratio fan noise: Contractor Report. Technical Report NASA CR-2188, Hamilton Standard, Windsor Locks, USA, 1973.

[187] Moreau, A. PropNoise Documentation - Modus 10. `https://propnoise.dlr.de/index.php/Modus10`, 2025.

[188] R. Storn and K. Price. Differential Evolution – A Simple and Efficient Heuristic for Global Optimization over Continuous Spaces. *Journal of Global Optimization*, 11(4):341–359, 1997.

[189] G. Ebenhoch. Personal Communication, September 21, 2023.

[190] S. Schade, R. Jaron, A. Moreau, and S. Guérin. Mechanisms to reduce the blade passing frequency tone for subsonic low-count OGV fans. *Aerospace Science and Technology*, 125(5), 2022.

[191] ICAO. Environmental Technical Manual - Vol.I: Procedures for the Noise Certification of Aircraft. `https://www2023.icao.int/environmental-protection/Documents/SGAR_2018_ETM_Vol_I.pdf`, 2018.

[192] Boeing Commercial Airplanes. High-Speed Civil Transport Study. Technical Report NASA CR-4233, Boeing Commercial Airplanes, Seattle, USA, 1989.

[193] FAA. Reduced and Derated Takeoff Thrust (Power) Procedures. Technical Report AC 25-13, Federal Aviation Administration, Washington, USA, 1988.

[194] M. Graebert, R. Jaron, C. V. Munoz, M. Plohr, and A. Moreau. Single- and Two-Stage Fan Designs for a Supersonic Airliner with Focus on Certification Noise Re-

duction. In *AIAA SCITECH 2025 Forum*, Reston, USA, 2025. American Institute of Aeronautics and Astronautics (AIAA).

[195] NLR. Report on noise certification level estimates for the final status of the Ma 1.8 airliner. Deliverable D5.21, SENECA Consortium, 2024.

[196] Society of Automotive Engineers. ARP866-A - Standard Values of Atmospheric Absorption as a Function of Temperature and Humidity. `https://www.sae.org/standards/content/arp866a/`, 1975.

[197] C. F. Chien and W. W. Soroka. Sound propagation along an impedance plane. *Journal of Sound and Vibration*, 43(1):9–20, 1975.

[198] G. Gabard. Boundary layer effects on liners for aircraft engines. *Journal of Sound and Vibration*, 381:30–47, October 2016.

Appendix I - Take-Off Profile Variation Results

T_{rel} [%]	PLR height [ft]	PLR ratio [%]	Del. rot. [ms^{-1}]	V_2 excess [ms^{-1}]	LAT Level [EPNdB]	FO Level [EPNdB]	CUM Level [EPNdB]	LAT Margin [EPNdB]	FO Margin [EPNdB]	CUM Margin [EPNdB]
70	200	80	0	20	81.48	88.46	250.14	17.51	9.55	34.44
70	200	80	18.7	40	78.39	87.61	246.2	20.6	10.4	38.38
70	200	80	0	40	79.26	86.65	246.11	19.73	11.36	38.47
70	200	80	18.7	72	77.98	86.87	245.05	21.01	11.14	39.53
70	200	80	29.9	72	76.95	85.9	243.05	22.04	12.11	41.53
70	200	90	0	20	81.39	90.8	252.39	17.6	7.21	32.19
70	200	90	0	40	78.83	88.66	247.69	20.16	9.35	36.89
70	200	90	18.7	40	78.24	88.97	247.41	20.75	9.04	37.17
70	200	90	29.9	72	76.64	85.98	242.82	22.35	12.03	41.76
70	35	70	8.3	20	81.4	85.78	247.38	17.59	12.23	37.2
70	35	70	18.7	40	79.33	85.59	245.12	19.66	12.42	39.46
70	35	70	26.6	55	76.43	84.49	241.12	22.56	13.52	43.46
70	35	70	29.9	72	77.29	83.35	240.84	21.7	14.66	43.74
70	35	80	0	20	81.33	88.46	249.99	17.66	9.55	34.59
70	35	80	8.3	20	81.54	88.45	250.19	17.45	9.56	34.39
70	35	80	0	40	79.49	85.97	245.66	19.5	12.04	38.92
70	35	80	18.7	40	78.53	86.81	245.54	20.46	11.2	39.04
70	35	80	29.9	72	77.29	83.88	241.37	21.7	14.13	43.21
70	35	80	18.7	72	78.29	84.33	242.82	20.7	13.68	41.76
70	35	90	0	20	81.51	90.77	252.48	17.48	7.24	32.1
70	35	90	8.3	20	81.12	90.87	252.19	17.87	7.14	32.39
70	35	90	0	40	78.87	88.58	247.65	20.12	9.43	36.93
70	35	90	18.7	40	78.27	88.92	247.39	20.72	9.09	37.19
70	35	90	18.7	72	77.46	85.37	243.03	21.53	12.64	41.55
70	35	90	29.9	72	76.85	84.66	241.71	22.14	13.35	42.87
70	35	100	8.3	20	79.07	92.17	251.44	19.92	5.84	33.14
70	35	100	18.7	40	78.19	90.59	248.98	20.8	7.42	35.6
70	35	100	26.6	55	75.79	88.37	244.36	23.2	9.64	40.22
70	35	100	29.9	72	76.7	85.22	242.12	22.29	12.79	42.46

T_{rel} [%]	**PLR height** [ft]	**PLR ratio** [%]	**Del. rot.** [ms^{-1}]	**V_2 excess** [ms^{-1}]	**LAT Level** [EPNdB]	**FO Level** [EPNdB]	**CUM Level** [EPNdB]	**LAT Margin** [EPNdB]	**FO Margin** [EPNdB]	**CUM Margin** [EPNdB]
59	200	80	0.1	20	83.22	84.24	247.66	15.77	13.77	36.92
59	200	80	19.1	40	79.73	84.27	244.2	19.26	13.74	40.38
59	200	80	9.4	40	80.81	84.94	245.95	18.18	13.07	38.63
59	200	80	9.4	20	81.84	85.42	247.46	17.15	12.59	37.12
59	200	90	9.4	20	81.49	87.53	249.22	17.5	10.48	35.36
59	200	90	0.1	20	82.13	87.34	249.67	16.86	10.67	34.91
59	200	90	0.1	40	81.2	85.93	247.33	17.79	12.08	37.25
59	200	90	19.1	40	79.7	85.66	245.56	19.29	12.35	39.02
59	200	90	9.4	40	80.1	85.23	245.53	18.89	12.78	39.05
59	35	70	9.4	20	82.7	83.28	246.18	16.29	14.73	38.4
59	35	70	19.1	40	80.46	81.61	242.27	18.53	16.4	42.31
59	35	80	0.1	20	83.11	84.16	247.47	15.88	13.85	37.11
59	35	80	9.4	20	82.1	84.99	247.29	16.89	13.02	37.29
59	35	80	19.1	40	80.12	82.04	242.36	18.87	15.97	42.22
59	35	80	9.4	40	80.93	81.6	242.73	18.06	16.41	41.85
59	35	90	9.4	20	81.56	87.46	249.22	17.43	10.55	35.36
59	35	90	0.1	20	82.09	87.39	249.68	16.9	10.62	34.9
59	35	90	9.4	40	80.31	84.32	244.83	18.68	13.69	39.75
59	35	90	0.1	40	81.4	84.29	245.89	17.59	13.72	38.69
59	35	90	19.1	40	79.81	85.47	245.48	19.18	12.54	39.1
59	35	100	9.4	20	81.29	88.83	250.32	17.7	9.18	34.26
59	35	100	19.1	40	79.42	86.61	246.23	19.57	11.4	38.35
59	35	100	19.9	55	78.12	83.4	241.72	20.87	14.61	42.86
53	200	80	10.1	20	83.13	82.48	245.81	15.86	15.53	38.77
53	200	90	10.1	20	82.68	84.39	247.27	16.31	13.62	37.31
53	35	80	10.1	20	83.47	80.77	244.44	15.52	17.24	40.14
53	35	90	10.1	20	82.84	84.32	247.36	16.15	13.69	37.22
53	35	100	10.1	20	82.3	86.18	248.68	16.69	11.83	35.9
53	35	100	12.3	40	81.28	82.3	243.78	17.71	15.71	40.8